INTERNATIONAL ATOMIC ENERGY AGENCY
UNITED NATIONS EDUCATIONAL, SCIENTIFIC AND CULTURAL ORGANIZATION
INTERNATIONAL CENTRE FOR THEORETICAL PHYSICS
I.C.T.P., P.O. BOX 586, 34100 TRIESTE, ITALY. CABLE CENTRATOM TRIESTE

UNITED NATIONS INDUSTRIAL DEVELOPMENT ORGANIZATION

INTERNATIONAL CENTRE FOR SCIENCE AND HIGH TECHNOLOGY

SMR/481 - 4

EXPERIMENTAL WORKSHOP ON
HIGH TEMPERATURE SUPERCONDUCTORS AND RELATED MATERIALS
(ADVANCED ACTIVITIES)

(26 November - 14 December 1990)

" Flux Lattices in Exotic Superconductors "

presented by:

D. BISHOP
AT&T Bell Laboratories
Murray Hill, NJ 07974
U.S.A.

FLUX LATTICES IN EXOTIC SUPERCONDUCTORS

David Bishop
ATT-Bell Laboratories
Murray Hill, New Jersey 07974

OUTLINE

1) Introduction to Flux Lattices in Superconductors

2) Flux Lattices in High Tc Superconductors
   - A) Static Structures
     - i) the flux quantum and the Little-Parks exp
     - ii) hexatics
     - iii) liquids
     - iv) phase transition from liquid to hexatic
     - v) chains
   - B) Dynamics of Flux Lattices
     - i) oscillator experiments and melting
     - ii) picovoltmeter experiments

3) Other Superconducting Systems
   - A) Heavy Fermion Superconductors
     - i) power law transport properties
     - ii) complex phase diagram-oscillator exp
     - iii) magnetism and neutrons
     - iv) flux lattices w/ neutrons
   - B) Two-Dimensional Superconductors
   - C) One-Dimensional Superconductors

4) Conclusions

PHYSICAL REVIEW B VOLUME 41, NUMBER 4 1 FEBRUARY 1990

Little-Parks oscillations of T_c in patterned microstructures of the oxide superconductor $YBa_2Cu_3O_7$: Experimental limits on fractional-statistics-particle theories

P. L. Gammel, P. A. Polakos, C. E. Rice, L. R. Harriott, and D. J. Bishop
AT&T Bell Laboratories, Murray Hill, New Jersey 07974
(Received 27 November 1989)

We report observation of Little-Parks oscillations in arrays with a 4-μm^2 plaquette area, fabricated from ĉ-axis-oriented $YBa_2Cu_3O_7$ films. Near the mean-field transition temperature the magnitude of the oscillations implies a zero-temperature coherence length $\xi(0)=15\pm2$ Å. For temperatures more than 1 K below the mean-field transition, the magnitude of the oscillations increases dramatically, apparently signaling a crossover to the dynamics of a Josephson-coupled network. Precise experimental limits can be placed on the value of the flux quantum, severely restricting any anomalous value which may be proposed on the basis of fractional-statistics-particle theories.

An important observation in the early days of superconductivity was the Little-Parks effect. In an ingenious experiment,[1] these workers were able to clearly show that the fluxoid, not the flux, is quantized in a multiply connected superconductor. The experiment consisted of a thin-walled superconducting cylinder whose transition temperature was measured as a function of the applied axial field. T_c was found to be periodic with a periodicity determined by the superconducting flux quantum $\Phi_0=hc/2e=20.7$ Gμm^2. Subsequent workers have studied single structures and arrays of both narrow wires and weak links.[2] In any periodic array, harmonics of the basic period may be produced because of coherence extending over several loops. Weak links within the array may introduce strong temperature dependence through the temperature dependence of the Josephson-coupling strength.

In this Rapid Communication, we report on the temperature dependence of resistance oscillations in patterned films of the high-T_c superconductor $YBa_2Cu_3O_7$. Oscillations have been previously reported[3] in bulk ceramics. However, our well controlled geometry permits quantitative treatment. The periodicity is determined by the superconducting flux quantum to a high precision. We are able to put strong limits on any anomalous values for the flux quantum which may have implications for recently proposed fractional-statistics-particle theories. From the magnitudes of the oscillations and the quadratic background near the mean-field transition temperature we can extract $\xi(0)=15\pm2$ Å, in accord with other measurements.[4] For temperatures more than 1 K below the mean-field transition T_c, we find a strong temperature dependence. This presumably represents a crossover to the behavior of a Josephson-coupled network. We have previously reported[5] weak link behavior in single junctions in the same size range as the wire width in these arrays. The temperature dependence expected for the array based on this work is in rough agreement with our measurements. In both the single junctions and the arrays this is a surprising result, since the usual size criteria for a Dayem bridge[6] are not satisfied. However, the amplitude of the oscillations never exceeds $\Delta T_c/T_c\sim5\times10^{-4}$, much smaller than the value $\Delta T_c/T_c=0.3$ predicted in Josephson-coupled networks.[2]

In a single ring satisfying $\xi,\lambda\gg w$, where ξ is the temperature-dependent coherence length, λ is the penetration depth, and w is the thickness of the ring; the Little-Parks effect is a simple consequence of the single-valued nature of the superconducting order parameter.[7] For a ring of radius R in a perpendicular field, the supercurrent velocity is $v_s=(\hbar/2mR)(n-\Phi/\Phi_0)$ where m is the electron mass, n is an integer, and the flux through the ring is Φ. The superconducting transition temperature will be reduced by an amount proportional to v_s^2. The exact result in the clean limit appropriate to $YBa_2Cu_3O_7$ is $(\Delta T_c/T_c)=[\xi(0)/R]^2(n-\Phi/\Phi_0)^2$ where $\xi(0)$ is the zero-temperature coherence length. Such oscillations are observed by sitting at fixed temperature and measuring the magnetoresistance. Temperature shifts are inferred from $\Delta T_c=\Delta R(H)(dT/dR)$.

For an array the situation is more complex. For integral numbers of flux quanta per plaquette and a square array,[8] the oscillation depth is $\Delta T_c/T_c=1.82[\xi(0)/a]^2(\pi/4)^2$ where a is the size of the square. In addition, the oscillations develop a cusplike shape.[9] Note that in terms of a magnetoresistance measurement, the value of temperature oscillation inferred should be independent of the temperature at which the sample is biased. In general, however, experiments[10] tend to show increased oscillation as the temperature or current bias is lowered. For an array consisting of wires of width w the oscillation in $T_c(H)$ will be superimposed on a thin-film background $T_c(H)=T_c(0)\{1-0.18[\pi wH\xi(0)/\Phi_0]^2\}$.

The films used in this work were 2000-Å thick deposited on (100) $SrTiO_3$ as described previously.[11] These films were c-axis oriented normal to the substrate with a T_c ($R=0$) of 89.0 K after photoprocessing and ion milling to produce the large-scale pattern. The 1-μm features shown in Fig. 1 were ion milled using a 20-KeV focused gallium beam. The ion-beam spot size, 0.2 μm, allowed features to be written down to 0.5 μm. Studies[5] using single junctions showed no appreciable degradation of the film quality for features larger than 0.6 μm. In both structures shown in Fig. 1, with a characteristic size of 1 μm, T_c was reduced by 0.3 K during the ion-beam writing and the

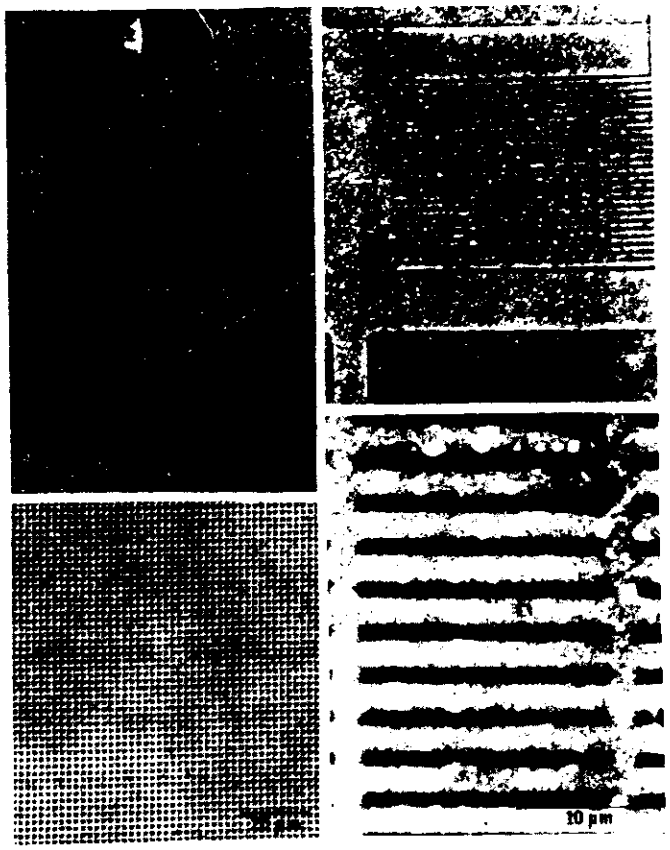

FIG. 1. Micrographs of the patterned films used in these measurements. On the left-hand side are two views of the square array. On the right-hand side are two views of a similarly patterned control. The large-scale pattern is produced by argon ion-beam milling with a photomask. The small-scale pattern is direct write ion milled using 20-keV gallium.

transition width was increased from 0.9 to 1.6 K (10%–90%). The pair of structures shown in Fig. 1 had $\rho(T)$ values equal to within 5% throughout the entire temperature range of this experiment.

Shown in Fig. 1 are several views of two arrays studied in this experiment. They were fabricated side by side from a single piece of film. Current and voltage leads were patterned by Ar-ion milling with a photoresist mask.[12] Contacts were Au pads evaporated onto a freshly milled surface, and had a contact resistance (77 K) less than 0.5 Ω. Six such pairs of arrays were studied during the course of this experiment. The data presented here stem from the pair with the sharpest and highest transition temperature. On the left-hand side in Fig. 1 is a 50×50 array of $1\ \mu m\times1\ \mu m$ holes in which we measured the resistance oscillations. Since the magnitude of the oscillations scales quadratically with $\xi(0)$, significant experimental effort was required. Using an estimate for the zero-temperature coherence length $\xi(0)\sim15$ Å, the mean-field estimate for the temperature oscillation is 0.12 mK. Two-stage temperature regulation gave a short-term stability of 0.05 mK with an oscillation due to the magnetoresistance of the final thermometer of 0.2 mK. To help remove the effect of these drifts and provide first-order temperature and magnetoresistance cancellation, the sample shown on the right-hand side in Fig. 1 could be used as a control. The holes in this case are $1\times20\ \mu m^2$. Any oscillation should be reduced in magnitude by a factor of $(1/20)^2$ relative to the array, and occur with a significantly different period.

The two samples could be used in a bridge configuration to measure differential magnetoresistance, although all of the data presented here are simple magnetoresistance measurements of the square array shown in Fig. 1 and drawn schematically in the inset to Fig. 3. With a measurement current of 2 μA at a frequency of 33 Hz, substantial averaging was required to obtain an acceptable signal-to-noise ratio. Our noise was 10 $nV/Hz^{1/2}$ referenced to the input of the voltage amplifiers. Transformers with ratios of 10, 100, or 1000 were used to impedance match the sample at different temperatures. Repeated field sweeps in both directions were averaged, dividing the field range into bins of 0.08 G. Typically 150 scans swept at a rate of 2 G/min (allowing a 0.3-Hz bandwidth) were averaged over a period of three days. The results shown here are insensitive to changes in measurement current or field sweep rate by factors of at least 5. The ultimate resistance resolution was $\Delta R/R\sim5\times10^{-7}$. This corresponds to nearly 1-μK resolution near T_c.

Shown in Fig. 2 are the changes in T_c inferred from the magnetoresistance data at various temperatures. The measured values of dR/dT have already been normalized out of the data. Two features are readily apparent. The first is a periodicity of ~5 G, corresponding to a flux quantum of $\sim20\ G\mu m^2$. The second is a sizable temperature dependence in contrast to the simple expectations of the mean-field limit discussed above. A zero-field offset, 1.8 G, has been removed from the data, and corresponds to the measured local magnetic field in the vicinity of our experiment. The gradual decay of the oscillations as the field is increased is due to inhomogeneities in the plaquette size. The decay envelope is about five oscillation periods as determined from the Fourier transform width (see inset to Fig. 4), which corresponds to 5% nonuniformity in the plaquette area. This is estimated based on a $\pi/2$ phase shift between the minimal and maximal area over five oscillations.

Shown in Fig. 3 is a plot of the peak positions for the 86.175-K data versus the number of flux quanta. The

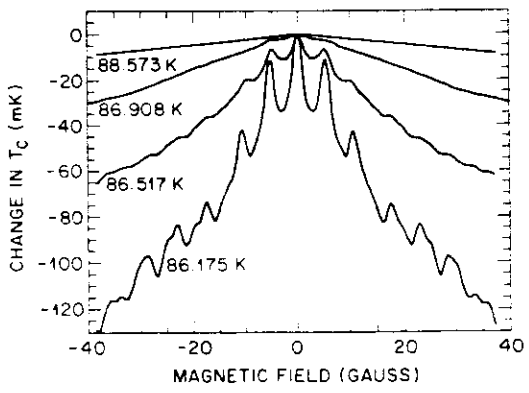

FIG. 2. Temperature oscillations inferred from the resistance oscillations and the measured dR/dT for four different measuring temperatures.

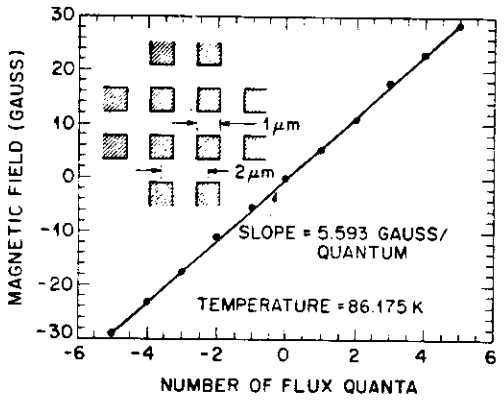

FIG. 3. The locations of the maxima for the 86.175-K data shown in Fig. 2 vs number of flux quanta per plaquette. The inset shows a schematic diagram of the sample with the nominal dimensions.

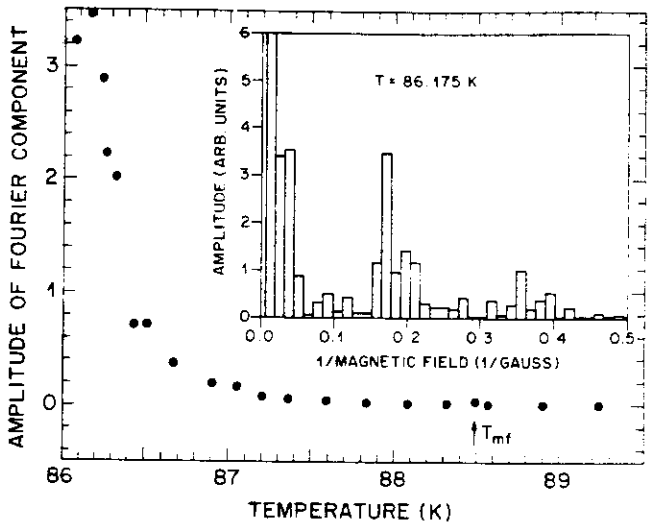

FIG. 4. The inset shows the Fourier transform of the 86.175-K data. The plot shows the amplitude of the peak in the Fourier transform (5.83-G period) as a function of temperature.

slope of the line is an accurate measure of the flux quantum in our film. This slope, 5.59 G/plaquette with an average plaquette area of 4 μm^2, gives $\Phi_0 = 22.4\ G\mu m^2$. Nominally, one should find $hc/2e = 20.7\ G\mu m^2$. The combined error in the field calibration (4%) and fabrication area (5%) is roughly 6.5%. Therefore, the observed deviation, 7%, is consistent with a flux quantum of exactly $hc/2e$.

Shown in the inset of Fig. 4 is the Fourier transform of the 86.175-K data. The peaks are at the fundamental frequency of 5.83 G, with harmonics present at 2.81 and 1.76 G (not shown). These harmonics stem from the nature of our array and correspond to fractional numbers of flux quanta per plaquette or coherence around two, three, or more boxes. The amplitude of the peak at $\frac{1}{2}$ quantum per plaquette is 25% of the fundamental. This compares favorably to calculations[13] for arrays which typically show about a 20% effect. It should be noted that arrays will give Fourier-transform peaks for all fractional fillings. A periodicity larger than the fundamental is either the result of inhomogeneities or a different value for the flux quantum.

There has been substantial theoretical interest in fractional-statistics-particle theories for superconductivity in the high-T_c materials. In these theories,[14,15] two-dimensional particles fractional-statistics particles have fractional statistics intermediate between those of bosons and fermions. If the phase change on exchanging two particles along a path enclosing no other particles is $\Theta = \pi(1 - 1/n)$, each particle carries a flux $\Phi = \Phi_0/n$. Only for the case of paired half fermions ($n = 2$), should the flux quantum correspond to the superconducting flux quantum as measured in this and other experiments. The additional structure seen here at $\frac{1}{2}$ and $\frac{1}{3}$ filling should not be treated as evidence for $n = 2$ or $n = 3$ particles, but rather as a manifestation of the long-range structure in the array. However, for the case $n = 1$, there should be no response in the array. The amplitude of oscillation at $\frac{1}{2}$ of the fundamental is 9.3% of the peak value, placing an upper bound on the admixture of $n = 1$ type excitations. Another consequence of fractional-statistics-particle theories is an orbital ferromagnetism, which can give rise to a nonsymmetric response with respect to field reversal. After subtraction of the 1.8-G remnant field, our results are symmetric to within 0.1 G. Decoration experiments[16] in zero nominal applied field have shown this field to be homogeneous on a 1-μm length scale. Any orbital ferromagnetism must necessarily cancel on these length and field scales. In the language of fractional-statistics-particle theories, this demands either antiferromagnetic-type coupling between planes or domain sizes of order 1 μm, and guarantees the absence of any manifestation of fractional-statistics particles in bulk transport coefficients.

In Fig. 4 a plot of the amplitude of the primary Fourier component of $\Delta T(H)$ is shown versus temperature. The oscillations are present at and below the mean-field transition temperature as defined by $R = 0.5R_N$. Above this temperature the effect is zero to within our resolution. Using a fit to the magnitude of the oscillations for the data within 1 K of the mean-field transition ($R = 0.1 \rightarrow 0.5R_N$), we can extract a zero-temperature coherence length $\xi(0) = 15 \pm 2$ Å, consistent with other determinations of this length. In addition, the quadratic magnetoresistance background (fit for $|H| < 15$ G) for the two points closest to the mean-field transition is consistent with this value and a width of 1 μm with 30% error bars. At lower temperatures, the background is dominated by other powers of field, and the quadratic contribution is difficult to extract. For temperatures more than 1.5 K below the mean-field transition, a sizable temperature dependence is present. At this point the resistance is $r \sim 10^{-2} R_N$. This is similar to the point at which thin-film screening experiments[17] show a divergence of λ, and could be explained as the onset of long-range phase coherence. In this case, the temperature dependence below this point would be a result of weak-link behavior in a Josephson-coupled array. Our measurements[5] of critical currents in weak links would predict[18] an effect linear in temperature, in rough accord with the data. As stated previously, for a Josephson-coupled array, one would expect $\Delta T_c/T_c \sim 0.3$. The maximum value observed in this

experiment was $\Delta T_c/T_c = 5\times10^{-4}$. The lowest temperature at which data were taken was limited by our resolution of small resistances. Alternate explanations for the temperature dependence based on the disappearance of pinning[19] or melting[20] at temperatures 1 K below the transition are also possible. We are presently limited in further exploration by the minimum linewidth capability of our focused ion-beam system.

In conclusion, we have reported the first observation of the Little-Parks effect in a high-T_c superconductor. Our results in ion-beam patterned $YBa_2Cu_3O_7$ arrays are consistent with a value of $hc/2e$ for the flux quantum. Combined with our decoration results, severe limitations can be placed on the range of parameters in fractional-statistics-particle theories. Analysis of the data at the mean-field transition give a zero-temperature coherence length $\xi(0) = 15$ Å in the plane. The effect has a surprisingly strong temperature dependence for temperatures well below T_c, which are likely to be a signature of a crossover to Josephson-coupled behavior.

We would like to thank D. A. Huse, C. M. Varma, B. Batlogg, and P. B. Littlewood for numerous helpful discussions.

[1]W. A. Little and R. Parks, Phys. Rev. A **113**, 97 (1964).

[2]A useful introduction to the extensive literature on this subject is the *Proceedings of the NATO Workshop on Coherence in Superconducting Networks, Delft, Netherlands, 1987,* edited by J. E. Mooij and G. B. J. Schon [Physica B **152**, No. 1&2 (1988)].

[3]R. Steinmann, P. Lejay, J. Chaussy, and B. Pannetier, Physica C **153–155**, 1487 (1988).

[4]U. Welp, W. K. Kwok, G. W. Crabtree, K. G. Vandervoort, and J. Z. Liu, Phys. Rev. Lett. **62**, 1908 (1989); W. C. Lee, R. A. Klemm, and D. C. Johnston, *ibid.* **63**, 1012 (1989).

[5]L. E. Harriott, P. A. Polakos, and C. E. Rice, Appl. Phys. Lett. **55**, 495 (1989).

[6]K. K. Likharev, Rev. Mod. Phys. **51**, 101 (1979).

[7]M. Tinkham, *Introduction to Superconductivity* (Krieger, Malabar, FL, 1980).

[8]P. Gandit, J. Chaussy, B. Pannetier, and R. Ramal, Physica B **152**, 32 (1988); J. Chaussy, B. Pannetier, R. Ramal, and J. C. Villegier, Phys. Rev. Lett. **53**, 1845 (1984); D. F. Hofstader, Phys. Rev. B **14**, 2239 (1976).

[9]See, for example, Q. Nui and F. Nori, Phys. Rev. B **39**, 2134 (1989).

[10]D. J. van Harlinger, K. N. Springer, G. C. Hilton, and J. Tien, Physica B **152**, 134 (1988).

[11]P. M. Mankiewich, J. H. Scofield, W. J. Skocpol, R. E. Howard, A. H. Dayem, and E. Good, Appl. Phys. Lett. **51**, 1753 (1987).

[12]S. Matsui, N. Takado, H. Tsuge, and K. Asakawa, Appl. Phys. Lett. **52**, 69 (1988).

[13]A simple argument is given in M. Tinkham, D. W. Abraham, and C. J. Lobb, Phys. Rev. B **28**, 6578 (1983).

[14]B. I. Halperin, J. March-Russell, and F. Wilczek (unpublished).

[15]J. March-Russell and F. Wilczek, Phys. Rev. Lett. **61**, 2066 (1988); Y.-H. Chen, F. Wilczek, E. Witten, and B. I. Halperin (unpublished).

[16]P. L. Gammel, D. J. Bishop, G. J. Dolan, J. R. Kwo, C. A. Murray, L. F. Schneemeyer, and J. V. Waszczak, Phys. Rev. Lett. **59**, 2952 (1987); and (unpublished).

[17]A. T. Fiory, A. F. Hebard, P. M. Mankiewich, and R. E. Howard, Phys. Rev. Lett. **61**, 1419 (1988); Appl. Phys. Lett. **52**, 2165 (1988).

[18]C. J. Lobb (private communication); D. A. Huse (private communication).

[19]A. F. Hebard, P. L. Gammel, C. E. Rice, and A. F. J. Levi, Phys. Rev. B **40**, 5243 (1989).

[20]P. L. Gammel, L. F. Schneemeyer, J. V. Waszczak, and D. J. Bishop, Phys. Rev. Lett. **61**, 1666 (1988).

Flux-Lattice Melting in Amorphous Composite In/InO_x Two-Dimensional Superconductors

P. L. Gammel, A. F. Hebard, and D. J. Bishop
AT&T Bell Laboratories, Murray Hill, New Jersey 07974
(Received 15 October 1987)

We report the phase diagram for magnetic fluxoids in two-dimensional In/InO_x superconducting films. The films are sputtered directly onto high-Q silicon oscillators. The melting of the vortex lattice is signaled by a peak in the attenuation and a shift of the resonant frequency of the oscillator, caused by the rapid change in mobility of the vortex array. The zero-field limit of the melting temperature can be fitted by the Kosterlitz-Thouless model. However, the magnetic field dependences disagree with the current theoretical picture.

PACS numbers: 74.60.Ge, 74.75.+t

With the applied field between H_{c1} and H_{c2} a type-II superconductor is permeated by an array of flux lines, each carrying one quantum of flux. Abrikosov[1] was the first to predict that these would form into a triangular lattice. Such lattices have been imaged with high-resolution Bitter-pattern techniques[2] and neutron scattering.[3] This lattice behaves as a solid with a well-defined shear modulus[4] at low temperatures and fields. In superconducting films in which the vortices are effectively two dimensional this solid undergoes a melting transition below the resistive transition temperature, T_c. It has been predicted[5,6] that this melting should be a Kosterlitz-Thouless (KT) type melting, mediated by the unbinding of dislocation pairs. Measurements on granular aluminum films have shown a vortex mobility transition consistent with such behavior.[7]

In this Letter we report mechanical measurements of flux-lattice melting and present the phase diagram as a function of temperature and magnetic field for the flux lattice in amorphous composite In/InO_x films. The observed phase diagram is qualitatively similar to the theoretical form, but has important quantitative differences. While the previously published theory[5] predicts no field dependence to the melting temperature in the intermediate-field regime, we see a linear dependence. Inclusion of H/H_{c2} correction would improve the qualitative agreement in the shape of the phase diagram.[8] The theory also predicts that the melting line should approach H_{c2} at low temperatures, while the measured line remains substantially below this value. The theory has one parameter, A_1, which may be used to fit the zero-field limit of the melting temperature, T_M. While A_1 can in principle be calculated, at present it has only been estimated. Our fitted value lies well within the estimate for a KT-type melting.

The experimental setup used in these experiments is shown schematically in the inset of Fig. 1. The basis of the experiment is a high-Q silicon oscillator.[9] By measurement of the resonant frequency and dissipation of the oscillator, the bulk modulus and dissipation in the vortex array can be determined. The oscillator was driven self-resonantly with use of a phase-locked loop.[9] The oscillators had a Q of 2×10^5 at 4.2 K, a frequency of 3 kHz, and a fractional frequency stability of 10^{-8}. The simplest beam-bending mode of the oscillator was

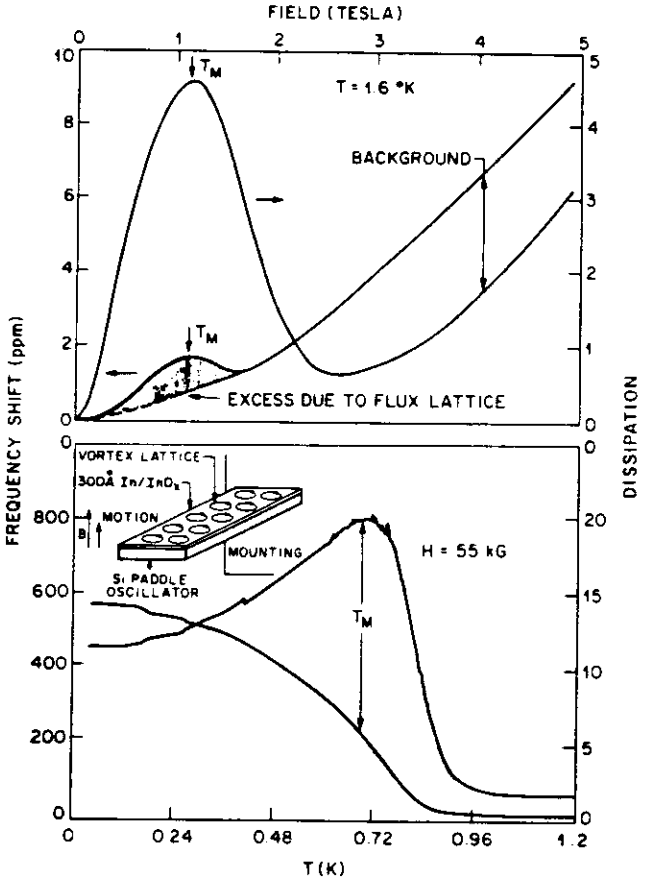

FIG. 1. Bottom: Temperature dependence at fixed magnetic field, or density of vortices. The vortex lattice melts at T_M. Inset: A schematic view of the experiment. Top: At fixed temperature, the vortex lines form a solid at low density and melt as the density is increased. The dissipation and frequency shift scale as H^2 both below and above melting. The melting point is identified as the peak in attenuation.

used. The direction of the motion was parallel to the applied field. To avoid nonlinear effects, a typical amplitude of motion used was 10 nm.

The In/InO_x films were deposited directly onto the oscillator by reactive ion-beam sputter deposition in a low-pressure oxygen environment. The films produced by this technique have been shown to be reproducible and homogeneous.[10] For these experiments, films which were smooth with a predominantly amorphous microstructure were used. Films were also deposited onto a piece of silicon from the same wafer for transport measurements. The resistive transition in zero field was quite sharp, 0.1 K, indicating uniform films. The mean-field transition temperature T_c was estimated from a 40% criterion, rather than a detailed fit to the Aslamazov-Larkin theory.[11] The magnetoresistance of the films was used to determine the upper critical field H_{c2} and the zero-field, vortex-antivortex KT transition temperature, T_{KT}.[12] For the values of $R_\square$ where melting was observed, T_{KT} was within 0.2 K of T_c. The film parameters for the samples studied in these experiments are shown in Table I.

The basic result of the oscillator experiment is shown in Fig. 1. With a uniform magnetic field applied perpendicular to the sample, an array of quantized vortex lines is present. For typical fields, 10 kG, the average spacing is 70 nm. Because the two-dimensional penetration depth, $\Lambda(T)=\lambda^2(T)/d$ where λ is the bulk penetration depth and d is the thickness of the film, is several millimeters, the vortices are strongly overlapping magnetically. However, since the average intervortex spacing $(H/\Phi_0)^{1/2} \gg \xi$ the vortex cores are still well separated. Φ_0 is the superconducting flux quantum and ξ is the coherence length.

When the vortex lattice is in the low-temperature solid phase, a simple physical picture for the oscillator response is possible. The vortex lattice will be collectively pinned, so that the vortices move with the film. In the bending-beam mode, the average vortex spacing, a_0, will oscillate as $\Delta a_0/a_0 \propto A\delta x\, e^{i\omega t}$ where A is the amplitude of oscillation, δ is the thickness of the oscillator, and x is the distance from the suspension point. This density modulation gives a coupling to longitudinal sound in the vortex array at the measurement frequency ω. In two dimensions, the elastic modulus for longitudinal sound is $B+\mu$ where $B \sim H^2$ is the bulk modulus and $\mu \sim H$ is the shear modulus. As a result of the long-range interaction between vortices $B \gg \mu$, and the shear contribution of the vortex array can be neglected.

TABLE I. Parameters for all the films studied.

d (Å)	$R_\square$ (Ω)	T_{c0} (K)	T_{KT} (K)	T_M (K)	A_1
400	313	3.23	3.04	2.24	0.546
500	367	3.00	2.79	2.00	0.483
300	572	2.84	2.58	1.85	0.516
200	904	3.08	2.80		
100	1728	3.22	2.85		

This coupling to longitudinal sound in the vortex array will depend on the relaxation rate of the flux lattice. Since the Hall angle is known to be small,[13] the response of the vortices is purely dissipative. For $T \ll T_M$ there will be a well-formed flux lattice which will remain collectively pinned even in the presence of weak disorder. This will make the relaxation rate for compression of the flux lattice, τ, very long, so that in this regime $\omega\tau \gg 1$ and the vortices will move with the underlying film. Thus an elastic modulus appropriate to longitudinal sound in the vortex lattice will be contributed to the elastic response of the oscillator. For $T \gg T_M$, thermal fluctuations will dominate the motion of the vortices. In this limit, the vortex fluid will relax rapidly ($\omega\tau \ll 1$) and the vortices will not contribute to the elastic response of the film. Near T_M, the compressional relaxation rate will be strongly temperature dependent and a crossover between the two regimes will occur. The peak in attenuation will occur for $\omega\tau \sim 1$, which is the experimentally defined melting temperature.

In the top half of Fig. 1, the dynamic response of the vortex array is examined at fixed temperature by sweeping of magnetic field, or vortex density. At low density, the vortices form a solid. In the solid phase, there is an additional stiffness and dissipation. Both these effects are proportional to H^2. As the solid melts with increasing density, the frequency shift and dissipation decrease. The shaded region in Fig. 1 represents the additional frequency shift due to the flux lattice. The maximum dissipation is identified as the density at which melting occurs. The melting may also be explored at fixed density as a function of temperature, as shown in the lower section of Fig. 1. The excess dissipation which is seen well below the transition temperature has also been observed in helium films,[14] and is associated with internal friction in the vortex solid. The melting temperature is again identified as the maximum in dissipation. The resulting phase diagram is consistent with that given by the field sweeps. In fact, if the curves in the top half of Fig. 1 are divided by the density dependence, H^2, the resulting picture is similar to that seen at fixed density.

If the sample is aligned parallel to the field so that no vortex lattice is present, there are no sharp features in the oscillator response such as those associated with melting. A small frequency shift and dissipation, both proportional to H^2, are still seen. These effects were also seen in an oscillator which had no superconducting film, and are associated with eddy currents in the gold film. This term is identified as the background in Fig. 1.

These data may be combined with the transport data to generate a phase diagram as shown in Fig. 2 for the 313-Ω/□ sample. The results for other samples are qualitatively similar, but the melting line is shifted to lower temperatures as the normal-state sheet resistance is in-

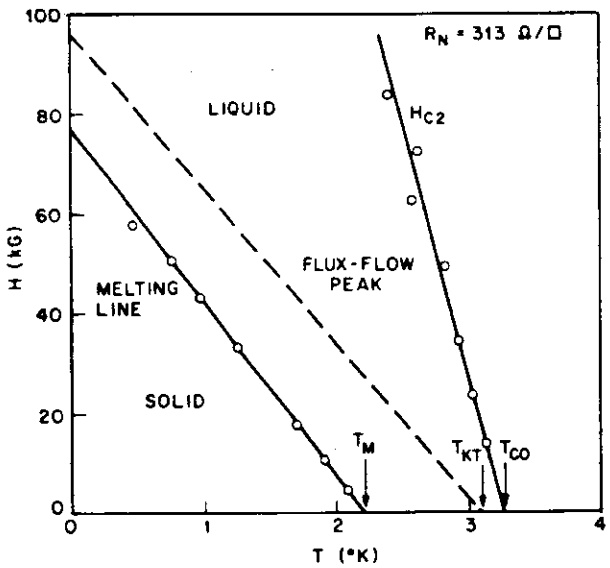

FIG. 2. H_{c2} is obtained from magnetoresistance. Together with the melting data from the oscillator, this is used to generate a phase diagram. Nonlinear I-V curves were used to determine the location of the peak in the volume pinning force.

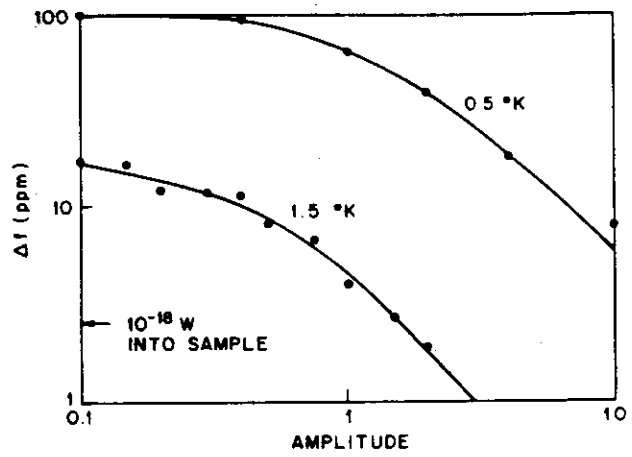

FIG. 3. As the oscillation amplitude is increased, the frequency shift on melting is reduced. The critical velocity increases as the temperature is lowered.

creased, although its slope remains nearly unchanged. The parameters for the three samples in which melting was observed are included in Table I. For normal-state sheet resistances in excess of 900 Ω/□, there was no evidence of solidification, down to 0.3 K, a factor of 4 below the expected melting temperature.

In order to understand the role of pinning in this experiment, I-V curves were measured on the transport samples. In a 400×100-μm^2 sample, the current required to induce 1 μV was defined as the critical current, I_c. The volume pinning force $F_p \propto HI_c$ showed a peak at low fields. The location of this peak is also sketched in Fig. 2. The data were obtained on a sample of higher $R_\square$, so that a larger region below T_c could be explored with our magnet. The data were found to obey the relation $H_{FF}=0.31H_{c2}$. The zero-field intercept was T_{KT}. The dashed line in Fig. 2 is given by this parametrization. Such peaks have been associated with collective pinning phenomena in the vortex array, for samples which showed a peak at high fields.[15] The melting phenomena which we are investigating is clearly distinct from collective pinning. In fact, the 1.3-kΩ/□ sample on which the flux-flow data were taken showed no melting transition.

The effect of increasing the amplitude of motion of the oscillator is shown in Fig. 3, where the frequency shift on melting is shown as a function of oscillation amplitude. For calibration, at an amplitude of 0.1 μm, about 10^{-16} W is dissipated into the 1-cm^2 sample. The critical amplitude increases somewhat as the temperature is reduced. We believe that this is evidence for motionally induced melting of the vortex lattice. A shift in the density at which melting occurs was not observed with increasing amplitude.

The phase diagram has been investigated theoretically[5] for $T_M \ll T_c$. In the intermediate-field regime $\Lambda^2 \gg H/\Phi_0 \gg \xi^2$ relevant to these experiments, the calculated T_M is independent of magnetic field, in contrast to our results. The next-order correction, H/H_{c2}, will suppress melting at high fields in better qualitative agreement with the experiment.[8] At $T=0$, the calculated melting line approaches H_{c2} as $(H-H_{c2})^2$ in the limit of no disorder. We find no departure from the linear slope of the melting line down to 50 mK, our lowest temperature where $H_{c2}\simeq300$ kG and melting occurs at 80 kG. In the presence of disorder, a perfect lattice is no longer expected. As a result of even small amounts of pinning, the quasi long-range order of the flux lattice is destroyed, and there is no sharp melting transition. However, for weak disorder, there will still be solid order out to long distances and pinning will not be too significant. As H approaches H_{c2} pinning becomes more important.[5] The transition width, which is found to be proportional to field, is further evidence for the increasing importance of disorder in high fields. The high-field phase at low temperatures has been conjectured to be an amorphous solid rather than a liquid.[8] The amorphous solid phase may also be responsible for the transition widths. In fact, for samples with normal-state sheet resistances greater than 900 Ω/□, the disorder is sufficiently great to inhibit the growth of a crystalline solid for all temperatures and densities.

In the limit of low normal-state sheet resistance, $R_\square/R_c \ll 1$, the calculated melting temperature with standard dirty-limit expressions is $T_c/T_M=(1+3.8R_\square/A_1R_c)$. $R_c=4.12$ kΩ/□ is a characteristic resistance near which superconductivity vanishes. This result can be compared to the zero-field extrapolation of the measured melting line to give the values of A_1 in Table I. For a KT-type transition, it is estimated[5] that 0.4

$< A_1 < 0.75$. The measured value $A_1 \simeq 0.5$ falls within this range. Because this experiment does not probe the shear modulus, the validity of the KT universal jump criterion $\mu(T_M)a_0^2/k_B T_M = 4\pi$, where a_0 is the lattice constant, cannot be determined.

The remarkable stiffness of the vortex solid is demonstrated by this experiment. Using the ratio of film thickness to that of the oscillator, 10^{-4}, we may estimate the magnitude of the elastic modulus of the vortex solid. At low temperatures, in an 80-kG applied field, the frequency shift on melting is of order 5×10^{-4}. This implies that the elastic modulus of the vortex lattice is nearly 10 times that of silicon at the lowest temperatures. The bulk modulus may be obtained from the total interaction energy of the vortex array,

$$[\Phi_0^2/8\pi^2\Lambda(T)]\int n(r)\ln(r-r')n(r')d^2r\,d^2r'.$$

The integral is cut off either by the finite system size or by $\Lambda(T)$. Either length scale is approximately 1 cm. Since the density is given by $n = H/\Phi_0$, this gives the observed H^2 dependence. The estimated modulus is 100 kbar for a lattice constant of 50 nm ($H = 20$ kG) which is similar to bulk silicon and in rough agreement with experiment.

In conclusion, we have used a novel high-Q mechanical-oscillator technique to study flux-lattice melting in amorphous In/InO_x thin-film superconductors. The phase diagram has been explored for a variety of normal-state resistances. A theory based on KT melting can qualitatively describe the data, but differs in its quantitative features. The theory contains one parameter which may be used to fit the zero-field extrapolation of the melting temperature for the different normal-state sheet resistances. However, the theory predicts a melting temperature independent of magnetic field. Our result, the melting temperature being reduced linearly with field, may be due to either the required H/H_{c2} corrections[8] to the theory or the increasing role of pinning at high fields. The observed bulk modulus of the vortex solid exceeds that of bulk silicon below 0.1 K in 80 kG fields, which can be understood in terms of the long-range interactions between vortices.

We would especially like to thank D. S. Fisher for numerous discussions and continuing interest in this experiment. We would also like to thank A. Millis for many helpful discussions and R. H. Eick for technical assistance.

[1]A. A. Abrikosov, Zh. Eksp. Teor. Fiz. **32**, 1442 (1957) [Sov. Phys. JETP **5**, 1174 (1957)].

[2]H. Trauble and U. Essman, J. Appl. Phys. **25**, 273 (1968).

[3]D. Cribier, B. Jacrot, L. M. Rao, and B. Farnoux, Phys. Lett. **9**, 106 (1964).

[4]E. Conen and A. Schmid, J. Low Temp. Phys. **17**, 331 (1974); A. L. Fetter and P. C. Hohenberg, Phys. Rev. **159**, 330 (1967).

[5]D. S. Fisher, Phys. Rev. B **22**, 1190 (1980).

[6]B. A. Huberman and S. Doniach, Phys. Rev. Lett. **43**, 950 (1979).

[7]A. T. Fiory and A. F. Hebard, Phys. Rev. B **25**, 2073 (1982).

[8]D. S. Fisher, private communication.

[9]R. N. Kleiman, G. K. Kaminsky, J. D. Reppy, R. Pindak, and D. J. Bishop, Rev. Sci. Instrum. **56**, 2088 (1985).

[10]A. F. Hebard and S. Nakahara, Appl. Phys. Lett. **41**, 1130 (1982).

[11]M. A. Paalanen and A. F. Hebard, Appl. Phys. Lett. **45**, 794 (1984).

[12]A. F. Hebard and M. A. Paalanen, Phys. Rev. Lett. **54**, 2155 (1985).

[13]Y. B. Kim and M. J. Stephen, in *Superconductivity*, edited by R. D. Parks (Dekker, New York, 1969), Vol. 2, pp. 1107–1167.

[14]D. J. Bishop and J. D. Reppy, Phys. Rev. Lett. **40**, 1727 (1978), and Phys. Rev. B **22**, 5171 (1980).

[15]P. H. Kes and C. C. Tsui, Phys. Rev. B **28**, 5126 (1983).

Evidence from Mechanical Measurements for Flux-Lattice Melting in Single-Crystal $YBa_2Cu_3O_7$ and $Bi_{2.2}Sr_2Ca_{0.8}Cu_2O_8$

P. L. Gammel, L. F. Schneemeyer, J. V. Waszczak, and D. J. Bishop
AT&T Bell Laboratories, Murray Hill, New Jersey 07974
(Received 8 July 1988)

We have studied flux-lattice melting in single crystals of $YBa_2Cu_3O_7$ and $Bi_{2.2}Sr_2Ca_{0.8}Cu_2O_8$ using a high-Q mechanical oscillator. In $YBa_2Cu_3O_7$ with an applied magnetic field $\mathbf{H}\perp\hat{\mathbf{c}}$, flux-lattice melting occurs at H_{c2} as in a conventional three-dimensional superconductor. However, for $\mathbf{H}\|\hat{\mathbf{c}}$ flux-lattice melting occurs 3.2 K *below* H_{c2}. We believe that this is evidence for a transition into a vortex-liquid state similar to that seen in two-dimensional superconducting films. For $Bi_{2.2}Sr_2Ca_{0.8}Cu_2O_8$ the effect is even more pronounced; with a bulk superconducting transition of 75 K, the flux-lattice melting in this material occurs in both orientations near 30 K.

PACS numbers: 74.60.Ge

The potential for applications of the high-T_c superconductors has produced an unprecedented amount of effort towards the understanding of their physical properties. Many of these applications will require high critical currents which will, in turn, make detailed knowledge of the microscopics of the superconducting flux lattice of importance. To obtain high critical currents, the formation of a flux lattice is crucial because the finite shear modulus of the lattice allows a relatively small number of pinning centers to pin all of the flux lines. A number of authors[1-4] have pointed out that there exist good reasons why the flux lattices in these materials might be unconventional. In this paper we report on mechanical measurements of flux-lattice melting in single crystals of $YBa_2Cu_3O_7$ (YBCO) and $Bi_{2.2}Sr_2Ca_{0.8}Cu_2O_8$ (BSCCO). We find that in these materials there is indeed unconventional behavior in the flux lattice. We find a general tendency for the flux lattice to melt well below H_{c2} into a vortex-liquid state similar to that seen in two dimensions.[5] We suggest that a Lindeman criteria for melting might qualitatively explain our results.

In conventional, three-dimensional superconductors the flux lattice is most often a triangular lattice with long-range positional order. In a finite magnetic field approaching $T_c(H)$, the flux lattice melts at T_c because the coherence length $\xi(T)$ diverges and the vortices cease to be well defined objects. Generally, in three dimensions, the lattice is stable and uninteresting over the entire superconducting phase diagram.

However, in two dimensions things can become more interesting.[6] The increased importance of thermal fluctuations in two dimensions produces a flux lattice without long-range positional order which can melt well *below* $T_c(H)$ into a vortex-liquid state. The suppression of the melting temperature T_M from the superconducting transition temperature depends strongly on the normal-state resistance of the film.[6] In the dirty limit, $T_c/T_M = 1+3.8R_\square/A_1R_c$ with $R_c = 4.12$ kΩ and $A_1 = 0.5$. Thus, the observation of a vortex-liquid state strongly suggests that the flux lattice is two dimensional in character.

There are also other possibilities for nonconventional behavior in the flux lattices in these materials. Nelson[7] has pointed out that at the high transition temperatures and for the small coherence lengths in these systems in the Lindeman criterion for melting can become relevant. In addition, even more complicated states can exist such as the vortex entanglement state suggested by Nelson.[2] Finally, if the superconducting state is anisotropic, symmetries of the flux lattice other than triangular can exist.[8,9] However, decoration experiments using the high-resolution Bitter pattern technique appear to rule this out.[3]

In this paper we report mechanical measurements of flux-lattice melting in YBCO and BSCCO and show that their phase diagrams are indeed nonconventional. The experimental setup used is shown in Fig. 1. The basis for the experiment is the high-Q silicon oscillator technique

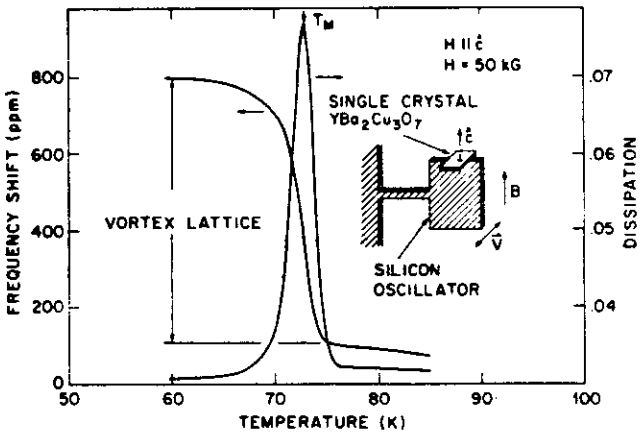

FIG. 1. The frequency and dissipation of the silicon oscillator as a function of temperature. The vortex mobility transition occurs at the peak in the attenuation, T_M. Below T_M, the vortex lattice is pinned and contributes to the elastic response. Inset: the geometry of the experiment. The oscillator was rotated in the plane of this drawing for other field orientations.

developed by Kleiman *et al.*[10] The oscillators were fabricated from *p*-type (110) silicon wafers 0.010 in. thick and patterned by means of photolithography and anisotropic etching. The silicon was coated with 100 nm of gold on both sides, which was used as part of a capacitive drive and detection scheme. The simplest beam-bending mode of the oscillator was used as indicated by the V in the drawing. The motion was driven self resonantly with use of a phase-locked loop. The structure had a Q of 10^5, a frequency of 2 kHz, and a frequency stability of 10^{-7} at 100 K. To avoid nonlinear effects, the amplitude at the end of the oscillator was kept well below 100 nm. This low amplitude represents an important difference between the oscillator technique and other similar measurements, particularly flux flow. In flux flow, there is no measurable signal until the flux lines have moved a macroscopic distance which then destroys the flux lattice that one wishes to observe. We typically dissipate 10^{-18} W in our measurement and can see effects of motionally induced melting at 10^{-16} W.

The superconducting crystal was epoxied to the silicon as shown. The single-crystal samples were grown as described elsewhere.[11] The YBCO crystals have a T_c of 87 K as measured by the Meissner effect, with a width of 3 K. The crystals contained many twins, usually in the form of long domains. The crystals were square flat platelets ~ 1 mm across and 0.1 mm thick, with the $\hat{c}$ axis perpendicular to the plane of the plates. While the upper critical filed, H_{c2}, was not measured on the crystals used, they are from batches from which several crystals were measured and found to give results similar to those reported by Worthington, Gallagher, and Dinger.[12]

The result of a typical measurement at fixed field as a function of temperature is shown in Fig. 1. Both the real and imaginary parts of the oscillator response are shown. Below the melting temperature, the bulk modulus of the vortex lattice contributes an additional stiffness to the oscillator. As the lattice melts, the response softens. This is accompanied by a peak in the dissipation. We define T_M, the melting temperature, as the location of the dissipation peak.

This identification can be justified as follows: For $T \ll T_M$ there is a well defined flux lattice which will remain pinned even in the presence of weak disorder. This will make the relaxation rate for compression of the flux lattice, τ, very long so that $\omega\tau \gg 1$ and the vortices will move with the underlying crystal. Thus, an elastic modulus appropriate to longitudinal sound in the vortex lattice will be added to the elastic response of the oscillator. For $T \gg T_M$, thermal fluctuations will dominate the motion of the vortices. In this limit the vortex liquid will rapidly relax ($\omega\tau \ll 1$) and the vortices will not contribute to the oscillator response. Near the melting temperature, T_M, the relaxation rate will be strongly temperature dependent. A peak in the dissipation will occur at $\omega\tau \sim 1$ which is our experimentally defined melting temperature. This identification is strengthened by comparison with similar measurements on a wide variety of other superconducting systems in which flux-lattice melting occurs at $T_c(H)$ with features identical to those shown here. This feature is *not* what is seen near flux-flow peaks[5] or depinning transitions.

Shown in Fig. 2 are these melting temperatures for YBCO as a function of magnetic field for $\mathbf{H} \perp \hat{c}$ and $\mathbf{H} \parallel \hat{c}$. For $\mathbf{H} \perp \hat{c}$, melting occurs at H_{c2} as in conventional three-dimensional superconductors. The critical-field slope defined by T_M agrees well with that measured at AT&T-Bell Laboratories and elsewhere,[12] and T_M extrapolates to $T_c(H=0)$. However, for $\mathbf{H} \parallel \hat{c}$ the flux-lattice melting line is suppressed *below* H_{c2} by ~ 3.6 K and it does *not* extrapolate to $T_c(H=0)$. In Fig. 2, H_{c2} for $\mathbf{H} \parallel \hat{c}$ is shown by the dashed line. We conclude that for this orientation the flux lattice melts into a vortex liquid before superconductivity is destroyed. This result is very similar to what is seen in two dimensions where flux-lattice melting can occur well below $T_c(H)$.[5] We suggest that the two-dimensional character of the system might be important for this behavior of the flux lattice. In this system the coherence length[12] is roughly equal to the spacing between the two-dimensional copper-oxygen planes and we suggest that the system could be in a crossover regime from a 3D system to a stack of decoupled 2D systems. Our experimental observations are consistent with our earlier flux-lattice decoration experiments[3] where at low temperatures and for $\mathbf{H} \perp \hat{c}$ we find only short-range (~ 1.5 lattice constants) positional order of the flux lines and at 77 K the images are consistent with a vortex-liquid state (i.e., no distinct, stable patterns of flux lines). We believe that the mechanical

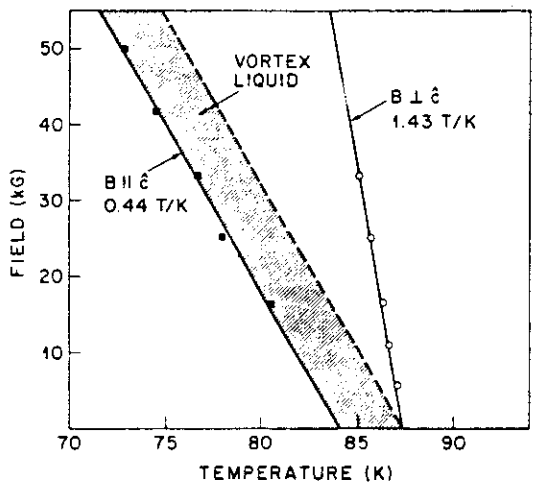

FIG. 2. The phase diagram for flux-lattice melting in YBCO. For $\mathbf{B} \perp \hat{c}$, the vortex mobility transition occurs at H_{c2}, as in three-dimensional superconductors. For $\mathbf{B} \parallel \hat{c}$, the vortex mobility transition occurs 3 K below H_{c2} (indicated by the dashed line). The shaded region is the vortex fluid.

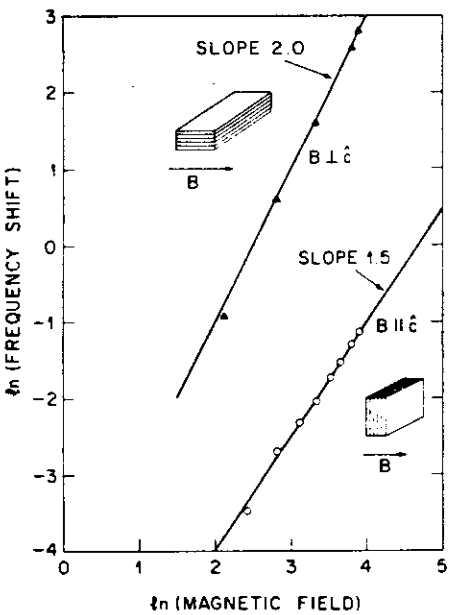

FIG. 3. The magnitude of the frequency shift for $\mathbf{H}\parallel\hat{\mathbf{c}}$ and $\mathbf{H}\perp\hat{\mathbf{c}}$ as a function of applied field.

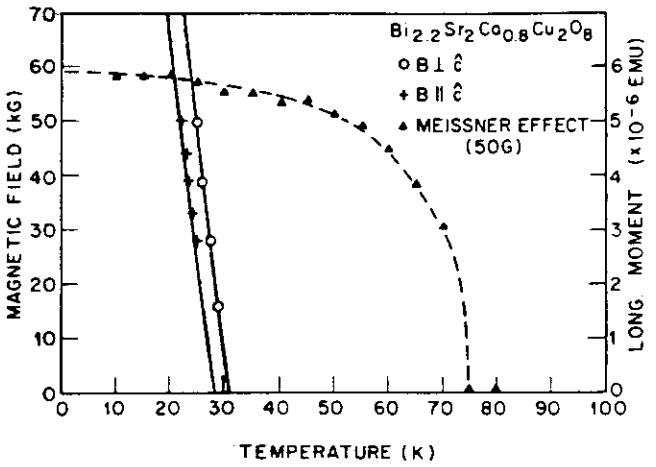

FIG. 4. The Meissner signal and the melting temperatures for single-crystal BSCCO for both field orientations.

measurements, in conjunction with the decoration experiments, provide evidence for melting and not merely flux line depinning.

Shown in Fig. 3 are the values of the frequency shift as a function of magnetic field for YBCO. We find that for $\mathbf{H}\perp\hat{\mathbf{c}}$ the response is significantly stiffer than for $\mathbf{H}\parallel\hat{\mathbf{c}}$ and that it varies as H^2. For $\mathbf{H}\parallel\hat{\mathbf{c}}$, we find that the resonse is soft and varies as $H^{1.5}$. For a conventional superconductor, the real response can be obtained from the total field energy and is proportional to H^2. For $\mathbf{H}\perp\hat{\mathbf{c}}$ we find this behavior. However, the weaker dependence for $\mathbf{H}\parallel\hat{\mathbf{c}}$ and the smaller magnitude suggests a much more disordered lattice with shorter-range order and weaker pinning consistent with the flux-lattice decoration images.[3]

We will now discuss BSCCO in which the coherence length is 4 times smaller[13] than the interplanar spacing and the effect on the melting temperatures is even more pronounced. Flux-lattice decoration experiments[14] in BSCCO at 4.2 K show similar patterns to those in YBCO. The flux quantum is $hc/2e$ and there is only short-range hexagonal order as was seen in YBCO. The mechanical measurements show an identical feature at the melting transition as was shown for YBCO. However, the transition temperature is much lower.

Shown in Fig. 4 is the phase diagram for flux-lattice melting in BSCCO. Also plotted is the Meissner signal for the same sample. Note that while bulk superconductivity sets in at 75 K the flux-lattice melting temperature is -30 K for both field orientations with $T_M(\mathbf{H}\parallel\hat{\mathbf{c}}) \leq T_M(\mathbf{H}\perp\hat{\mathbf{c}})$. This strong reduction in the melting temperature for a material with a coherence length much shorter than the interplanar spacing suggests that this might be the relevant parameter in determining whether the flux-lattice melting is described by two- or three-dimensional physics. This conclusion has severe implications for potential applications. If, as is widely believed, the high transition temperatures are related to the two-dimensional character of the planes, then, as the interplanar coupling decreases, the flux-lattice melting temperature will go down making many applications impossible for very high-temperature superconductors. The similarity of the response for both field orientations is quite surprising given the strong anisotropy of the system. Varma[15] recently has made arguments based on entropy considerations in which the transition for $\mathbf{H}\parallel\hat{\mathbf{c}}$ is from two to three dimensions and for $\mathbf{H}\perp\hat{\mathbf{c}}$ from one to three dimensions with the expectation that the transition temperatures should be similar. Clearly this surprising result needs to be better understood.

There are other experiments which also suggest that the flux lattices can melt well below T_c. In ceramic samples of YBCO, the critical currents[16] have been found to be extremely low within 2 K of T_c. In BSCCO in finite magnetic fields, it has been found that J_c drops abruptly[17] at ~ 30 K. In YBCO, SQUID noise is found to diverge below T_c.[18] We conclude that these observations are the result of the flux-lattice melting behavior that we have observed in the oscillator experiments and are consistent with our results. For example, we predict that flux noise will be much less for devices in which $\mathbf{H}\perp\hat{\mathbf{c}}$ in comparison with those for $\mathbf{H}\parallel\hat{\mathbf{c}}$ as is standard at the moment. Therefore, superconducting devices should be made from films with the $\hat{\mathbf{c}}$ axis in the plane.

At the moment it is difficult to give an unambiguous theoretical interpretation to our results. The vortex entanglement theory of Nelson[2] predicts new phases which are primarily low-field phases (near H_{c1}). It is unclear whether such phases could exist in the high-field regime where we see our transitions. The Kosterlitz-Thouless

vortex unbinding theory is appealing.[6] However, the large suppression for $\mathbf{H} \perp \hat{\mathbf{c}}$ in BSCCO is hard to reconcile with this idea. The final possibility is simply that the small coherence lengths and high transition temperatures make thermal-fluctuation or Lindeman-induced melting much more likely.

We are currently studying larger samples at low fields to search for any additional low-field phases as suggested by Nelson. Neutron-scattering studies of flux-lattice melting would be most interesting as it would provide real structural information about these phases. A limitation of our technique is that we can only identify transitions between flux-lattice phases and obtain very little information about the structures of the phases themselves.

Finally, we note that in very recent measurements[19] on single-crystal thallium compounds with a T_c of 110 K that melting occurs at approximately 40 K, strengthening our surmise that this is a general feature of these compounds.

In conclusion, we have studied flux-lattice melting in single-crystal YBCO and BSCCO. Unlike in conventional three-dimensional superconductors which melt at T_c, these materials show flux-lattice melting well below $T_c(H)$. We argue that this is a general feature of these materials with severe implications for potential applications. At the moment we have no clear theoretical understanding of the phenomena, although some type of fluctuation-induced melting transition enhanced because of the short coherence lengths seems possible.

We would like to thank D. Nelson, C. M. Varma, B. Batlogg, B. van Dover, D. S. Fisher, W. F. Brinkman, B. I. Halperin, and A. P. Ramirez for numerous helpful discussions.

[1]M. Rice, Z. Phys. B **67**, 141 (1987), and references therein.

[2]D. R. Nelson, Phys. Rev. Lett. **60**, 1973 (1988), and references therein.

[3]P. L. Gammel, D. J. Bishop, G. J. Dolan, J. R. Kwo, C. A. Murray, L. F. Schneemeyer, and J. V. Waszczak, Phys. Rev. Lett. **59**, 2592 (1987).

[4]M. Tinkham, Helv. Phys. Acta (to be published).

[5]P. L. Gammel, A. F. Hebard, and D. J. Bishop, Phys. Rev. Lett. **60**, 144 (1988).

[6]D. S. Fisher, Phys. Rev. B **22**, 1190 (1980).

[7]D. R. Nelson, private communication.

[8]R. N. Kleiman, P. L. Gammel, E. Bucher, and D. J. Bishop, to be published.

[9]L. Gor'kov, to be published.

[10]R. N. Kleiman, G. K. Kaminsky, J. D. Reppy, R. Pindak, and D. J. Bishop, Rev. Sci. Instrum. **50**, 2088 (1985).

[11]L. F. Schneemeyer, J. V. Waszczak, T. Siegrist, R. B. van Dover, L. W. Rupp, B. Batlogg, R. J. Cava, and D. W. Murphy, Nature (London) **328**, 601 (1987); L. F. Schneemeyer, R. B. van Dover, S. H. Glarum, S. A. Sunshine, R. M. Fleming, B. Batlogg, T. Siegrist, J. H. Marshall, J. V. Waszczak, and L. W. Rupp, Nature (London) **332**, 423 (1988).

[12]T. K. Worthington, W. J. Gallagher, and T. R. Dinger, Phys. Rev. Lett. **59**, 1160 (1987).

[13]T. T. M. Palstra, B. Batlogg, L. F. Schneemeyer, and R. J. Cava, to be published.

[14]P. L. Gammel, L. F. Schneemeyer, J. V. Waszczak, and D. J. Bishop, to be published.

[15]C. M. Varma, private communication.

[16]M. A. Dubson, S. T. Herbert, J. J. Calabrese, D. C. Harris, B. R. Patton, and J. C. Garland, Phys. Rev. Lett. **60**, 1061 (1988).

[17]B. van Dover, L. F. Schneemeyer, E. M. Gyorgy, and J. V. Waszczak, to be published.

[18]J. C. Clarke, private communication.

[19]P. L. Gammel, D. J. Bishop, D. Ginley, and J. Schirber, to be published.

Comment on "Evidence from Mechanical Measurements for Flux-Lattice Melting in Single-Crystal $YBa_2Cu_3O_7$ and $Bi_{2.2}Sr_2Ca_{0.8}Cu_2O_8$"

In a recent Letter Gammel *et al.*[1] reported on nice measurements of frequency and dissipation of oscillating superconductors and concluded from these data the melting of the flux-line lattice (FLL) at a certain temperature. We argue about this conclusion.

First, if the magnetic field **B** and motion **V** were as depicted in Fig. 1 of Ref. 1 then there should be *no effect at all*: A superconductor moving without rotation in a homogeneous field B does not feel any force nor torque by this field. Thus, the curves called $\mathbf{B}\|\hat{\mathbf{c}}$ in Ref. 1 should not be taken seriously. They reflect a spurious effect which might be due to a small misalignment or inhomogeneity of **B** but, more likely, is caused by a *torsional vibration* coupled to the linear vibration due to the off-axis epoxied sample. The resulting sample rotation, not mentioned in Ref. 1, periodically tilts the slightly pinned flux lines relative to **B** and has a similar effect as in the case $\mathbf{B}\perp\hat{\mathbf{c}}$ explained in the next point. Therefore, the difference between the effects for $\mathbf{B}\|\hat{\mathbf{c}}$ and $\mathbf{B}\perp\hat{\mathbf{c}}$ *does not reflect crystal anisotropy but just the different geometries.*

Second, if the field is rotated, case $\mathbf{B}\perp\hat{\mathbf{c}}$, a magnetic restoring force originates from the *tilt* (not motion) of the flux lines with respect to **B** when these are pinned to a periodically rotating material. This nontrivial effect was studied in amorphous[2] and ceramic[3] reeds. The resulting frequency enhancement is caused by two effects: (a) the tilt modulus of the FLL,[4] $c_{44}\approx B^2/\mu_0$ (this is a *volume* effect) and (b) the partial expulsion of field changes which are so small that they cannot unpin all flux lines (this differential Meissner effect depends on the sample *shape* and field orientation). For thin vibrating reeds it causes large enhancements of frequency and damping in *longitudinal* field,[2] but only weak (second order) effects in *transversal* fields. The geometries in Ref. 1 are difficult to treat quantitatively. In any case, the changes of frequency and damping *do not reflect the bulk modulus* of the FLL[4] ($c_{11}-c_{66}\approx B^2/\mu_0$) which, by the way, is nearly the same in a flux-line lattice and liquid. These changes might depend on the *shear modulus* of the FLL[4] ($c_{66}\ll c_{11}$) via the collective pinning strength which increases with decreasing c_{66}.[4]

Third, the peak observed in the attenuation near B_{c2} very likely does not reflect FLL melting but has the same origin as the peak observed near B_{c2} in superconducting vibrating reeds.[2,5] There, motion of the flux lines relative to the twin boundaries or other pins causes *hysteretic damping* due to elastic instabilities ("plucking" of flux lines). This damping mechanism exists even at extremely small vibrational amplitudes though, in principle, the viscous damping of moving flux lines should dominate at still smaller amplitudes. It would be helpful to measure the amplitude dependence before one dares a new interpretation.

Fourth, while two-dimensional FLL's are indeed interesting *dynamically*, three-dimensional FLL's are not uninteresting as claimed in Ref. 1. In fact, even *statically* these appear to be always entangled (contain screw dislocations[4]). This is suggested by an abrupt jump (by factors of 8 to 80) observed in the critical current of weak-pinning films when B is increased to a critical value B_{c0}.[6] This jump reflects a sharp transition from two- to three-dimensional pinning, i.e., from order to disorder along the flux lines, and occurs even at $T=0$. This transition should also occur in weak-pinning ceramics with sufficiently short flux lines.

E. H. Brandt,[(1)] P. Esquinazi,[(2)] and G. Weiss[(3)]
[(1)]Max-Planck Institut für Metallforschung
Institut für Physik
D-7000 Stuttgart 80, Federal Republic of Germany
[(2)]Physikalisches Institut
Universität Bayreuth
D-8580 Bayreuth, Federal Republic of Germany
[(3)]Institut für Angewandte Physik II
Universität Heidelberg
D-6900 Heidelberg, Federal Republic of Germany

Received 31 October 1988
PACS numbers: 74.60.Ge

[1]P. L. Gammel, L. F. Schneemeyer, J. V. Waszczak, and D. J. Bishop, Phys. Rev. Lett. **61**, 1666 (1988).

[2]E. H. Brandt, P. Esquinazi, H. Neckel, and G. Weiss, Phys. Rev. Lett. **56**, 89 (1986); J. Low Temp. Phys. **63**, 187 (1986); E. H. Brandt, J. Phys. (Paris), Colloq. **48**, C8-31 (1987).

[3]C. Duran, P. Esquinazi, J. Luzuriaga, and E. H. Brandt, Phys. Lett. A **123**, 485 (1987); P. Esquinazi and C. Duran, Physica (Amsterdam) **153-155C**, 1499 (1988).

[4]E. H. Brandt and U. Essmann, Phys. Status Solidi (b) **144**, 13 (1987); E. H. Brandt, Phys. Rev. B **34**, 6514 (1986).

[5]P. Esquinazi, H. Neckel, G. Weiss, and E. H. Brandt, J. Low Temp. Phys. **64**, 1 (1987); P. Esquinazi and E. H. Brandt, Jpn. J. Appl. Phys. **26**, 1513 (1987).

[6]R. Wördenweber and P. H. Kes, Phys. Rev. B **34**, 494 (1986); E. H. Brandt, Phys. Rev. Lett. **57**, 1347 (1986).

Kleiman *et al.* Reply: In our technique[1] the sample is affixed to a high-Q mechanical oscillator. The oscillator is vibrated in its resonant mode, but as opposed to previous measurements[2] with our technique the sample itself is *not* stressed. The increased stiffness and dissipation are due only to the tilting of the sample with respect to the magnetic field, which is easily understood and calculable. In the strong pinning limit the increased stiffness in a magnetic field is due to an effective magnetization of the sample resulting from flux pinning on the time scale of the measurement. Dissipation arises from the motion of the flux lines relative to the crystal via the Stephen-Bardeen[3] mechanism, as the flux lines depin. Because of the small samples and low residual damping of the oscillator it is possible to maintain very low amplitudes and dissipation levels, which we have demonstrated are essential for studying intrinsic properties of the samples such as flux-lattice melting.

Brandt, Esquinazi, and Weiss[4] correctly point out that Fig. 1 of our Letter is misleading. While the bulk of the motion associated with the cantilever mode which we employ is a translation with respect to the field which does not couple to the flux lattice, it also includes a contribution from rotation with respect to the field, which does give a coupling to the flux lattice. This coupling is intentionally kept small to reduce the damping of the oscillator by keeping the axis of rotation parallel to the field to within $\sim 1°$. Nonetheless, it is the relative orientation of $\mathbf{H}$ and the $\hat{\mathbf{c}}$ axis of the *sample* that will determine the properties of the sample if they are anisotropic. This is independent of the geometry of the *oscillator* with respect to the field.

Brandt, Esquinazi, and Weiss have suggested that the dissipation we observe is due to hysteretic damping as was seen in previous experiments on superconducting vibrating reeds. This would suggest a strongly amplitude-dependent damping. In our measurements the linearity of the response has been verified, and good agreement with Stephen-Bardeen-type viscosities is found. They also suggest that our effect is similar to the flux-pinning peak previously seen near H_{c2} in weak-pinning materials. We point out that in our measurements on $Bi_{2.2}Sr_2Ca_{0.8}Cu_2O_8$ (BSCCO) the observed transition occurs at roughly 0.2% of H_{c2}.

As we stated in our paper we feel that our results can be interpreted as indirect evidence for flux-lattice melting via the following mechanism. The torque from rotation of the sample in a magnetic field is $\mathbf{M}\times\mathbf{H}$. If the flux lattice is a solid, the relaxation time of the magnetization is much longer than the period of the oscillator and the torque due to the sample magnetization is added to the restoring force of the oscillator. However, as the lattice melts, the relaxation time becomes much shorter than the oscillator period and the response softens. The dissipation peak occurs at $\omega\tau = 1$, which we identify as the melting temperature. While the interesting question of the frequency dependence is not addressed by this measurement, it was on the basis of this model and our observations that we conjectured that the flux lattice was melting well below T_c.

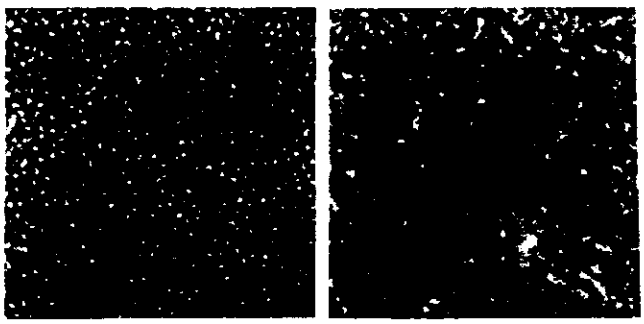

FIG. 1. Simultaneous flux-lattice decorations of YBCO (left) and BSCCO (right) at 15 K in a field of 20 G. In contradistinction to YBCO, the flux lines in BSCCO move significantly during the decoration time (~ 1 sec) providing convincing visual evidence that the flux lattice in BSCCO is melted into a liquid significantly below T_c.

To verify this interpretation of our mechanical measurements we have carried out a series of flux-lattice decorations[5] at different temperatures. Shown in Fig. 1 are decorations at 15 K for both $YBa_2Cu_3O_7$ (YBCO) and BSCCO in an applied field of 20 G. The decoration takes place over approximately 1 sec as the magnetic particles strike the surface. The YBCO which, at 15 K, is well below the melting temperature shows stable, discrete flux lines as do both YBCO and BSCCO at 4.2 K. However, at 15 K the flux lines for the BSCCO are blurred and show evidence of motion during the decoration. As 15 K is approaching the melting temperature, we feel that this is convincing visual evidence that the flux lattice is indeed melting well below T_c in BSCCO as we had concluded from our mechanical measurements.

R. N. Kleiman, P. L. Gammel, L. F. Schneemeyer, J. V. Waszczak, and D. J. Bishop
AT&T Bell Laboratories
Murray Hill, New Jersey 07974

Received 4 January 1989
PACS numbers: 74.60.Ge

[1]P. L. Gammel *et al.*, Phys. Rev. Lett. **61**, 1666 (1988).
[2]P. Esquinazi, H. Neckel, G. Weiss, and E. H. Brandt, J. Low Temp. Phys. **64**, 1 (1986).
[3]M. J. Stephen and J. Bardeen, Phys. Rev. Lett. **14**, 112 (1965).
[4]E. H. Brandt, P. Esquinazi, and G. Weiss, preceding Comment, Phys. Rev. Lett. **62**, 2330 (1989).
[5]P. L. Gammel *et al.*, Phys. Rev. Lett. **59**, 2592 (1987).

Mechanical Measurements of the Flux Lattice in the Heavy-Fermion Superconductor UPt_3

R. N. Kleiman, P. L. Gammel, E. Bücher, and D. J. Bishop
AT&T Bell Laboratories, Murray Hill, New Jersey 07974
(Received 28 September 1987)

We report mechanical measurements of the flux lattice in UPt_3. In the superconducting state the flux lattice that is formed in the sample when a magnetic field is applied contributes a restoring force and a dissipation term to a high-Q mechanical oscillator, when the oscillator and sample are tilted with respect to the static magnetic field. In addition to the characteristic response for a type-II superconductor that gives $H_{c2}(T)$, we observe an unexpected dissipation peak along two lines in the (H,T) plane within the superconducting state. The evidence suggests transitions between three different superconducting phases, and hence a complex phase diagram for UPt_3 is proposed.

PACS numbers: 74.60.Ge, 74.70.Tx

Soon after the discovery of the heavy-fermion superconductors, it was recognized that they represent a new class of materials in which the pairing mechanism for superconductivity may not be of the conventional phonon-mediated, singlet BCS type.[1] Considerable subsequent work suggest that these materials are likely to be superconductors with anisotropic higher-angular-momentum pairing states.[2] For example, in UPt_3 the pairing is thought to be d wave.[3] With higher-angular-momentum pairing, the possibility exists of transitions between different superconducting states, as in superfluid ^{3}He. Furthermore, the anisotropic nature of the superconducting state in these materials suggests that the flux lattice formed when a magnetic field between H_{c1} and H_{c2} is applied will have a complex character. The symmetry of the flux lattice can depend in a complex way on the density of the flux lines (i.e., the applied magnetic field) and the underlying symmetry of the order parameter. The cores of the flux lines themselves can, in general, be anisotropic depending on the orientation of the magnetic field with respect to the order parameter, which we presume to be pinned to the crystalline axes in the hexagonal UPt_3. For example, in ^{3}He, which is the only known anisotropic superfluid state, transitions between phases with singly and doubly quantized vortices, symmetric and asymmetric, core structures, and singular and nonsingular core structures have been considered theoretically[4] and investigated experimentally.[5] The observation of analogous transitions between different superconducting states or textures would be certain evidence of higher-angular-momentum pairing in the heavy-fermion superconductors.

In this paper we present results on the flux lattice in UPt_3 using a novel high-Q mechanical oscillator technique.[6,7] We observe dissipation peaks indicative of a complex phase diagram with three distinct superconducting phases in the (H,T) plane. Our work complements that of Müller *et al.*[8] and Qian *et al.*[9] who observe an attenuation peak in high-frequency ultrasound measurements of UPt_3 along the higher-field phase line reported in this paper. In addition, we observe a feature above $H_{c2}(T)$ which we believe is due to flux penetration into the superconducting sheath, at the higher field of $H_{c3}(T)$. We find that $H_{c3} \approx 1.7H_{c2}$ in agreement with the standard theory of Saint-James and de Gennes[10] developed for isotropic superconductors.

In our apparatus a large single crystal of UPt_3 ($\sim$0.5 cm^3) is affixed to a high-Q BeCu mechanical oscillator, as shown schematically in the inset to Fig. 3. The $\hat{c}$ axis of the crystal, the applied magnetic field **H**, and the rotational axis of the oscillator are all parallel to within $-2°$. ac susceptibility coils placed around the sample allow us to independently measure T_c. The resonant frequency ($\sim$600 Hz) and dissipation of the oscillator are measured in the experiment. In a type-II superconductor, the applied magnetic field produces a flux lattice in the sample for $T < T_c$ and $H_{c1} < H < H_{c2}$. The force and dissipation associated with tilting the crystal with respect to the static magnetic field are reflected as small changes in the oscillator response. The oscillator has a Q of $\sim 10^6$ with a frequency resolution of 1 part in 10^8. This gives high sensitivity to the small changes in mechanical damping and restoring force due to the presence of the flux lattice. Changes in the damping and restoring force of the oscillator signify the transitions at H_{c1}, H_{c2}, and H_{c3} and between the three superconducting phases. It is the superconducting phase diagram of UPt_3 which is the subject of this paper. A more detailed discussion of the mechanical oscillator technique for the study of type-II superconductors can be found in Ref. 7.

The additional restoring force on the crystal in the presence of the applied magnetic field is due to the pinning of the flux lines to the crystal.[11] In the limit of strong pinning, the pinned flux lines give rise to an effective dynamic sample magnetization because the rate of flux penetration through the surface barrier is slow as compared to the oscillator frequency. When operated in the torsional mode, this results in a restoring torque $\tau = MH \sin^2\theta_0 = BH \sin^2\theta_0$ on the oscillator, where θ_0 is the angle between the rotational axis of the oscillator ω

and the applied magnetic field H. If H and ω were perfectly aligned ($\theta_0=0$), there would be no restoring torque, whereas $\theta_0=90°$ gives too large a response for convenient measurements with our apparatus. In our experimental configuration, $\theta_0\sim 2°$ is chosen in order to keep the damping and changes in frequency low, allowing a sensitive high-Q measurement over the whole range of H and T. This choice is also crucial in order to keep the measurement in the low-amplitude limit, i.e., where the amplitude of the flux-line motion (here ~ 10 Å) is small as compared to the lattice constant of the flux lattice. Large amplitudes of flux-line motion are found to mechanically melt the flux lattice that we wish to observe.

The additional dissipation term is due to the relative motion of the unpinned flux lines with respect to the crystal. There is a viscosity associated with the relative motion due to microcurrents which are driven through the normal cores, as calculated by Stephen and Bardeen.[12] We have verified that the oscillator response is linear with drive amplitude; thus we can be sure that the damping is viscous and not in a hysteretic regime at the amplitude of operation. In the strong-pinning limit, which holds well at low fields and temperatures, $(\Delta f/f)\propto BH$ and there is no dissipation because all of the flux lines are pinned to the crystal. Near H_{c2} the flux pinning begins to weaken and finally vanishes at H_{c2}. Consequently, the restoring force from the pinned flux lines vanishes at H_{c2}. As the flux lines depin, the free vortices give rise to dissipation since they move relative to the crystal lattice. Just below H_{c2} there is a dissipation peak when the majority of flux lines depin. Above H_{c2} the dissipation is due to the eddy-current damping of the normal metal.

Shown in Fig. 1 are the real and imaginary parts of the oscillator response as a function of applied magnetic field at fixed temperature (upper) and as a function of temperature at fixed magnetic field (lower). Looking first at the lower figure, we see that in the superconducting state there is an additional stiffness (-50 ppm) associated with the flux pinned inside the sample. The damping (Q^{-1}) is low and is due to the residual eddy-current damping of the normal-metal oscillator. As the flux lattice melts at $T_c(H)$, the real part of the response softens, accompanied by a large dissipation peak in the imaginary component. In the normal region ($T>T_c$ ~ 0.53 K) eddy-current damping is large, but the real part of the response vanishes since the magnetic field penetrates uniformly throughout the sample. The dissipation *peak* occurs at H_{c2} as measured by the ac susceptibility. We believe that the shoulder above the peak is due to H_{c3} and will be discussed below. In the upper figure the response as a function of magnetic field at fixed temperature is shown. The real part of the response is quadratic in field as discussed above. However, if one divides out the quadratic field dependence (as done in the upper figure) then the field dependence of the normalized response is qualitatively similar to the temperature dependence of the response shown in the lower figure.

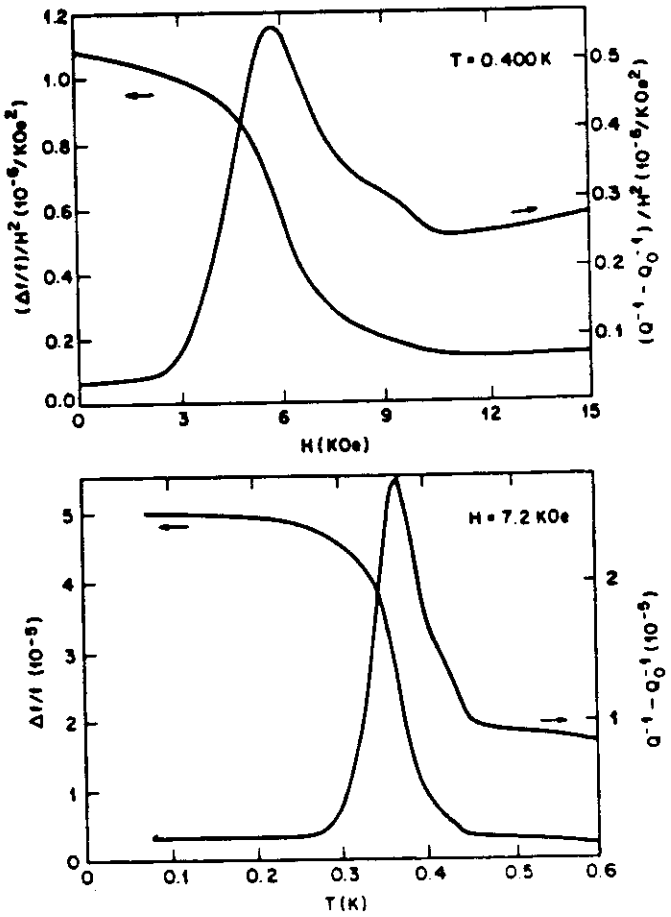

FIG. 1. Top: The normalized frequency shift and dissipation of the oscillator with the UPt_3 sample attached, at fixed temperature ($T=0.400$ K) as a function of magnetic field with $\mathbf{H}\parallel\hat{\mathbf{c}}$. We identify the large peak as H_{c2} and the shoulder as H_{c3}. Bottom: The frequency shift and dissipation at fixed magnetic field ($H=7.2$ kOe) as a function of temperature. The features are the same as in the upper figure.

Shown in Fig. 2 is the normalized dissipation on a more sensitive scale as a function of magnetic field at fields below H_{c2}. At the lowest temperature (0.076 K) we observe two dissipation peaks *below* H_{c2} which we believe indicate transitions between three distinct superconducting phases. Measurements on conventional superconductors show no such additional structure in the superconducting state.[7] The dissipation peaks are small compared to the one observed at H_{c2}, and cannot be seen easily at the scale shown in Fig. 1. No corresponding feature is observed in the real part of the response. As the temperature is increased the peaks move together, and at 0.3 K and 5.5 kOe they meet at a tricritical point. We have checked carefully for hysteresis and all the

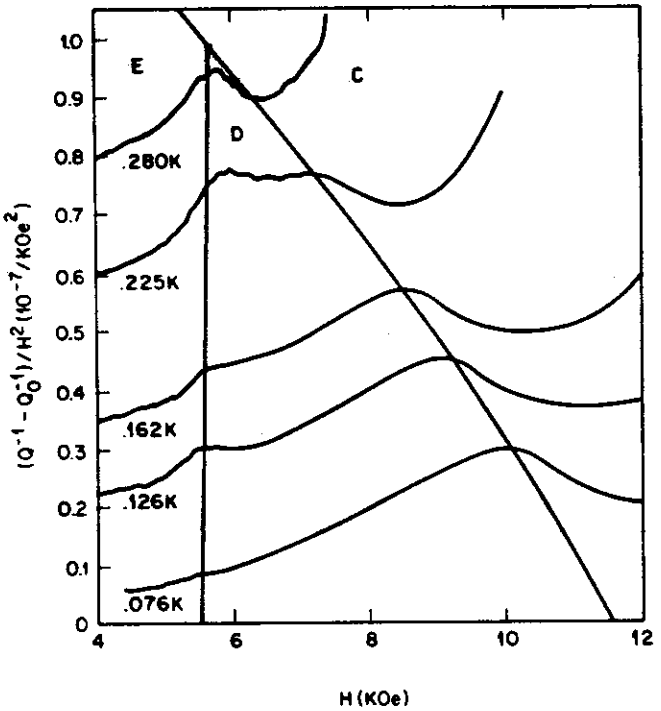

FIG. 2. The normalized dissipation of the oscillator at a series of temperatures as a function of field below H_{c2}, on an expanded scale. The offsets between curves corresponding to different temperatures are arbitrary. The attenuation peaks indicate transitions between three distinct superconducting phases, which meet at a tricritical point (0.3 K and 5.5 kOe). The lines are merely a guide to the eye. It is the peak positions that are plotted in Fig. 3.

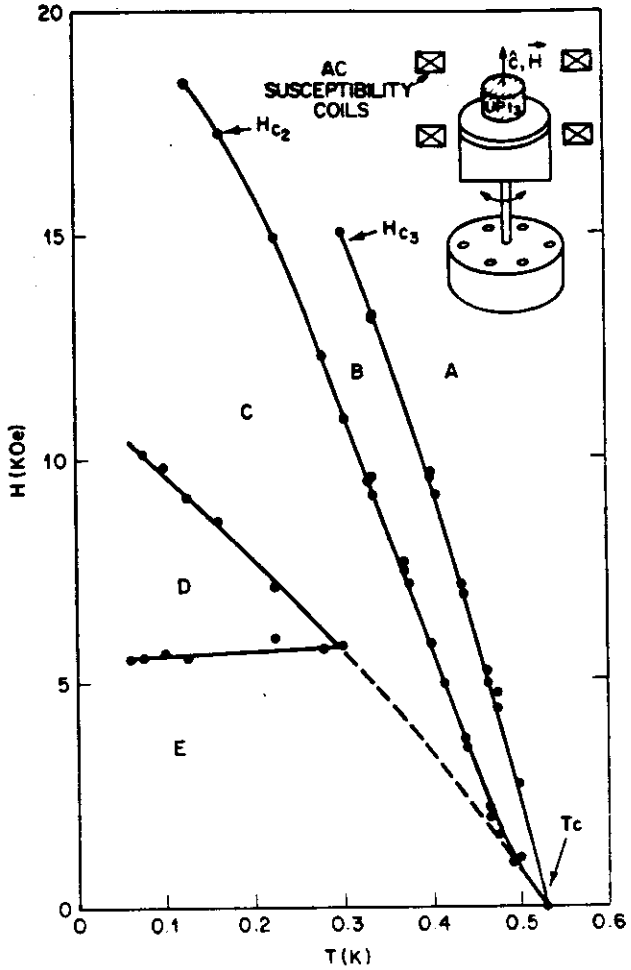

FIG. 3. Proposed phase diagrams for UPt_3. A: normal metal; B: sheath superconductivity; C, D, and E: superconducting states. The dashed line connecting the tricritical point and T_c is suggested to complete the phase diagram. A schematic drawing of the experimental apparatus is shown in the upper right-hand corner.

transitions appear to be second order or only weakly first order. Shown in Fig. 3 is our proposal for the superconducting phase diagram of UPt_3. The dashed line in the phase diagram is based on the assumption that the upper phase line is proportional to $H_{c2}(T)$ and hence meets the H_{c2} line at T_c. It is interesting to note that the change in the character of the transition from the solid line to the dashed line is also observed in the ultrasound measurements.[8]

In our opinion, the three bulk superconducting phases are most likely to be ones with different symmetries of the flux lattice. In an isotropic superconductor with large κ, the flux lattice is triangular[13] at all fields below $H_{c2}(T)$ and temperatures[9] below T_c. However, the difference in free energy between the square and triangular lattices is quite small and the calculation must be done to second order to obtain the proper equilibrium configuration. Since the energy balance is so delicate it is quite likely that in an anisotropic superconducting state the symmetry of the flux lattice will reflect the underlying symmetry of the order parameter. For example, cubic anisotropy is known to stabilize a square flux lattice in low-κ conventional superconductors.[14] Our model is that the observed dissipation peaks correspond to transitions between superconducting phases with flux lattices of different symmetry. The additional dissipation in the neighborhood of the transition arises because of the motion of the flux lines relative to each other and to the crystal lattice, as the flux lattice changes symmetry. The fact that there is no softening of the real part of the response at these transitions, as at $H_{c2}(T)$, confirms the fact that the dissipation peaks observed cannot simply be attributed to monotonic changes in the pinning forces.

Recently, Müller *et al.*[8] and Qian *et al.*,[9] in ultrasound measurements, have also seen evidence for a complex phase diagram in UPt_3. They observe an attenuation peak along one phase line which is similar to that which we find between region C and the combined areas of D and E. The fact that there is no significant frequency dependence to the position of the phase line over six decades of frequency is strong evidence that the dissipation peaks observed in *both* measurements are due to a

true phase transition in the superconducting state and not a simple artifact of flux pinning. However, they find no evidence for a tricritical point. Müller *et al.*[8] find evidence in the susceptibility for a hysteretic phase at low fields within our region E. Their measurements were made with H tilted with respect to the $\hat{c}$ direction by 21°. We find no evidence for such a phase in our experiment with $\mathbf{H} \| \hat{c}$. Clearly, it would be important to investigate the phase diagram of UPt_3 with the magnetic field oriented perpendicular to the $\hat{c}$ direction, in order to compare to theories for different anisotropic superconducting states.

In Fig. 1 there is a shoulder in the real and imaginary parts of the oscillator response above $H_{c2}(T)$ which we believe to be the response due to H_{c3}. In a type-II superconductor, the critical field for the destruction of sheath superconductivity is higher than H_{c2} because of specular reflection of the quasiparticles at the interface.[10] This makes it harder to insert a quantum of flux into a region the size of a coherence length and superconductivity is not destroyed until one reaches a field larger than H_{c2} which is denoted as H_{c3}. The position of the observed feature is plotted in Fig. 3 and tentatively denoted as H_{c3}.

Saint-James and de Gennes[10] have calculated H_{c3} for an isotropic superconducting state and find $H_{c3} = 1.695 H_{c2}$ in good agreement with experiments in conventional superconductors.[15] Our measurements agree well with this value giving $H_{c3} \approx 1.7 H_{c2}$. In general, one would expect this relationship to be modified for an anisotropic state. However, recent measurements suggest that the most likely superconducting gap structure for UPt_3 is one with a line of nodes in the basal plane.[3] This would produce isotropic vortices for the case of the magnetic field parallel to the $\hat{c}$ axis (our case). Seen in that light the agreement with isotropic theory is not surprising. Clearly, measurements with different field orientations will prove interesting as the theory of Saint-James and de Gennes will require modification for anisotropic superconducting states.

In conclusion, we have studied the properties of the flux lattice in UPt_3 using a novel mechanical oscillator technique. We find evidence for a complex phase diagram with three distinct superconducting phases. The phase diagram we propose differs from that derived from the ultrasound measurements in the observation of an additional phase line at intermediate fields. We suggest that the phases which we see represent states with different symmetries of the flux lattice. However, it is also possible that the observed transitions are occurring instead in the cores of the individual flux lines. Clearly, neutron-scattering experiments are called for to elucidate the nature of these phases and their symmetry.

We would like to thank B. Batlogg, C. M. Varma, G. Aeppli, and S. Schmitt-Rink for numerous stimulating discussions.

[1]C. M. Varma, in *Moment Formation in Solids*, edited by W. J. L. Buyers (Plenum, New York, 1984), and Bull. Am. Phys. Soc. **29**, 404 (1984); P. W. Anderson, Phys. Rev. B **30**, 1549 (1984).

[2]D. J. Bishop, C. M. Varma, B. Batlogg, E. Bücher, Z. Fisk, and J. L. Smith, Phys. Rev. Lett. **53**, 1009 (1984); Z. Fisk, H. R. Ott, T. M. Rice, and J. L. Smith, Nature (London) **320**, 124 (1986), and references therein.

[3]K. Miyake, S. Schmitt-Rink, and C. M. Varma, Phys. Rev. B **34**, 6554 (1986); S. Schmitt-Rink, K. Miyake, and C. M. Varma, Phys. Rev. Lett. **57**, 2575 (1986).

[4]A. L. Fetter, in *Progress in Low Temperature Physics*, edited by D. F. Brewer (North-Holland, Amsterdam, 1986), Vol. 10, p. 1.

[5]P. L. Gammel, T.-L. Ho, and J. D. Reppy, Phys. Rev. Lett. **55**, 1708 (1985).

[6]See, for example, R. N. Kleiman, G. K. Kaminsky, J. D. Reppy, R. Pindak, and D. J. Bishop, Rev. Sci. Instrum. **56**, 2088 (1985), and references therein.

[7]R. N. Kleiman, P. L. Gammel, E. Bücher, and D. J. Bishop, to be published.

[8]V. Müller, Ch. Roth, D. Maurer, E. W. Scheidt, K. Lüders, E. Bücher, and H. E. Bömmel, Phys. Rev. Lett. **58**, 1224 (1987).

[9]Y. J. Qian, M-F. Xu, A. Schenstrom, H-P. Baum, J. B. Ketterson, D. Hinks, M. Levy, and B. K. Sarma, Solid State Commun. **63**, 599 (1987).

[10]D. Saint-James and P. G. de Gennes, Phys. Lett. **7**, 306 (1964).

[11]B. H. Heise, Rev. Mod. Phys. **36**, 64 (1964).

[12]M. J. Stephen and J. Bardeen, Phys. Rev. Lett. **14**, 112 (1965); John Bardeen and M. J. Stephen, Phys. Rev. **140**, A1197 (1965).

[13]D. Criber, B. Jacrot, L. Madhau Rao, and B. Farnoux, in *Progress in Low Temperature Physics*, edited by C. J. Gorter (North-Holland, Amsterdam, 1967), Vol. 5, p. 161.

[14]B. Obst, Phys. Lett. **28A**, 662 (1969).

[15]See, for example, B. Serin, in *Superconductivity*, edited by D. Parks (Dekker, New York, 1969), Vol. 2, p. 969.

PHYSICAL REVIEW B VOLUME 40, NUMBER 10 1 OCTOBER 1989

Mechanical measurements of two-dimensional flux lattices: Observation of two-stage melting

P. L. Gammel, A. F. Hebard, and D. J. Bishop
AT&T Bell Laboratories, Murray Hill, New Jersey 07974
(Received 17 July 1989)

Using a high-Q silicon mechanical oscillator we have studied flux lattice melting in two-dimensional amorphous composite In/InO_x superconducting films. In addition to the previously observed solid and liquid phases, the flux lattice exhibits a third stable phase, intermediate between the solid and liquid, which exists at high sheet resistances, large magnetic fields, and low temperatures. For a range of sheet resistances, this phase coexists at a tricritical point with the liquid and solid phases. In the limit of high sheet resistance, only this new phase is stable, preempting the solid phase. We argue that this intermediate phase is unlikely to be a hexatic phase, and is more likely to be an amorphous solid phase.

When the applied magnetic field is between the lower critical field, H_{c1}, and the upper critical field, H_{c2}, a type-II superconductor will be permeated by an array of flux lines, each with one quantum of flux $hc/2e$. As predicted by Abrikosov[1] and subsequently verified by numerous experiments,[2] in three dimensions, these lines form a triangular lattice with long-range positional order and a well-defined shear modulus. However, in thin superconducting films it is possible to study a flux-line lattice which is two dimensional. In this case, the interactions between vortices are logarithmic and a Kosterlitz-Thouless–type melting should occur.[3,4]

For two-dimensional systems Halperin and Nelson[5] and Young[6] argued that melting should occur in two stages. As the temperature is increased, at the first transition, the dislocation pairs unbind and destroy the quasi-long-range positional order of the two-dimensional solid. At this transition the orientational order should remain essentially unchanged. At the second transition, the lattice disclinations unbind, and destroy the orientational order to result in a high-temperature liquid phase with exponential decay of both the orientational and positional correlations. The intermediate, or hexatic phase is expected to be characteristic of all two-dimensional melting. This hexatic phase has been identified and studied in a variety of two-dimensional systems, including freely suspended liquid-crystal films[7] and colloidal systems.[8]

In this Rapid Communication we report on mechanical measurements of flux lattice melting in amorphous composite In/InO_x superconducting films. The films are sufficiently thin so that the flux lattice is two-dimensional in character. We will present data which indicates that in addition to the previously observed solid and liquid phases for the two-dimensional flux lattice there also exists an intermediate phase in which there is only very short-range positional order for the flux lines. This phase is stabilized by increasing the disorder which may be accomplished by increasing either the magnetic field or the sheet resistance of the films. Although this new phase occurs between the solid and liquid phases, and coexists with them at a tricritical point, we argue that it is unlikely to be a hexatic phase, although its detailed identification remains an open question.

The experimental apparatus is shown in Fig. 1. It is similar to that used in Ref. 9. The experiment consists of a high-Q silicon oscillator[10] onto which a thin ($\sim$100 Å) In/InO_x film is grown by reactive ion beam sputter deposition in a low-pressure oxygen environment. The films used in this experiment were smooth with an amorphous composite microstructure.[11] Transport measurements on samples deposited simultaneously onto silicon from the same wafer as the oscillator served to characterize the films. The resistive transitions in zero field were always sharp (≤ 0.1 K), indicating uniform films. The superconducting transition in zero field has been shown[12] to be the result of a Kosterlitz-Thouless phase transition describing the thermally induced dissociation of bound vortex-antivortex pairs. Homogeneity of the films over long length scales is a prerequisite for this observation since unbinding of the largest pairs dominates the transition.

The oscillators were operated self-resonantly in the simplest beam-bending mode as shown in Fig. 1. The oscillators typically had a Q of 2×10^5, a resonant frequency of 3 kHz and a frequency stability of $1:10^{-8}$. By measuring the resonant frequency and dissipation of the oscillator, the bulk modulus of the vortex lattice and dissipation can be determined.

The oscillator's response to the presence of a vortex lattice is as follows. At low temperatures, the vortex lattice will be pinned so that the vortices will move with the film.

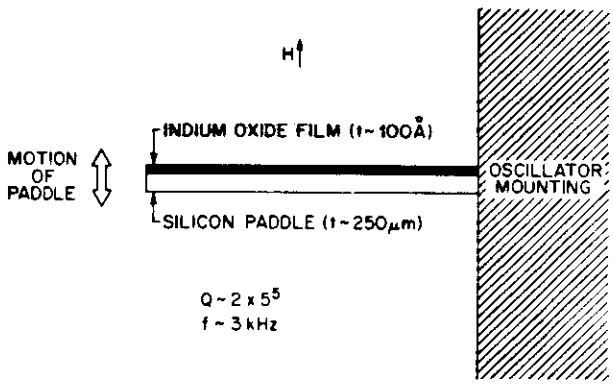

FIG. 1. A schematic diagram of the mechanical oscillator.

In the cantilever mode used here the average vortex spacing will oscillate as $\Delta a_0/a_0 \sim Ax\delta e^{i\omega t}$, where A is the amplitude of the oscillation, x the distance from the suspension point, and δ the thickness of the oscillator. This density modulation gives a coupling to longitudinal sound in the vortex array at the frequency of oscillation. In two dimensions the elastic modulus for longitudinal sound is $B+\mu$ where $B \propto H^2$ is the bulk modulus and $\mu \propto H$ is the shear modulus. As a result of the long-range interaction between vortices, $B \gg \mu$ and the contribution due to shear can be ignored.

This coupling to longitudinal sound will depend on the relaxation rate of the flux lattice. Since the Hall angle is known to be small[13] the response is purely dissipative. At low temperatures, $T \ll T_M$, there is a well-formed flux lattice which remains pinned to the substrate. In this regime, the relaxation rate τ for compression of the flux lattice is very long and $\omega\tau \gg 1$. Hence, the vortices move with the underlying film. The vortex lattice will then contribute to the elastic response of the oscillator. For $T \gg T_M$, thermal fluctuations will dominate the motion of the vortices. In this regime the vortex fluid will relax rapidly ($\omega\tau \ll 1$). The vortices are decoupled from the film and there will be no contribution to the oscillator's response from the elastic properties of the flux lattice. Near T_M this rate will be strongly temperature dependent and a crossover between the two regimes will occur with a dissipation peak and a softening of the oscillator's response at $\omega\tau \sim 1$. We define this dissipation peak as the melting temperature as in Ref. 9. The subject of this paper is a second dissipation peak which occurs at higher fields and generally lower temperatures than our previous study. We feel that this indicates a transition into either a hexatic phase or, which we argue is more likely, an amorphous glass phase of the two-dimensional flux lattice.

Shown in Fig. 2 is the frequency shift and dissipation for a film with $R_\square = 343\ \Omega/\square$ at 80 kG. The feature labeled T_M is the melting temperature where there is a large (off scale) dissipation peak and a frequency shift of ~ 1700 ppm. The second feature, which we believe is the transition to an amorphous glass phase, is labeled T_G. It is accompanied by a small dissipation peak and a frequency shift of ~ 5 ppm. Shown in Fig. 3 is the phase diagram in both field and temperature for the melting and glass

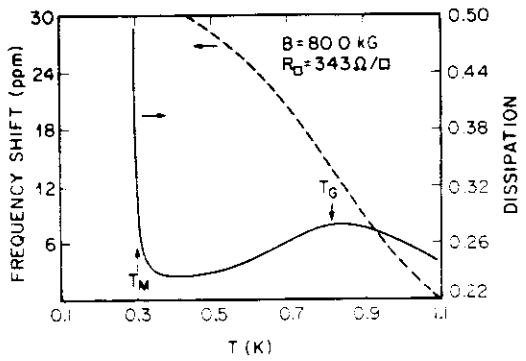

FIG. 2. The frequency shift and dissipation are shown as a function of temperature at a field of 80 kG for a film with a sheet resistance of 343 Ω/□.

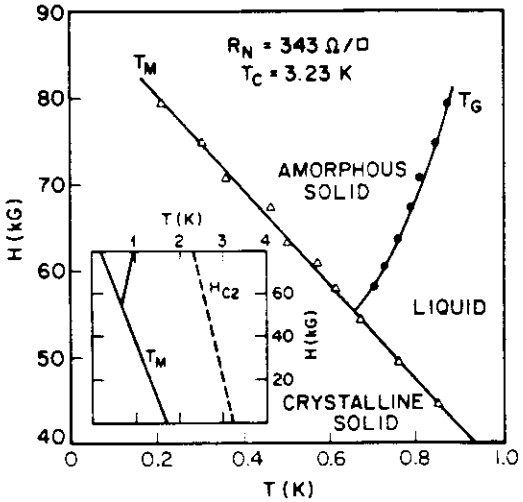

FIG. 3. The phase diagram is shown as a function of field and temperature for all three phases of the flux lattice for the same film as in Fig. 2.

transitions. These data are for the same film as shown in Fig. 2. Note that the three phases meet at what appears to be a tricritical point.

Shown in Fig. 4 is the phase diagram for a film with a sheet resistance of 904 Ω/□. As was shown in Ref. 3, when the sheet resistance is increased, the melting temperature is reduced according to the formula

$$\frac{T_c}{T_M} = \left(1 + 3.8\frac{R_\square}{A_1 R_c}\right) \tag{1}$$

with $R_c = 4.12$ kΩ/□ and A_1 predicted to lie in the range $0.4 < A_1 < 0.75$. Experimentally,[9] it was found that $A_1 \approx 0.5$ for In/InO_x films. For the sample shown in Fig. 4 the solid phase has disappeared, preempted by the new phase. As the sheet resistance is increased, the T_G line moves down in field. In Fig. 4, T_G for the $R_\square = 343\ \Omega/\square$

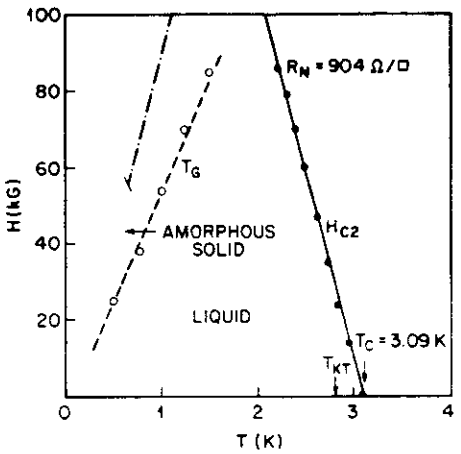

FIG. 4. The phase diagram is shown for a film with $R_\square = 904$ Ω/□. Note the absence of a solid phase. The dash-dotted line is T_G for the film with $R_\square = 343$ Ω/□. Note that the T_G line moves down as the disorder is increased.

film shown in Fig. 2 is shown as the dash-dotted line.

Clearly this third phase cannot arise from gross sample inhomogeneities as these films are known to be very uniform, with their properties completely determined by $R_{\square}$. In addition, the slope of the T_G line is opposite to that of T_M. Since earlier measurements[9] have shown the effect of increasing disorder on melting is a reduction of T_M, with little change in the field-dependent slope, T_G could not represent a portion of the sample with a different $R_{\square}$. This new phase is clearly favored by increasing disorder. These measurements are all below the collective pinning peak due to flux flow as independently measured in these samples. This means that in this regime, as the field is increased the effectiveness of pinning increases and the flux lattice is increasingly disordered. The data in Figs. 3 and 4 show that this increase in disorder pushes the transition temperature higher. Also, as the sheet resistance is increased and the solid phase is inhibited, the new phase becomes favored over a larger part of the phase diagram.

A qualitative analysis of the magnitudes of the frequency shift shows that this phase is not a solid with a long mechanical relaxation time. The bulk modulus of the solid phase may be obtained from the total interaction energy of the vortex array

$$\frac{\Phi_0^2}{8\pi^2\Lambda(T)}\int n(r)\ln(r-r')n(r')d^2r\,d^2r'. \qquad (2)$$

The vortex density is $n(r)=B/\Phi_0$. The integral is cut off by either the size of the system, or $\Lambda(T)$, the effective two-dimensional penetration depth. In the solid phase, this gives the observed H^2 dependence of the frequency shift and also the approximate magnitude (1700 ppm at 80 kG). However, the transition to the glass phase shows only a 5 ppm shift suggesting much shorter mechanical relaxation rate and a weaker coupling to the film.

The observed magnitudes of the oscillator response are consistent with either hexatic phase or an amorphous glass phase. We feel that the hexatic phase is an unlikely explanation of our observations based on the following three reasons. First, theoretical analysis[3] and simulations[14] have suggested that the hexatic phase is not particularly sensitive to disorder. In particular, it should be no more sensitive than the melting temperature itself. However, there is no evidence that increasing disorder stabilizes the hexatic phase and causes the liquid to hexatic transition to occur at *higher* temperatures.

The second reason is that the mechanical response of a hexatic phase has been extensively studied theoretically.[15] The hexatic phase should have a mechanical response identical to that of a liquid. This would make the hexatic-liquid transition unobservable in an experiment such as ours. It should be noted, however, that in mechanical measurements of freely suspended films[16] the hexatic-liquid transition *is* seen and is characterized by a small (100 times smaller than at the solid-hexatic transition) dissipation peak. In our experiment the feature at T_G is approximately 300 times smaller than that at T_M.

The third reason is, as is shown in Ref. 15, that as the density is increased, the hexatic phase should become less favored. This is in contrast to the observed intermediate phase, which is observed at high fields (high flux line density).

Because of these reasons we feel that this newly observed phase is more likely to be an amorphous glass stabilized by the disorder.[17] It is an open question as to whether T_G is a true phase transition as has been suggested for flux lattices in the high-T_c superconductors[18] or merely a crossover point in the dynamical response of the vortex liquid. Clearly more theoretical and experimental work is required to address these issues.

In conclusion, we have measured melting in two-dimensional flux lattices. We have found the first experimental evidence in this system for a new phase which occurs intermediate between the liquid and solid phases with a tricritical point where all three phases can coexist. This phase is stabilized by increasing disorder in the flux lattice. We argue that it is unlikely to be a hexatic phase, and is probably an amorphous glass. The details of the identification are as yet incomplete.

We would like to thank D. Fisher, M. P. A. Fisher, and D. Nelson for numerous technical discussions and continuing interest.

[1]A. A. Abrikosov, Zh. Eksp. Teor. Fiz. **32**, 1442 (1957) [Sov. Phys. JETP 5, 1174 (1957)].

[2]See, for example, H. Trauble and U. Essman, J. Appl. Phys. **25**, 273 (1968).

[3]D. S. Fisher, Phys. Rev. B **22**, 1190 (1980).

[4]B. A. Huberman and S. Doniach, Phys. Rev. Lett. **43**, 950 (1979).

[5]B. I. Halperin and D. R. Nelson, Phys. Rev. Lett. **41**, 121 (1978).

[6]A. P. Young, Phys. Rev. B **19**, 1855 (1979).

[7]M. Cheng, J. T. Ho, S. W. Hui, and R. Pindak, Phys. Rev. Lett. **61**, 550 (1988).

[8]C. A. Murray and D. H. van Winkle, Phys. Rev. Lett. **58**, 1200 (1987).

[9]P. L. Gammel, A. F. Hebard, and D. J. Bishop, Phys. Rev. Lett. **60**, 144 (1988).

[10]R. N. Kleiman, G. K. Kaminsky, J. D. Reppy, R. Pindak, and D. J. Bishop, Rev. Sci. Instrum. **56**, 2088 (1985).

[11]A. F. Hebard and S. Nakahara, Appl. Phys. Lett. **41**, 1130 (1982).

[12]A. F. Hebard and A. T. Fiory, Phys. Rev. Lett. **50**, 1603 (1983); A. T. Fiory, A. F. Hebard, and W. C. Glaberson, Phys. Rev. B **28**, 5075 (1983).

[13]Y. B. Kim and M. J. Stephen, in *Superconductivity*, edited by R. D. Parks (Derker, New York, 1969), Vol. 2, pp. 1107–1167.

[14]D. Nelson, M. Rubinstein, and F. Spaepen, Philos Mag. A **46**, 105 (1982).

[15]A. Zippelius, B. I. Halperin, and D. R. Nelson, Phys. Rev. B **22**, 2514 (1980).

[16]R. Pindak (private communication).

[17]D. S. Fisher (private communication).

[18]M. P. A. Fisher, Phys. Rev. Lett. **62**, 1415 (1989).

Magnetic Order in the Different Superconducting States of UPt_3

G. Aeppli,[1,2] D. Bishop,[1,2] C. Broholm,[1,2] E. Bucher,[1,3] K. Siemensmeyer,[4] M. Steiner,[5] and N. Stüsser[4]

[1]*AT&T Bell Laboratories, 600 Mountain Avenue, Murray Hill, New Jersey 07974*
[2]*Risø National Laboratory, Roskilde, DK-4000, Denmark*
[3]*University of Konstanz, Konstanz 7750, West Germany*
[4]*Hahn-Meitner Institute, 1000 Berlin 39, Germany*
[5]*University of Mainz, Mainz 6500, West Germany*

(Received 26 April 1989)

We use neutron diffraction to show that superconductivity affects the magnetic order in UPt_3. The different superconducting states identified in previous bulk measurements can be associated with different behaviors of the magnetic order parameter. The data suggest that the coupling between the multicomponent superconducting and magnetic order parameters leads to the variety of superconducting phases of UPt_3.

PACS numbers: 74.70.Tx, 75.25.+z

UPt_3 continues to fascinate because of its unusual superconductivity,[1] simultaneous antiferromagnetic tendencies,[2] and large carrier masses.[3] Early experiments were concerned primarily with the superconducting properties in zero magnetic field, with results strongly indicating anisotropic d-wave pairing. More recently, attention has shifted to anomalies found within the superconducting phase for nonzero applied fields H by torsional-oscillator,[4] ultrasound,[5] and specific-heat[6] measurements. In the present paper, we describe neutron-diffraction data which show that these anomalies are best understood in the context of coupled superconducting and (static) magnetic order parameters. Specifically, we show that the $(1, \frac{1}{2}, 0)$ magnetic Bragg intensity decreases with decreasing temperature for $T \lesssim 0.4$ K and $H = 0$. Even more interesting is that it can be made to increase at $T = 0.1$ K by applying a field *perpendicular* to the basal planes and ordered moments of UPt_3. However, the intensity is T and H dependent only in the low-H, low-T superconducting state delineated by the most pronounced bulk anomalies.

Before presenting our results, we recall that UPt_3 is hexagonally close packed (space group $P6_3/mmc$) with two U atoms per unit cell. The locations of Bragg peaks are expressed in reciprocal-lattice units, where $a^* = b^* = 4\pi/(a\sqrt{3}) = 1.264$ Å and $c^* = 1.285$ Å. The magnetic order[2,7] in UPt_3 involves a doubling of the unit cell along an a^*-type direction in the basal planes, with the ordered moment also parallel to this direction. The ordered moment is small [$(0.02 \pm 0.01)\mu_B$/U atom] but comparable to that for other superconducting heavy-fermion systems, such as URu_2Si_2[8] and $U_{1-x}Th_xBe_{13}$.[2,9] The Néel temperature is $T_N \approx 5$ K, which is close to where several transport and thermodynamic anomalies occur.[10] The $(\frac{1}{2}, 0, 1)$ intensity was previously measured for $T \gtrsim 0.25$ K: It rises in proportion to $T_N - T$ until it reaches a plateau below $T \approx 0.5$ K.

We performed our neutron scattering experiments using the triple-axis spectrometer TAS7 installed in the cold-neutron guide hall of the DR-3 reactor at Risø National Laboratory, Denmark. Both the monochromator and analyzer were pyrolitic graphite, set for the (002) reflection, while cooled Be filters eliminated higher-order contamination of the incident beam. Except where explicitly mentioned, no collimators were installed; we note, however, that the divergence of the beam incident on the monochromator was 20′ as given by the neutron

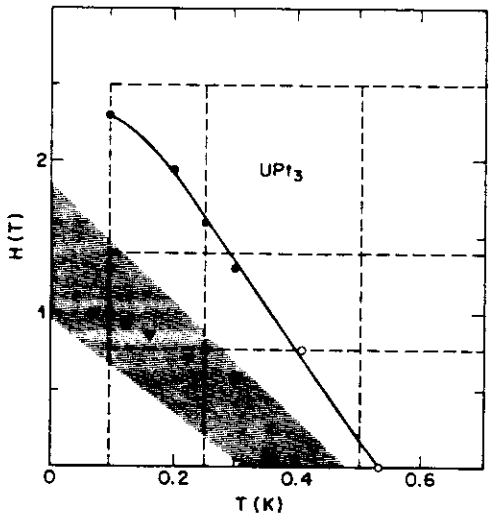

FIG. 1. Phase diagram for superconducting UPt_3. Open and closed circles represent $H_{c2}(T)$ found from constant-field and -temperature sweeps, respectively, of ac susceptibility measured *in situ* as described in text. Open triangles are locations of torsional-oscillator anomalies in Ref. 4. Shaded area represents boundary between states where antiferromagnetic intensity varies with field and temperature and where it is H and T independent. Dashed lines are trajectories followed to accumulate diffraction data.

guide. The neutron energy was 5 meV. We mounted four UPt_3 crystals, each a cylinder of roughly 4 cm in length (c|| growth direction) and 6 mm in diameter, so that their crystallographic axes coincided to within better than 1°, on a copper sample holder. A fifth crystal mounted on the holder was the core of a mutual inductance coil used for monitoring the ac susceptibility during the neutron scattering experiment. The assembly was attached to the cold finger of an Oxford Instruments dilution refrigerator such that the c axes of the crystals were parallel to the (vertical) field produced by a split-coil superconducting magnet. The entire refrigerator was installed on the sample table of the spectrometer whose (horizontal) scattering plane coincided with the $(hk0)$ zone of UPt_3.

The UPt_3 crystals were the same as those used in the earlier cold-neutron scattering study; growth procedures and experiments relating to their quality and purity are described elsewhere.[7] Figure 1 shows the superconducting phase diagram for these samples. The solid and open circles represent $H_{c2}(T)$ found from the ac susceptibility χ_{ac} measured *in situ* for constant fields and temperatures, respectively. The phase transition was identified as occurring where χ_{ac} reached 10% of its diamagnetic limit. For $H=0$, the corresponding transition temperature is $T_c=0.53$ K.

Figure 2 shows the $(1,\frac{1}{2},0)$ Bragg intensities and ac susceptibilities measured along the constant-H and constant-T trajectories indicated by the dashed lines in Fig. 1. At all fields for $T>T_c$, the intensity increases monotonically with decreasing T until $T\approx T_c$, in agreement with the measurements of the $(\frac{1}{2},0,1)$ reflection.[7] The most important new result is that at the lowest fields and temperatures, the $(1,\frac{1}{2},0)$ intensity is actually reduced (by -5%) with respect to its value at T_c. Another remarkable result is that fields larger than 1 T restore the full Bragg intensity (observed at T_c) even at the lowest temperature (0.1 K). Finally, the Bragg intensity is independent of field at T_c. This observation, together with the knowledge that the ordered moments are within the basal plane and that fact that the magnetic susceptibility is lowest when measured parallel to c,[11] the direction of the magnetic field in this experiment, clearly implies that the anomalous behavior of the magnetic intensity is due to the superconductivity of UPt_3. Interestingly, however, the Bragg intensity becomes independent of field and temperature when according to the ac susceptibility data, the samples are still well within the superconducting regime. While occurring far from the boundary defined by $H_{c2}(T)$, the Bragg intensity saturates near anomalies found in the superconducting state by torsional-oscillator and ultrasound-attenuation measurements; the arrows in Fig. 2 represent the reported positions of torsional-oscillator anomalies.[4]

To obtain a quantitative summary of how the magnetic intensity behaves in the H-T plane, we have fitted our

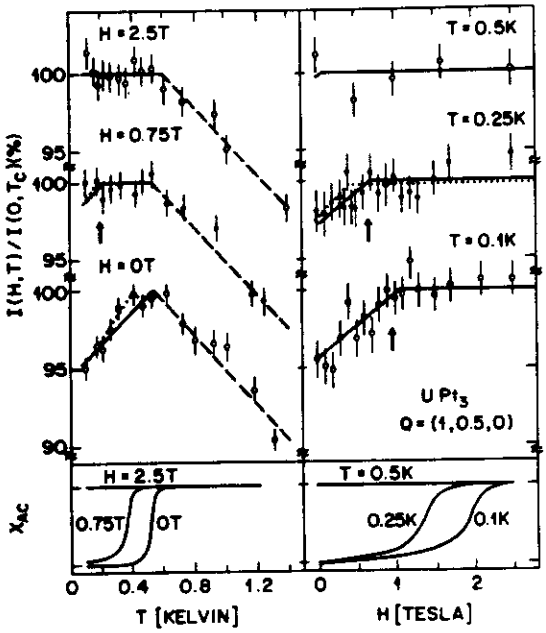

FIG. 2. Normalized and background-corrected temperature-dependent (left-hand column) and field-dependent (right-hand column) $(1,\frac{1}{2},0)$ magnetic Bragg intensities (upper frames) and ac susceptibilities (lower frames). Temperature sweep for $H=1.4$ T is not shown because it is indistinguishable from that for $H=2.5$ T. Solid and dotted lines are derived from fits described in text. At $H=0$ and $T=0.5$ K, the observed peak intensity is 245 counts/min on a background of 48 counts/min.

data for $T<0.55$ K by the form

$$I(H,T)=\begin{cases} I_0 \text{ for } H>H'(T), \\ I_0-c[H'(T)-H] \text{ for } H\le H'(T), \end{cases} \quad (1)$$

where $H'(T)=H_0'(1-T/T_c')$.

We obtain the best results for $T_c'=0.39$ K and $H_0'=1.4$ T. The statistically weighted χ^2 increases by 10% from its minimum if T_c' is raised (lowered) by 0.09 (0.08) K, or if H_0' is raised (lowered) by 0.5 (0.4) T. The shaded region in Fig. 1 separates the regimes where the Bragg intensity is saturated and where it is still H and T dependent. The shading is used to indicate the uncertainty, established by the error analysis just described, in the location of the boundary between the two regimes. All of the "phase boundaries" reported previously for superconducting UPt_3 fall within the shaded region. This is true not only for $H\gg H_c$ (see, e.g., open triangles which mark positions of maxima in dissipation measured by the use of a torsional oscillator[4]), but also for $H=0$, where the data are slightly more consistent with Eq. (1) when $T_c'\neq T_c$ (dotted lines in Fig. 2) rather than when $T_c'=T_c$ (solid lines in Fig. 2), in agreement with specific-heat data indicating two superconducting transitions.[6] Thermodynamic measurements on crystals of the type used here are underway and will help to de-

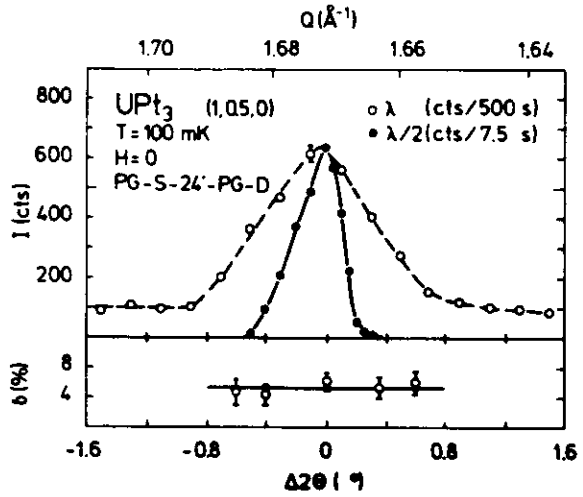

FIG. 3. Upper frame shows longitudinal (θ-2θ) scan through magnetic $(1,\frac{1}{2},0)$ and nuclear (2,1,0) reflections observed with first- and second-order neutrons, respectively, using the same spectrometer configuration, which differs from that of Fig. 2 by the addition of a 24′ collimator after the monochromator. $\Delta 2\theta$ is the deviation in scattering angle from peak position; Q is the momentum transfer. Lower frame represents the Q dependence of the ratio of magnetic intensities I_N and I_S at 540 mK and 100 mK, respectively, with $H=0$: $\delta=(I_N-I_S)/(I_S-I_B)$, where I_B = background signal = 12 counts per minute.

cide where bulk superconductivity sets in (χ_{ac} generally gives a higher value for T_c) and whether our samples undergo two transitions in zero field.

Figure 2 shows intensities measured for constant scattering angle. To determine whether the new effects are due to a change in the overall amplitude, or to a broadening or a shift of the Bragg peak, we have measured the shape of the magnetic scattering peak with higher momentum resolution. In the upper frame of Fig. 3, the magnetic peak is compared to the (2,1,0) nuclear Bragg profile determined using $\lambda/2$ neutrons. On account of the wavelength-dependent divergence of the neutrons in the guide, the $\lambda/2$ profile does not give the resolution width for λ directly. However, it can be used to make a rough estimate (0.016 $Å^{-1}$ full width at half maximum) which implies that as for the $(\frac{1}{2},0,1)$ magnetic reflection,[7] the $(1,\frac{1}{2},0)$ peak is not resolution limited; its width corresponds to a magnetic correlation length of order 150 Å. The lower frame of Fig. 3 shows the effect of reducing the temperature to 0.1 K. We have plotted the fractional increase δ of background-corrected intensities (the background was measured to be temperature independent) from 0.1 to 0.5 K, respectively. To eliminate the influence of small irreproducibilities in the spectrometer setting, the data were taken at both temperatures for each point in the scan before moving to the next point. The constant δ seen in Fig. 3 implies that the line shape and position of the $(1,\frac{1}{2},0)$ magnetic peak remain unchanged between the superconducting and normal states of UPt_3. In other words, the intensity changes associated with superconductivity are due to changes in the overall amplitude of the elastic magnetic scattering. This result excludes scenarios where magnetic order is nucleated at discrete defects, and the finite range associated with the penetration of the order into the otherwise unperturbed host is modified by the superconductivity.

Largely because of ultrasound-absorption measurements,[1] UPt_3 has been classified as an anisotropic superconductor where the gap function vanishes at lines on the Fermi surface. The unconventional pairing is commonly thought[12] to be d wave, and mediated by the antiferromagnetic fluctuations observed by inelastic neutron scattering.[2] The corresponding superconducting order parameter ψ can be represented by vectors $\xi_1\hat{\mathbf{x}}-\xi_2\hat{\mathbf{y}}$, where ξ_1 and ξ_2 are complex coefficients, and $\hat{\mathbf{x}}$ and $\hat{\mathbf{y}}$ are translations in the basal planes of UPt_3. Theorists have proposed several descriptions of the superconducting phases of UPt_3: (i) The two different superconducting states are characterized by either $\xi_1=i\xi_2$ or $\xi_1\xi_2=0$ (i.e., $\psi=\hat{\mathbf{x}}$ or $\hat{\mathbf{y}}$).[13] (ii) The microscopic superconducting order parameter is the same for both states, which differ only in the nature of the associated vortex cores.[5] (iii) The two states are $\xi_1=i\xi_2$ (for low T and H) and $\xi_1=ir\xi_2$, where r is a nonzero real number.[14]

Specific-heat and ultrasound measurements rule out proposal (i), as described elsewhere.[5,6] Since the magnetic order parameter can only couple to the microscopic superconducting order parameter, the transition between different states as described in (ii) would be invisible in the present neutron scattering experiments. Furthermore, the zero-field transition would not be split as shown by specific-heat measurements[6] and suggested by our data. Thus, (ii) is also ruled out. Proposal (iii), which incorporates the reduced space-group symmetry associated with the magnetic order, does allow for the splitting of the zero-field transition. However, the vector character of the magnetic order parameter and the related broken time-reversal invariance are not taken into account.

In view of the shortcomings of existing theory, not the least of which is the absence of predictions for the field and temperature dependence of the magnetic order parameter, we describe here the framework[15] within which our data might eventually be understood. We begin by noting that the coupling of the vectors representing superconducting (ψ) and magnetic (ϕ) order parameters involves both their amplitudes, as for ordinary s-wave superconductors, and their relative orientation, a quantity which of course does not exist for ordinary superconductors. Couplings involving amplitudes arise from the usual pair-breaking mechanisms which yield competition between superconductivity and magnetism. Taking only such couplings into account, the interpretation of our data would be that there are two different superconduct-

ing order parameters, with pair wave functions such that the coupling would be greatly reduced or even zero in the high-field, high-temperature state. Different interpretations are possible when we consider coupling terms involving the relative orientations of ψ and ϕ. These terms appear because of the inevitable and not necessarily pair-breaking interactions between the angular momentum of the Cooper pairs and the ordered moment. As their name implies, they lead to the possibility of orientation of ψ by ϕ when $|\psi|$ is small, which it is for H near $H_{c2}(T)$. On the other hand, when $|\psi|$ is large, ψ can actually *reorient* ϕ. Thus, ψ acts much as an *in-plane* magnetic field on UPt_3: As long as its amplitude (strength) is below a certain critical value (spin-flop field) due to the basal-plane anisotropy, ϕ will maintain its orientation, while for larger $|\psi|$, ϕ will be rotated. In the latter situation, the magnetic Bragg intensities will change because of the dipole selection rules. Measurements of more than a single Bragg peak are needed to determine the relative importance of amplitude and orientation effects. for example, since the rotation of the moments will occur within the basal planes (the in-plane anisotropy energies are small compared to the out-of-plane energies), it would be essentially undetectable at the $(\frac{1}{2},0,1)$ Bragg point studied previously.[7] If the result of Ref. 7, namely that the $(\frac{1}{2},0,1)$ intensity is T independent for $T < T_c$, were to hold to the lower temperatures of the current experiment, we would have strong evidence that the intensity changes observed at $(1,\frac{1}{2},0)$ are due primarily to a reorientation of ϕ.

In summary, we have shown that there are at least two microscopically distinct states of superconducting UPt_3, as characterized by the behavior of the magnetic order parameters. The fact that superconductivity influences the static magnetic scattering and that it does so in a way which changes its overall amplitude but not its shape demonstrates that antiferromagnetism and superconductivity coexist and interact at the microscopic level in our samples of UPt_3.

We are grateful to J. Als-Nielsen and J. Kjems for their hospitality, support, and encouragement at Risø National Laboratory, E Blount and C. M. Varma for helpful discussions, and R. Joynt, H. Monien, and K. Machida for preprints.

[1]D. Bishop *et al.*, Phys. Rev. Lett. **53** 1009 (1984); B. S. Shivaram *et al.*, Phys. Rev. Lett. **56**, 1078 (1984); D. Jaccard, J. Floquet, P. Lejay, and S. L. Tholence, J. Appl. Phys. **57**, 3082 (1985).

[2]A review of neutron scattering work is given by G. Aeppli *et al.*, J. Magn. Magn. Mater. **76-77**, 385 (1988), and J. Kjems and C. Broholm, *ibid.*, 371 (1988). Muon-spin rotation data are summarized by R. H. Heffner *et al.*, Los Alamos National Laboratory report, 1988 (to be published).

[3]G. R. Stewart, Z. Fisk, J. O. Willis, and J. L. Smith, Phys. Rev. Lett. **52**, 679 (1984); L. Taillefer *et al.*, J. Magn. Magn. Mater. **63-64**, 372 (1987).

[4]R. N. Kleiman, P. L. Gammel, E. Bucher, and D. J. Bishop, Phys. Rev. Lett. **62**, 328 (1989).

[5]A. Schenstrom *et al.*, Phys. Rev. Lett. **62**, 332 (1989); V. Muller *et al.*, Phys. Rev. Lett. **58**, 1224 (1987).

[6]R. A. Fisher *et al.*, Phys. Rev. Lett. **62**, 1411 (1989); K. Hasselbach, L. Taillefer, and J. Floquet, Centre de Recherches sur les Trēs Basses Températures, CNRS, report, 1989 (to be published).

[7]G. Aeppli *et al.*, Phys. Rev. Lett. **60**, 615 (1988). See also C. Broholm *et al.*, in *Magnetic Excitations and Fluctuations I*, edited by U. Balucani, S. Lovesey, M. Rasetti, and V. Tognetti (Springer-Verlag, Berlin, 1987), p. 162; and P. Frings, B. Renker, and C. Vettier, Physica (Amsterdam) **15B**, 499 (1988).

[8]C. Broholm *et al.*, Phys. Rev. Lett. **58**, 1467 (1987).

[9]B. Batlogg *et al.*, Phys. Rev. Lett. **55**, 1319 (1985).

[10]J. Odin *et al.*, J. Magn. Magn. Mater. **76-77**, 223 (1988); A. de Visser, Ph.D. thesis, Universiteit van Amsterdam, 1986 (unpublished).

[11]P. H. Frings and J. Franse, Phys. Rev. B **31**, 4355 (1985).

[12]K. Miyake, S. Schmitt-Rink, and C. M. Varma, Phys. Rev. B **34**, 6554 (1986); M. T. Beal-Monod, C. Bourbonnais, and V. J. Emery, Phys. Rev. B **34**, 7716 (1986); M. R. Norman, Phys. Rev. Lett. **59**, 232 (1987); W. Puttika and R. Joynt, Phys. Rev. B **37**, 2372; H. Monien and C. J. Pethick NORDITA report, 1988 (to be published); M. Ozaki and K. Machida, Cornell University report (to be published).

[13]G. E. Volovik, J. Phys. C **21**, L221 (1988).

[14]R. Joynt, Supercond. Sci. Technol. **1**, 210 (1988).

[15]E. Blount, C. M. Varma, C. Broholm, and G. Aeppli (to be published).

Observation of Hexagonally Correlated Flux Quanta In $YBa_2Cu_3O_7$

P. L. Gammel, D. J. Bishop, G. J. Dolan, J. R. Kwo, C. A. Murray,
L. F. Schneemeyer, and J. V. Waszczak
AT&T Bell Laboratories, Murray Hill, New Jersey 07974
(Received 26 August 1987)

The high-resolution Bitter pattern technique has been used to reveal the magnetic structure of single-crystal samples of high-T_c superconductor $YBa_2Cu_3O_7$ at 4.2 K. Typical patterns consist of hexagonally correlated, singly quantized vortices of flux $hc/2e$. That is, the structures are comparable to those that would be observed in conventional type-II superconductors under similar conditions.

PACS numbers: 74.70.Ya, 74.60.Ge

The way in which a superconductor breaks into normal and superconducting regions when magnetic flux is admitted involves fundamental aspects of its superconducting properties and metallurgy. Abrikosov's prediction[1] of a triangular array of vortices in the mixed state of type-II superconductors was central to his landmark contribution to the understanding of those materials. These vortices, each corresponding to a quantum of magnetic flux, were shown explicitly in high-resolution Bitter patterns by Träuble and Essmann[2] and by Sarma.[3] Similar information should be of use in the investigation of the fundamental properties and difficult materials properties of the new high-T_c materials. Some emerging theories[4] allow for the possibility of a flux quantum of hc/e rather than $hc/2e$, for example, and many experiments are explained in terms of inhomogeneities in the materials[5] or intrinsic inhomogeneities of the superconducting state.[6,7] It is even in question whether the materials are completely superconducting since magnetization data are often described in terms of the fraction of flux excluded by a sample of inconvenient shape and incompletely described microstructure. Our Bitter pattern experiments on $YBa_2Cu_3O_7$ crystals at 4.2 K show the individual vortices and indicate a strong tendency toward hexagonal ordering in the predominant patterns.

The Bitter pattern technique uses very small magnetic particles to sense the field at the surface of a magnetic material. The particles ("smoke") are made by evaporation of a magnetic material in a background of inert gas. The particles drift to the sample surface and preferentially "decorate" regions where there is a magnetic field. A sketch of the apparatus is shown in Fig. 1. Once on the surface, the particles are found to be immobile, presumably held in place by van der Waals forces. The sample is warmed to room temperature and the particle pattern is examined by scanning electron microscopy. The technique is limited to low fields and by its nature senses only the magnetic structure at a sample surface. Details of the technique as we use it are described in previous work.[8]

About fifteen successful decoration experiments have been performed on bulk samples of $YBa_2Cu_3O_7$. The single-crystal samples were grown from partially melting Y_2O_3-BaO-CuO mixtures and annealed in oxygen as described previously.[9] The crystals are known to be single-phase material with composition near stoichiometry but with many twins, usually in the form of long "domains." The material is orthorhombic with a large (1.17 nm) spacing between the planes perpendicular to the c axis. Usually the samples were flat platelets $\simeq 1$ mm in size with the broad surface perpendicular to the c axis, i.e., parallel to the basal plane. The magnetic field was oriented perpendicular to this surface. For some platelets the surface appeared smooth but for others waves and spirals arising in the crystal growth were apparent. The crystals were part of batches having $T_c \approx 92$ K although measurements of T_c were not made on the specific crystals decorated. Usually several small crystals were picked from a batch and decorated at the same time. The patterns considered successful on the

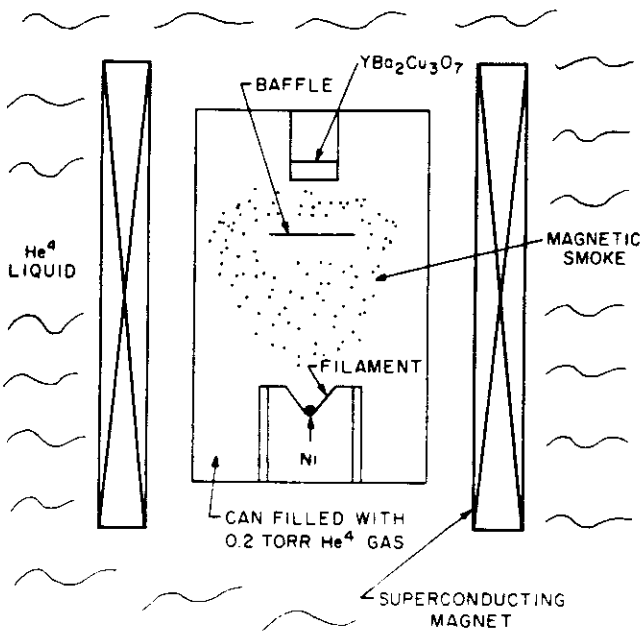

FIG. 1. Sketch of the decoration apparatus.

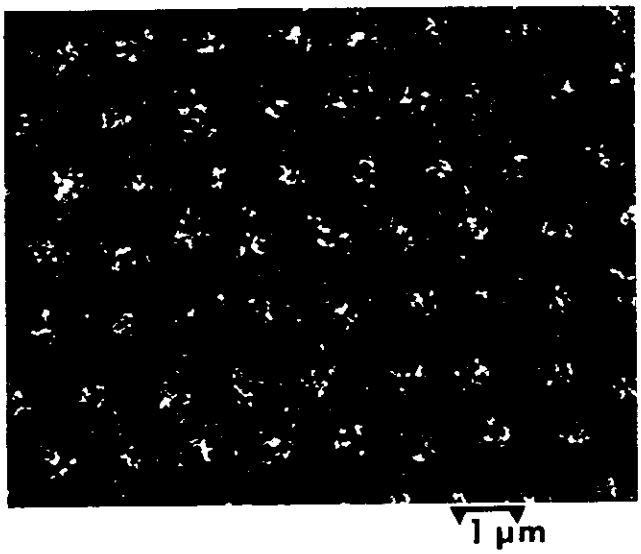

FIG. 2. Flux spots in a $YBa_2Cu_3O_7$ sample decorated after cooling in a field of 13 G.

different pieces were generally similar in character, implying a similarity in other properties. Experiments were conducted usually by cooling from room temperature in a fixed field, since this procedure gave the most uniform structures and seems *a priori* most likely to do so. A piece of Pb foil was decorated with the samples in many experiments. The observation of typical intermediate-state patterns implies that the temperature rise during decoration was modest (Pb has $T_c = 7.2$ K) and that the decoration procedure was effective. At 77 K we observed no flux-related patterns, and so our observations are directly pertinent only to low temperatures. We will discuss this further in our conclusion.

Figure 2 shows one of the patterns observed. The scanning electron microscope micrograph shows the particles as light on a dark background and is typical of the pattern observed everywhere on the sample and on another decorated at the same time. The sample was cooled to 4.2 K in a magnetic field of 13 G; this is also the local field within experimental error if the flux quantum is $hc/2e$. Figure 3(a) shows a similar pattern on one of the samples cooled in a 51-G field. The irregular shape of the spots in the figures is a consequence of interactions between the particles. Nevertheless, the spots are overall similar in spacing and brightness over the entire samples. Very similar patterns are observed in ordinary type-II superconductors, but highly ordered lattices are observed when flux pinning is small.[9] We conclude from the overall uniformity that the spots correspond to singly quantized vortices and that inhomogeneities on a scale at or near the vortex spacing must be small, i.e., that the samples are completely superconducting. The absence of a well defined lattice does imply some inhomogeneity or pinning, however, even in these crystal samples. Further, portions of many samples showed strong correlations to surface structures such as growth spirals and, possibly, to the twinning "domain" structure known to exist in the crystal. These pinning effects notwithstanding, we believe that the more regular patterns demonstrate that the Abrikosov lattice should be considered the equilibrium model state.

The vortices are clearly highly correlated in the small area shown in Fig. 2. Figure 3(a) shows a larger region of one of a set of samples cooled in a 52-G field. Computation[10] of the autocorrelation function, $G(\delta x, \delta y)$, of a digitized version of Fig. 3(a) shows the hexagonal trend more dramatically in Fig. 3(b). The pattern of brightness of Fig. 3(a) does not accurately replicate the shape

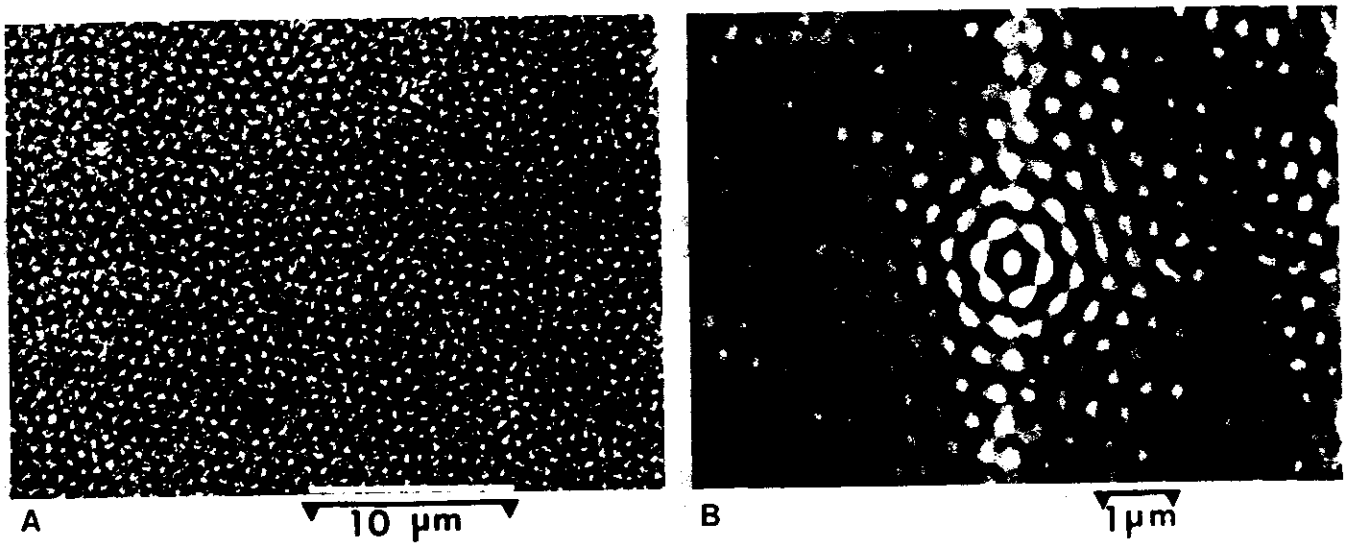

FIG. 3. (a) Typical area of a sample cooled in a 52-G field. (b) Central portion of the autocorrelation function of the pattern in (a).

and size of each vortex because of the large variations in size and shape of the magnetic particles, the bright patches in the micrograph. Even though the magnetic particles do not decorate each vortex in an identical manner, the underlying vortex structure determines on average the particle positions. The centers of intensity of each of the bright particles were located by a simple algorithm.[10] An autocorrelation function of the resulting image of particle centers produced an identical falloff of the central hexagonal region to that of Fig. 3(b). The autocorrelation function is defined as

$$G(\delta x,\delta y)=\int I(x+\delta x,y+\delta y)I(x,y)d(x)d(y),$$

where $I(x,y)$ is the image brightness. Essentially, $G(\delta)$ gives the probability of finding a similar degree of brightness in the image if one moves $\delta=(\delta x,\delta y)$ from any point. The four rings of sixfold peaks near the center ($\delta x=\delta y=0$) of the figure indicate that one has high probability of finding another fluxoid if one moves the indicated direction and distance from any fluxoid site. The decay of intensity of the peaks as one moves larger distances confirms that the correlation length for hexagonal order is roughly 2.5 lattice parameters of the fluxoid lattice, a fact that is evident from the size of a hexagonal "grain" in the original image. The sixfold symmetry of the detail in Fig. 3(b) indicates a strong tendency towards local hexagonal ordering. In the low-field limit one would assume the ordering would become stronger for stronger fields, i.e., as the vortices become more compressed and interact more strongly. In our experiments, all patterns were qualitatively similar to the one discussed here. At the highest field attempted, the field was still only 170 G and vortices were resolved in only a few small areas. Elsewhere a distinct threefold symmetry was discernible in a noisy background but the evidence for a more nearly perfect lattice was inconclusive.

For samples with sufficiently uniform flux density, a sampling of the spot density in several sample regions was used to provide an estimate of the overall sample flux and an upper bound on the flux quantum. Since there is no general agreement at this time on the microscopic or phenomenological basis of superconductivity in the new compounds, the value of the flux quantum is still in question theoretically. But experiments based on Josephson effects[11,12] and on flux jumps in cylinders[13] show a flux quantum $hc/2e$. Our test is of a somewhat different nature but should confirm these proofs and assure that the mixed state consists of vortices of the same quantum. In principle, one could measure the local field of a specified region and then count the vortices in this region to measure Φ_0 in a decoration experiment. We have not attempted to do this but can use our knowledge of the field history to set a bound on Φ_0 and thereby distinguish between $hc/2e$ and hc/e as the fluxoid. If a sample is cooled in a constant field the total flux in the specimen must clearly be less than the applied flux since some flux will be expelled. Figure 4 shows the sampled flux line or spot density for several experiments as a function of the field in which the samples were cooled. If all of the applied flux were trapped in the specimens the density would be given by one of the dashed lines depending on whether Φ_0 is $hc/2e$ or hc/e. In each experiment the line density was less than that required if $\Phi_0=hc/2e$; that is the data are consistent with this value since some flux would be expelled. All of the points except one are inconsistent with $\Phi_0=hc/e$ since the line density would then correspond to larger flux than the applied value, i.e., flux would have to be absorbed when the samples became superconducting. The one marginal point is merely inconclusive. Therefore, $\Phi_0=hc/2e$.

Our failure to observe a pattern at 77 K suggests several possible interpretations. Negative results occur for a variety of reasons in this kind of experiment, so that such results are inconclusive ultimately. Nevertheless, we believe we should have observed a pattern in the several attempts had the structure been strictly analogous to the 4.2 K structure. Taking the observations at face value, the experiments indicated a homogeneous penetration of flux throughout the specimens. This may reflect a temporally unstable distribution of flux since T/T_c is high. However, we cannot rule out other possibilities: that the samples are not homogeneously superconducting so that flux enters on a scale finer than our resolution; that there is a fundamentally different kind of state at the high temperature; or that there is a surface

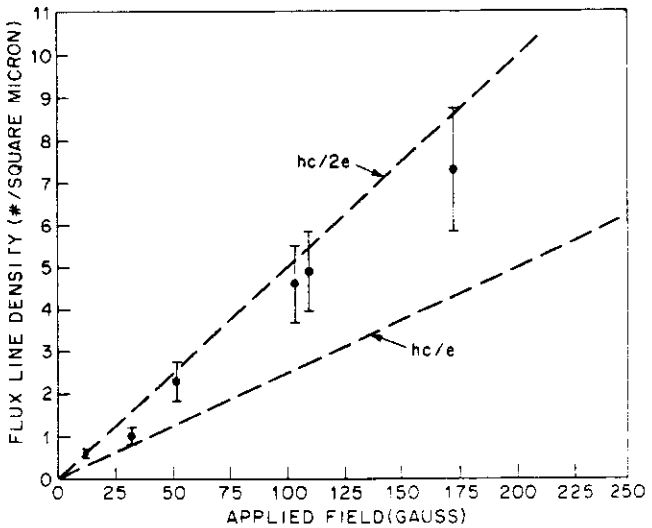

FIG. 4. Sampled flux-spot density on several samples plotted at the field in which the samples were cooled. The dashed lines are the densities which would be observed if all of the magnetic flux were trapped and if the flux quantum were either $hc/2e$ or hc/e. The data exclude hc/e as a possibility since the observed spot density would then correspond to a total sample flux greater than the applied value.

layer which has low T_c so that the bulk structure is masked. More difficult and comprehensive experiments are necessary to distinguish which, if any, of these is the case. Recently, Ourmazd *et al.*[14] reported dilute vortices and fine-scale magnetic structures of unusual character in polycrystalline, ceramic samples at 77 K. It is not implausible that the more disordered material with its stronger pinning would have a more stable flux structure. However, the patterns observed by Ourmazd *et al.* are rather unusual and the corroborative link to the applied field is weak. Also, we should point out the observation by us of some rather unusual patterns under decoration conditions where electrical rather than magnetic effects should dominate. We believe that at least some of the patterns reported by Ourmazd *et al.* are of this kind. These patterns may be of independent interest in understanding the new materials, but can have no direct relation to the magnetic structure of the superconducting state.

In conclusion, we have observed the magnetic structure in $YBa_2Cu_3O_7$ crystals at 4.2 K and found patterns strongly reminiscent of the analogous structures in low-T_c, type-II superconductors. The implications are that the crystals are uniform superconductors with a magnetic structure consisting of singly quantized vortices of quantum $hc/2e$ and with a tendency to form hexagonally ordered arrays. None of this can be shown to apply at 77 K, the only other temperature studied. It seems unlikely to us that this failure reflects anything exotic about the new superconductors since the low-temperature behavior is so ordinary.

We gratefully acknowledge technical discussions and assistance from P. W. Anderson, C. H. Chen, and D. Washington. We thank A. Ourmazd for showing and discussing his results and R. Wenk for assistance in the image-digitizing software.

[1]A. A. Abrikosov, Zh. Eksp. Teor. Fiz. **32**, 1442 (1957) [Sov. Phys. JETP **5**, 1174 (1957).

[2]H. Träuble and U. Essmann, J. Appl. Phys. **25**, 273 (1968).

[3]N. V. Sarma, Philos. Mag. **17**, 1233 (1968).

[4]P. W. Anderson, G. Baskaran, Z. Zou, and T. Hsu, Phys. Rev. Lett. **58**, 2790 (1987); Steven A. Kivelson, Daniel S. Rokhsar, and James P. Sethna, to be published.

[5]D. W. Johnson, Jr., E. M. Gyorgy, W. W. Rhodes, R. J. Cava, L. C. Feldman, and R. B. van Dover, Adv. Ceram. Mater. **2**, 364 (1987).

[6]B. Goldfarb, A. F. Clark, A. I. Braginski, and A. J. Panson, to be published.

[7]J. C. Phillips, to be published.

[8]G. J. Dolan and J. Silcox, Phys. Rev. Lett. **30**, 603 (1973), and J. Low Temp. Phys. **15**, 111,133 (1974); G. J. Dolan, thesis, Cornell University, 1973 (unpublished).

[9]L. S. Schneemeyer, J. V. Waszczak, T. Siegrist, R. B. van Dover, L. W. Rupp, B. Batlogg, R. J. Cava, and D. W. Murphy, Nature (London) **328**, 601 (1987).

[10]C. A. Murray and D. H. Van Winkle, Phys. Rev. Lett. **58**, 1200 (1987).

[11]W. R. McGrath, H. K. Olsson, T. Claeson, S. Eriksson, and L. G. Johansson, to be published.

[12]R. H. Koch, C. P. Umbach, G. J. Clark, P. Chaudhari, and R. B. Laibowitz, Appl. Phys. Lett. **51**, 200 (1987).

[13]C. E. Gough, M. S. Colclough, E. M. Forgan, R. G. Jordan, M. Keene, C. M. Muirhead, A. I. M. Rae, N. Thomas, J. S. Abell, and S. Sutton, Nature (London) **326**, 855 (1987).

[14]A. Ourmazd, J. A. Rentschler, W. J. Skocpol, and D. W. Johnson, Jr., to be published.

Observation of a Hexatic Vortex Glass in Flux Lattices of the High-T_c Superconductor $Bi_{2.1}Sr_{1.9}Ca_{0.9}Cu_2O_{8+\delta}$

C. A. Murray, P. L. Gammel, and D. J. Bishop
AT&T Bell Laboratories, Murray Hill, New Jersey 07974

D. B. Mitzi and A. Kapitulnik
Stanford University, Stanford, California 94305
(Received 27 February 1990)

We observe hexatic order in Abrikosov flux lattices in very clean crystals of the high-T_c superconductor $Bi_{2.1}Sr_{1.9}Ca_{0.9}Cu_2O_{8+\delta}$, by *in situ* magnetic decoration of the flux lattice at 4.2 K. Analysis of the decoration images shows that the positional order decays exponentially with a correlation length of a few lattice constants while the orientational order persists for hundreds of lattice constants and decays algebraically with an exponent $\eta_6 = 0.06 \pm 0.01$. Our results confirm recent theoretical speculation that the positional order should be far more sensitive to disorder than the orientational order and that the low-temperature ordered phase of the flux lines in these systems might be a hexatic glass.

PACS numbers: 74.60.Ge

The behavior of the statics and dynamics of magnetic-flux lattices in the high-T_c superconductors has triggered considerable experimental and theoretical effort.[1-6] In this paper we provide convincing evidence, in agreement with recent theoretical suggestions,[7,8] that the low-temperature, low-field ordered phase of magnetic-flux lattices in Bi-Sr-Ca-Cu-O is a novel phase of condensed matter—the hexatic vortex glass. This phase is characterized by short-range (few lattice constant) positional order which decays exponentially and long-range bond-orientational order which persists for hundreds of lattice constants. We find that the orientational order decays in a power-law fashion with a small exponent $\eta_6 = 0.06$ consistent with theory[9] for two-dimensional (2D) equilibrium hexatics and previous 2D simulations.[10] This may indicate a quasi-2D nature of the flux lines upon field cooling. In contrast to what we see here, in the vortex-liquid regime previously seen at higher temperatures,[6] one observes blurred flux lines and tracks indicating significant motion of the flux lines on the time scale of the measurement.

The experiments described here consist of the Bitter-pattern technique for decorating the magnetic-flux lattices in high-quality single crystals of Bi-Sr-Ca-Cu-O. This technique uses very small ferromagnetic particles to sense the field at the surface of a magnetic material. The "smoke" is made by evaporating a magnetic material in a background of inert (helium) gas. The sample is first field cooled to trap the flux. Magnetic Ni particles of size ~ 50 Å are then evaporated, thermalized in the gas, and then drift to the sample surface and preferentially decorate regions where there is a magnetic field. Once on the surface, the particles are held immobile by the van der Waals forces. The sample is then warmed to room temperature and examined using scanning electron microscopy. Details of the technique as we implement it are given in previous work and the references therein.[2]

The samples we have used for this study consist of high-quality, single crystals of $Bi_{2.1}Sr_{1.9}Ca_{0.9}Cu_2O_{8+\delta}$. This material was chosen because of its low pinning as evidenced by muon-spin-relaxation experiments[11] and the absence of twinning domains which have been shown to pin and orient the flux lattice in Y-Ba-Cu-O.[2,12] The single crystals were grown using a directional solidification process as described in Ref. 13. The crystals are typically in the form of thin sheets with basal-plane dimensions of up to several cm^2 and thicknesses up to 100 μm. The lattice constants, $a_0 = 5.413(2)$ Å, $b_0 = 5.411(3)$ Å, and $c_0 = 30.91(1)$ Å, were determined using a four-circle x-ray diffractometer. As is typical in these materials, an incommensurate periodicity of $4.7(1)b_0$ was observed along the b axis. The crystals, as extracted from the melt, demonstrated a large, sharp (< 5 K 10%–90% transition width) Meissner transition with an onset at 88 K, indicative of a homogeneous, bulk superconductor.

Shown in Fig. 1 are two decoration images taken on a single crystal at different locations on its surface. The

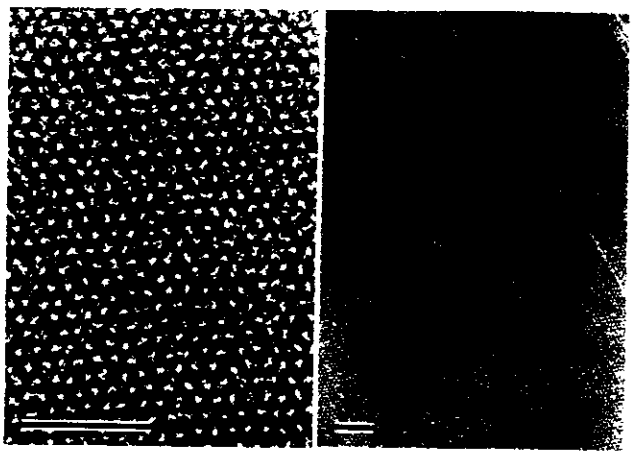

FIG. 1. Two decoration images taken on different regions of a single crystal of $Bi_{2.1}Sr_{1.9}Ca_{0.9}Cu_2O_{8+\delta}$ at a field of 20 G with a decoration temperature of 4.2 K. The bars are 10 μm in length.

crystal surfaces used in these experiments were freshly cleaved in air just before the decoration. The nominal magnetic field used was 20 G applied parallel to the c axis of the crystal and the decorations were done at 4.2 K after field cooling. Each flux line is marked with a clump of magnetic particles which shows up as a white spot in the photographs. As reported previously,[2] the flux quantum as measured here and elsewhere is consistent with $hc/2e$ and excludes the value hc/e.

The decoration images in Fig. 1 were digitized with a video frame grabber, and the centers of the largest clumps of particles were located by image-analysis algorithms described in detail elsewhere.[14] Care was taken to correct for any image distortion introduced by the video camera. The positions of the largest clumps, assumed to correspond to the location of the vortex lines, were then used to analyze the translational and orientational order of the vortices. We estimate that the accuracy of locating the centers of the vortices is comparable to or better than a radius of a large clump which is $0.14a$, where a is an average nearest-neighbor spacing of the large clumps.

Shown in Fig. 2 is a Delaunay triangulation[15] for the left-hand image presented in Fig. 1 consisting of 405 centers. In this construction each flux line is represented by a vertex and the lines emanating from it are the bonds to its uniquely defined nearest neighbors. In the figure the nearest neighborhoods of nonsixfold-coordinated flux lines are shaded in order to reveal the defect structure.

The most relevant 2D defects for the destruction of long-range translational order are free dislocations[9] or isolated pairs of fivefold- and sevenfold-coordinated particles, interstitials that exist as fourfold-coordinated particles with a pair of sevenfold-coordinated neighbors, and vacancies which often show up as eightfold-coordinated centers with two fivefold-coordinated centers. We observe in the larger-scale image containing 6763 vortices an approximately equal interstitial and vacancy density of roughly 0.4% each and free-dislocation density of approximately 1.5%, counting clusters with nonzero local Burgers vector.

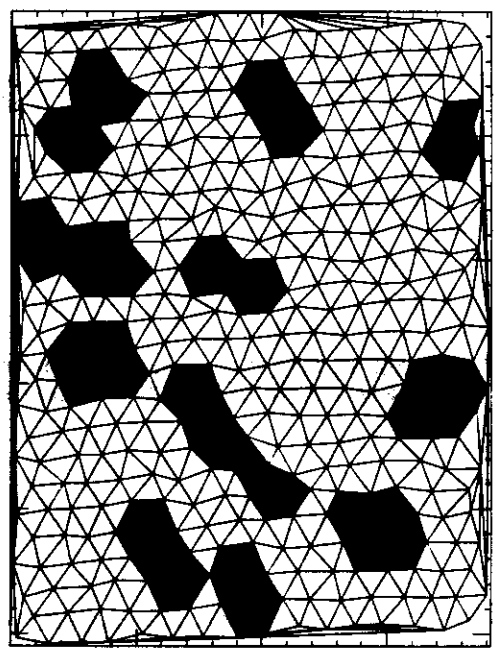

FIG. 2. A Delaunay triangulation for the smaller-scale image on the left-hand side in Fig. 1. An isolated dislocation is located in the upper right, and a cluster with net Burgers vector is located at the left, just above the center of the image.

The net concentration of dislocations observed is much larger than that which could be caused by a gradient in the field (or density of vortices). For our images this gradient is measured by counting vortices and is found to be $<1(1)\%$ in the short image direction and $<2.5(1)\%$ in the long image direction. This measured density gradient will introduce a density of unbound dislocations that is $\sim 0.04\%$ with an average separation of $\sim 40a$. The intrinsic free-dislocation-density average separation is $\sim 10a$, which is quite close to the measured translational correlation length.

The image in Fig. 2, and a similar defect analysis of the larger-scale image of Fig. 1, is strikingly reminiscent of that obtained for 2D colloidal hexatics.[16] If one sights along rows of particles, one can clearly see that there exists long-range orientational order, while the dislocations, interstitials, and vacancies in the defective neighborhoods limit the positional order to only a few nearest neighbors. The analysis can be made quantitative by extracting from the images shown in Fig. 1 the orientational and positional correlation functions.

The orientational correlation function $g_6(r)$ used here is the correlation function of the orientational order parameter[9] $\psi_6(\mathbf{r}) \equiv (1/n_j)\sum_j e^{i6\theta_j}$ for a vortex located at $\mathbf{r}$, where θ_j is the angle with respect to the x axis of the bond to the jth nearest neighbor, summed over all n_j nearest neighbors in the image, determined by a Voronoi polyhedron analysis.[15] Its decay measures directly the spatial falloff of bond-orientational order of the system.

Figure 3 is the central result of this paper. Shown in Fig. 3 is a plot of the orientational correlation function $g_6(r)$. Also shown for comparison is the translational correlation function $g_G(r)$ for two different directions in the lattice, also for the larger-scale image. The translational correlation function $g_G(r)$ measures the decay of the translational order parameter $\psi_t(\mathbf{r}) = e^{i\mathbf{G}\cdot\mathbf{r}}$ at a location $\mathbf{r}$, where $\mathbf{G}$ is any reciprocal-lattice vector.[9] Its decay directly measures the spatial falloff of translational order of a specific wavelength. The orientational order is sufficiently long range in these images that positions of the first reciprocal-lattice vectors $|G_0|_i = 4\pi/a_i\sqrt{3}$ were easily located to an accuracy of better than 0.05% by performing a Fourier transform of the data. Here a_i is the nearest-neighbor separation in one of the three symmetry directions of $i = 1,2,3$ of the lattice. We have plotted in Fig. 3 the extreme cases for G_0 with the shortest and longest correlation lengths.

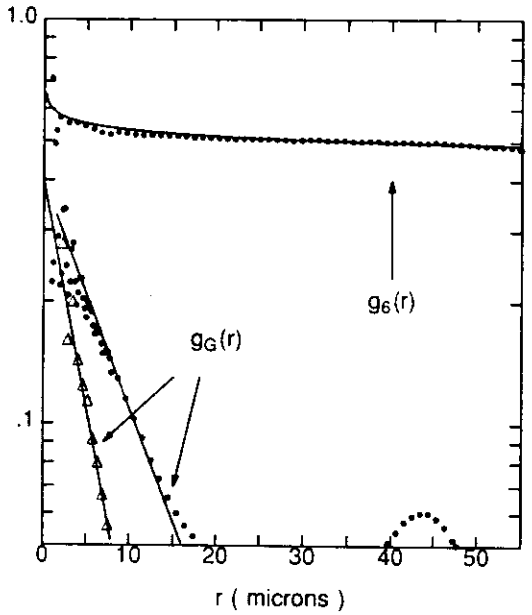

FIG. 3. Two extreme translational correlation functions $g_G(r)$ and the orientational correlation function $g_6(r)$ on a semilogarithmic plot for the larger-scale image in Fig. 1.

We find a slight anisotropy of 9(1)% and 8(1)% in the -b plane of the lattice for the smaller- and larger-scale nage, respectively, slightly smaller than that previously bserved on the Y-Ba-Cu-O a-b plane.[17] We see for the ıree different directions a fast exponential decay with :anslational correlation lengths of 5(1), 6(1), and 8(1) verage nearest-neighbor spacings in the three directions ɔr the smaller-area image and 3.6(5), 4.6(5), and 7(1) verage nearest-neighbor spacings for the larger-area nage.

The longer translational correlation lies in the direcon of the longest reciprocal-lattice vector, which is roıted 90° from the longest real-space vortex spacing. In ıe larger-area image of Fig. 1, the longest reciprocalıttice vector is in a direction that is 31.6° counterclockise from the obvious line defect in the larger-scale imge in the lower right. As the ratios of the effective ıasses range between $m_a/m_b \approx 1.5$ and 2.2 for this ma:rial[18] we expect a distortion of the perfect hexagonal :al-space lattice by the ratio of penetration depths $\lambda_b/\lambda_a = (m_a/m_b)^{1/2} \approx 1.2$–1.5, with the long direction along ıe b axis.[17,19] We have x rayed the sample and find ıat the $Bi_{2.1}Sr_{1.9}Ca_{0.9}Cu_2O_{8+\delta}$ crystal a axis is rotated 1° counterclockwise from the defect with the fluxttice real-space direction rotated 2.5° counterclockwise om the defect. Then the b axis is rotated 83.9° clockise from the line defect. We conclude the defect is not ɔviously a twin boundary, for which this angle should : 45°. Of the three different reciprocal-lattice direcɔns, the direction of the shortest translational correlaɔn length is 6.7° clockwise from the b direction of the ttice. The closest real-space direction of the average ttice is 2.5° removed in angle from the defect as well, so that its effect on the order of the lattice seems to be quite local.

Figure 3 suggests several things. The first is that, while the translational order is decaying exponentially on a scale of (4–10)a, the orientational order is decaying only very slowly. A fit with an exponential decay for this curve yields an effective orientational correlation length of 250a. The second point is that the data are consistent with a power-law decay where $g_6(r)$ varies as $r^{-\eta_6}$ with the exponent η_6 having the value 0.06(1). We have analyzed in a similar fashion four regions on three different crystals. All gave similar results to that quoted above. For η_6 we have found the values of 0.06(1) and 0.06(2) from different places on sample 1 at 20 G, 0.05(2) from sample 2 at 80 G, and 0.30(5) from sample 3 at 10 G. For ξ we find 2.5(5), 3.2(5), 3(1), and 3.2(5) nearest-neighbor lattice constants for the four samples studied, as determined from the angularly averaged pair-correlation function $g(r)$. The larger value of η_6 found for the 10-G data suggests that as H_{c1} is approached, the lattice is more disordered with a more liquidlike response with shorter-range orientational order.

The present work needs to be compared and contrasted with previous magnetic decorations on high-T_c single crystals. Our early work[2] on both Y-Ba-Cu-O and Bi-Sr-Ca-Cu-O observed flux lattices which showed a tendency for triangular order, but *both* the positional and orientational order for those lattices was found to decay approximately exponentially with correlation lengths of a few lattice constants. In the present work, on much cleaner samples, the positional correlation length is similar to the previous work but the orientational length has increased dramatically. This suggests that for our best materials we are now in an intermediate regime of disorder for the lattices in these materials. Dolan *et al.*[12] have also seen very-high-quality flux lattices in both Y-Ba-Cu-O and Bi-Sr-Ca-Cu-O single crystals with real-space images similar to those presented here, suggesting long-range orientational order, although the type of quantitative analysis we have presented here has not yet been done on those images.

After the idea of a hexatic phase was first introduced by Nelson and Halperin,[9] the issue of disorder and the decay of positional and orientational order was discussed by a number of workers in a variety of contexts. Nelson, Rubinstein, and Spaepen[10] discussed the effects of disorder on the orientational and positional correlations in their simulations on planar arrays of spheres. They were the first to point out that random disorder couples much more strongly to positional than to orientational correlations.

Nelson and Halperin's theory[9] for 2D hexatics with thermal disorder, as opposed to those with the quenched-in disorder found here, indicate that the exponent η_6 should be 0.25 at the hexatic-to-fluid transition, decreasing to zero at the hexatic-to-crystal transition. This is consistent with observations in 2D col-

loidal[16] systems with thermal disorder. Simulations in systems of 2D arrays of hard spheres[10] with trapped random dislocations find a value of $\eta_6 = 9c/\pi$, where c is the fraction of dislocation cores. This relation was obtained through a cumulant expansion of $g_6(r)$ within continuum elastic theory. In our case if we take as an estimate of c the fractional area of Voronoi polyhedra in which there is net Burgers vector ($\sim 1.5\%$), then $\eta_6 \sim 0.04$, which is close to our observed result. This simple analysis shows that the dislocations are responsible for the large part of *both* the short-range positional order as well as the quasi-long-range orientational order.

The detailed nature of the low-temperature ordered phase is the subject of a recent paper by Chudnovsky.[7] In that work he suggests that in the limit of strong pinning disorder, the in-plane positional order of vortices should be only short ranged while the orientational order should be long ranged (infinite), leading to a hexatic vortex glass. However, in that work, dislocations were not explicitly put in. In work done simultaneously and independently by Marchetti and Nelson,[8] the effects of dislocation loops in the 3D vortex lattice of combination screw and edge character have been included. They suggest that, similar to Chudnovsky, the positional order should fall off exponentially and the orientational order will be long ranged. Within the framework of the present theoretical understanding, there are at least two ways one can understand our experimental observations. In the first scenario, the hexatic vortex glass which we see at low temperatures is a vestige of a high-temperature hexatic liquid state which then gets quenched in as the temperature is lowered due to the low mobility of the edge dislocations (or vortices). In the second scenario, favored by Chudnovsky, the hexatic glass is not a nonequilibrium vestige of a high-temperature state but is the true low-temperature ground state which is produced by the competition between disorder in the system and the repulsive interactions between the lines. At the moment it is not clear to us which scenario is the appropriate one.

In conclusion, we have presented data which we feel provide convincing evidence for the observation of a hexatic vortex glass in superconducting flux lattices in the high-T_c superconductor $Bi_{2.1}Sr_{1.9}Ca_{0.9}Cu_2O_{8+\delta}$. In this state the positional order falls off exponentially with a correlation length of a few lattice constants while the orientational order persists for hundreds of lattice constants and has algebraic long-range order.

The authors would like to thank G. J. Dolan, D. Fisher, M. P. A. Fisher, D. Huse, P. Littlewood, and D. Nelson for many stimulating discussions. Two of the authors would like to acknowledge support received from AT&T (D.B.M.) and the NSF (A.K.). This work was supported in part by the Joint Services Electronic Program under Grant No. N00014-84-K-0327 and by the Stanford Center for Materials Research through the NSF Department of Materials Research.

[1]A. C. Mota, A. Pollini, P. Visani, K. A. Müller, and J. G. Bednorz, Phys. Rev. B **36**, 4011 (1987).

[2]P. L. Gammel, D. J. Bishop, G. J. Dolan, J. R. Kwo, C. A. Murray, L. F. Schneemeyer, and J. V. Waszczak, Phys. Rev. Lett. **59**, 2592 (1987).

[3]D. R. Nelson, Phys. Rev. Lett. **60**, 1973 (1988); D. R. Nelson and S. Seung, Phys. Rev. B **39**, 9153 (1989).

[4]Y. Yeshurun and A. P. Malozemoff, Phys. Rev. Lett. **60**, 2202 (1988).

[5]P. L. Gammel, L. F. Schneemeyer, J. V. Waszczak, and D. J. Bishop, Phys. Rev. Lett. **61**, 1666 (1988).

[6]R. N. Kleiman, P. L. Gammel, L. F. Schneemeyer, J. V. Waszczak, and D. J. Bishop, Phys. Rev. Lett. **62**, 2331 (1989).

[7]E. M. Chudnovsky, Phys. Rev. B **40**, 11 355 (1989).

[8]M. C. Marchetti and D. R. Nelson, Phys. Rev. B **41**, 1910 (1990).

[9]B. I. Halperin and D. R. Nelson, Phys. Rev. Lett. **41**, 121 (1978); D. R. Nelson and B. I. Halperin, Phys. Rev. B **19**, 2457 (1979).

[10]D. R. Nelson, M. Rubinstein, and F. Spaepen, Philos. Mag. A **46**, 105 (1982).

[11]D. R. Harshman, R. N. Kleiman, D. Mitzi, and A. Kapitulnik (to be published).

[12]G. J. Dolan, G. V. Chandrasekar, T. R. Dinger, C. Field, and F. Holtzberg, Phys. Rev. Lett. **62**, 827 (1989).

[13]D. B. Mitzi, L. W. Lombardo, A. Kapitulnik, S. S. Laderman, and R. D. Jacowitz, Phys. Rev. B **41**, 6564 (1990).

[14]D. H. Van Winkle and C. A. Murray, J. Chem. Phys. **89**, 3885 (1988).

[15]F. F. Preparata and M. L. Shamos, *Computational Geometry: An Introduction* (Springer-Verlag, New York, 1985).

[16]C. A. Murray, D. H. Van Winkle, and R. A. Wenk, "Phase Transitions" (to be published); C. A. Murray, W. O. Sprenger, and R. A. Wenk (to be published).

[17]G. J. Dolan, F. Holtzberg, C. Field, and T. R. Dinger, Phys. Rev. Lett. **62**, 2184 (1989).

[18]S. Martin, A. T. Fiory, R. M. Fleming, L. F. Schneemeyer, and J. V. Waszczak, Phys. Rev. Lett. **60**, 2194 (1989); S. Martin (private communication).

[19]L. J. Campbell, M. M. Doria, and V. G. Kogan, Phys. Rev. B **38**, 2439 (1988).

SQUID Picovoltometry of $YBa_2Cu_3O_7$ Single Crystals: Evidence for a Finite Temperature Phase Transition in the High Field Vortex State

P.L. Gammel, L.F. Schneemeyer and D.J. Bishop

AT&T Bell Laboratories
Murray Hill, New Jersey 07974

ABSTRACT

Using a SQUID picovoltmeter, we have measured current-voltage curves of $YBa_2Cu_3O_7$ microtwinned crystals as a function of temperature in fields from 1 to 6 Tesla. The data constitute evidence for a finite temperature phase transition in the vortex state. Exponents derived within the framework of the vortex glass model are found to be similar to thin film values. Strongly temperature dependent correlations, involving up to 10^5 vortices near the transition, combined with the qualitative failure of thermal activation models to fit our data support the existence of a phase transition.

PACS numbers: 74.60.Ge, 74.70.Vy

SQUID Picovoltometry of $YBa_2Cu_3O_7$ Single Crystals: Evidence for a Finite Temperature Phase Transition in the High Field Vortex State

P.L. Gammel, L.F. Schneemeyer and D.J. Bishop

AT&T Bell Laboratories
Murray Hill, New Jersey 07974

The statics and dynamics of fluxoids in the mixed state of the high temperature superconductors have generated intense interest and controversy. This is for two important reasons. First, an understanding of vortex interactions may help in obtaining high critical currents. Second, the mixed state is an excellent system in which to probe the decay of positional and orientational correlations and the nature of phase transitions in the presense of disorder.

The first evidence for unconventional behavior of the flux lattice in $YBa_2Cu_3O_7$ (YBCO) came from measurements of the decay of magnetization. An irreversibility line was found[1] which was associated with thermally activated depinning of single flux lines[2]. High-Q mechanical oscillator measurements[3], suggested a more controversial interpretation, namely a melting transition from an ordered phase into a high temperature flux liquid. The high temperatures, short coherence lengths and large $\hat{c}-$axis anisotropies were postulated to increase the importance of thermal fluctuations to allow a melting transition resembling that seen in two-dimensional superconducting films[4,5]. A phase transition in three dimensions is also predicted by Lindemann theories[6,7] and models of entangled flux liquids[8].

These simple phase transition models fail[9] to incorporate the disorder which leads to pinning. Larkin and Ovchinnikov[10] showed that disorder leads to the

destruction of long range positional order in the flux lattice in all dimensions less than four. Hence, in three dimensions, pinning should dominate. An extensive literature explaining transport data in terms of thermally activated flux-flow (TAFF) and flux creep has emerged[11]. These models postulate the existence of a finite resistivity for all T>0 and only weakly temperature dependent crossover currents for the onset of nonlinearities.

More recently disorder has been included in theories which do involve a phase transition. Following the work of Ebner and Stroud[12], Fisher et al[13] have postulated a vortex glass transition. Alternatively, Marchetti and Nelson[14] have examined the entanglement model with disorder, drawing an analogy to polymer glasses. In both theories, a phase transition is signaled by the vanishing of the zero frequency resistance. Koch et al[15] have analyzed thin film I-V curves in terms of the vortex glass model, although the strength of their scaling has been criticized[16]. A phase with orientational order only-such as an hexatic-may also be stable in some part of the phase diagram[17]. Worthington et al[18] have measured I-V curves on single crystal YBCO which they use to argue for the presence of an hexatic at high temperatures with a quasi-first order melting transition into an ordered phase at lower temperatures.

In this letter we report on I-V curves of YBCO in fields of 1 to 6 Tesla applied parallel to the $\hat{c}$-axis with sub-picovolt resolution. It was our reasoning that I-V curves at and near linear response at the picovolt level would provide the largest testable differences between the various theories. Our measurements of the temperature dependence of both the linear response resistivity and onset of nonlinear response strongly constrain theoretical fitting parameters and have allowed us to rule out a class of thermal activation models.

In our experiment, voltages were measured using a modified BTI[19] SQUID voltmeter. To adapt to the high temperatures involved, we used an input circuit consisting of NbTi wires soldered to a silver backbone and embedded in an epoxy and copper housing. The temperature gradient from 4K to the sample temperature was designed to occur over the final 3cm of the SQUID input circuit. The field gradients for the high field magnet were engineered in conjunction with magnetic shielding to minimize the fields on the input circuit. With the sample chamber at 100K, and an applied field of 6 telsa, the SQUID noise corresponded to a sensitivity of $1\text{pV}/\sqrt{\text{Hz}}$. Owing to a contact resistance of $\sim 1\Omega$ with this sample, the experimental noise was $7\text{pV}/\sqrt{\text{Hz}}$. With a typical bandwidth of .01Hz, this gave us a sub-picovolt measurement capability.

The sample is identical to one used in a previous report by Palstra et al[11]. It is a thin slab 2mmx1mmx20μm with voltage leads 1mm apart. The thin direction is the $\hat{c}-$axis. The crystal is heavily twinned in the ab plane. The zero field superconducting transition is sharp in our measurement, with the resistance dropping by approximately two decades per 0.1K over the range $0.5 > R/R_N > 10^{-6}$. The normal state resistivity of $64\mu\Omega-$cm is further evidence for the high quality of this sample. With a T_c in zero field of 88.033K, however, the transition is suppressed from optimal. For $R/R_N > 10^{-2}$ the data are identical to those reported earlier[11].

The basic data consist of two types. At each field, a series of isothermal I-V curves, as shown in the inset to fig. 3, constitute the bulk of the data. These curves were taken in two ways, which gave identical results. In the first, the voltage was measured at discrete current intervals. In the second, linear current sweeps of 1000 sec each were pieced together and averaged to cover the current range. In both types of measurement,

the effective system bandwidth was .01Hz. A second type of measurement, in which the current was square wave chopped at .001Hz, with lockin detection, was used to determine the linear response value of the resistance for those data sets where the I-V curves showed a linear range. This value was always equal, within experimental errors, to the value obtained by fitting the linear part of the I-V curve. The current range over which this was applicable forms an integral part of the discussion of the data below.

We will focus on the data at 6.0 Tesla. Data at other fields are similar, except as explicitly noted. The curves in the inset to fig. 3, separated by approximately 0.1K, show a crossover from linear to non-linear behavior as the current is increased. In fig. 1, the crosses indicate the temperature dependence of the linear response data. The inverse logarithmic temperature derivative of R/R_N is displayed, where R_N is the linear extrapolation with temperature of the normal state resistance. This quantity has a straightforward interpretation within several models of fluxoid dynamics and will be used as a test of their validity. A linear plot of R/R_N vs. T shows the same qualitative features, including a shoulder at $R/R_N \sim 0.2$, as noted previously[18]. The dashed line is our simulation of the TAFF model suggested by Griessen[16]. In his model, complexity is introduced in two ways. First, the sample is envisioned as a parallel summation of channels with different activation energies, with a distribution defined by a log-normal curve. In addition, each channel is shunted by a Bardeen-Stephen term. Despite this, the dashed line in fig. 1, which arises from the linear response part of our simulations[21] of his theory, is indistinguishable from $e^{-U/kT}$. There is clear disagreement with the data. The disagreement with other TAFF models[16] is equally severe.

However, a good fit to our data is found within the framework of the vortex glass model[13]. In the scaling regime of this model, the resistance should vanish as $R \sim (T-T_g)^{\nu(z-1)}$. This implies that the plot shown in fig. 1 of $(\partial \ell n R/\partial T)^{-1}$ vs. T should be a straight line which extrapolates to zero at T_g with a slope $1/\nu(z-1)$. The data shown in fig. 1 give $T_g = 74.0K$ and $\nu(z-1) = 6.5$. Another way of fitting this data, shown in fig. 2, is $\log(R/R_N)$ vs. $\log(T-T_g)$. For a proper choice of T_g, the solid points should lie on a straight line with slope $\nu(z-1)$. The values thus determined are consistent with fig. 1 and give overall $T_g = 74.0 \pm 0.2K$ and $\nu(z-1) = 6.5 \pm 1.5$. Deviations from scaling set in $\sim 3K$ above T_g. For other fields, not shown, the width of the scaling region is reduced roughly in proportion to $T_c - T_g$, where T_c is the zero field transition temperature.

For the nonlinear data, the simplest fit is again shown in the inset in fig. 1. The average power law fit to the I-V curve over the ranges $10^{-6} > V > 10^{-7}$ (solid symbols) and $10^{-7} > V > 10^{-8}$ (open symbols) is shown. As the voltage scale is reduced, the deviations from linearity are pushed to lower temperature and become more abrupt. For vortex glass scaling, at $T = T_g$ one has $V \sim J^{(z+1)/2}$. While extrapolation with temperature to T_g is difficult, we estimate $z = 3.4 \pm 1.5$ from these data, comparable to what is presented below. We define a crossover current J_{sc} from V/IR=2. Normalizing to $J_o = J_{sc}(74.811K) = 2.5 \times 10^3 A/m^2$, the data are shown in fig. 2 as the open symbols. The onset of nonlinearities with current defined by a TAFF model is simply $J_{sc} \sim T$, which is a constant over the range fig. 2 and clearly disagrees with the data. Within the vortex glass model the crossover current vanishes at the transition as $J_{sc} \sim (T-T_g)^{2\nu}$, which is the straight line shown in the figure. This gives $\nu = 2.0 \pm 1$. Note the remarkable

temperature dependence of J_{sc}, which varies by a factor of ~50 over less than 3K in temperature at 75K. This is extremely difficult to generate within a flux creep or flow scenario. Following Fisher et al[13], we may use this current to define a length scale via $\xi_d = (ck_B T/\phi_o J)^{1/2}$. This is the length scale over which the current J can affect thermal distributions. At our lowest temperature $\xi_d \sim 15\mu m$ implying cooperative motion of $\sim 10^5$ vortices. This length scale is almost a factor of 50 larger than that extracted by Koch et al[15] from their thin film work. The exponent ν from our nonlinear data can be combined with our linear response data to give $\nu = 2 \pm 1$ and $z = 4.3 \pm 1.5$ within the framework of the vortex glass theory. At a field of 4.0 Tesla, Koch et al. found $\nu = 1.8$ and $z = 4.7$.

Within the vortex glass theory, for $T > T_g$ the linear response resistance R and the crossover current J_{sc} can be used to scale all the I-V curves as shown in fig. 3. For those data sets with $\frac{V}{IR} > 4$, R could not be determined from the data, and were chosen to make the plot in fig. 3 a smooth curve. These values were consistent with the vortex glass scaling hypothesis for both the vanishing of the resistance and the current scale. Shown for comparison are the functional forms extracted from TAFF (solid line) which is simply $\sinh(J/J_o)$ and the scaling function found by Koch et al[15] (open circles). The curves were adjusted to agree at $\frac{V}{IR} = 8$. As already stated, the data show a significant qualitative departure from TAFF. Here, however, we also find differences from other data used to advocate a vortex glass transition. Three reasons could account for this departure. First, the thin film data of Koch et al focused on large nonlinearities. Their scaling was least accurate near linear response, where this comparison is made.

Alternatively, both data sets may be correct, and the difference in ξ_d may represent a different scaling function for crystals as opposed to films. Of course, it may be that the dependence of the scaling function on sample points to a failure of the vortex glass hypothesis.

Shown in fig. 4 is our composite phase diagram for the vortex state of YBCO. H_{c2} was taken from Welp et al[23], shifted to agree with our zero field T_c. The solid symbols are derived from fits to the vortex glass hypothesis. The prediction of the vortex glass model for this phase diagram is shown by the solid line, $H_g \sim (T_c - T_g)^{4/3}$. This arises from the zero field temperature dependence of the coherence length in the fluctuation regime. Mean field theory would give a linear $T_g(H)$, which is shown by the dashed line. In this case, even near zero field there could be a transition below T_c. Such an effect has been noted in low field magnetization data[24]. More extensive low field experiments are required to resolve this dilemma.

In conclusion, we have used a SQUID based picovoltmeter to measure the I-V curves of microtwinned YBCO crystals at and near linear response. The data represent significant evidence for a finite temperature phase transition in the vortex state. At our lowest temperature, the current scale for nonlinearities implies a coherence length $\xi_d \sim 15\mu m$ for vortex motion. Such a coherence volume incorporates $\sim 10^5$ vortices, which strongly suggests that only many particle theories with a phase transition will be able to explain our results. Our data significantly disagree with the predictions of present TAFF theories. Much of the data can be described within the framework of the vortex glass model with $\nu = 2 \pm 1$ and $z = 4.3 \pm 1.5$. However, departures from earlier data with respect to the scaling function leave open questions as to the details of this model.

We would like to thank D.A. Huse, D. Nelson, D.S. Fisher, S. Coppersmith, A.F. Hebard, T.A. Worthington, B. Battlogg and P.B. Littlewood for numerous helpful discussions. We would like to thank R. Koch for sending us details of his fits to the scaling function and R. Griessen for responding to our questions about his thermal activation model.

REFERENCES

[1] K.A. Muller, M. Takashige and J.G. Bednorz, Phys. Rev. Lett. 58, 1143 (1987). A.P. Malozemoff et al., Phys. Rev. B38, 7203 (1988).

[2] Y. Yeshurun and A.P. Malozemoff, Phys. Rev. Lett. 60, 2202 (1988).

[3] P.L. Gammel et al., Phys. Rev. Lett. 61, 1666 (1988). R.N. Kleiman et al., Phys. Rev. Lett. 62, 2331 (1989).

[4] B.A. Huberman and S. Doniach, Phys. Rev. Lett. 43, 950 (1979). D.S. Fisher, Phys. Rev. B22, 1190 (1980).

[5] P.L. Gammel, A.F. Hebard and D.J. Bishop, Phys. Rev. Lett. 60, 144 (1988).

[6] M.A. Moore, Phys. Rev. B39, 136 (1989).

[7] A. Houghton, H.A. Pelcovits and A. Sudbo, Phys. Rev. B40, 6763 (1989).

[8] D.R. Nelson, Phys. Rev. Lett. 60, 1973 (1988). D.R. Nelson and H.S. Seung, Phys. Rev. B39, 9153 (1989). D.R. Nelson, J. Stat. Phys. 57, 511 (1989). M.C. Marchetti and D.R. Nelson, Phys. Rev. B41, 1910 (1990). L. Xing and Z. Tesanovic, Phys. Rev. lett. 65, 794 (1990).

[9] E.H. Brandt et al., Phys. Rev. Lett. 62, 2330 (1989).

[10] A.I. Larkin and Yu. N. Ovchinnikov, J. Low Temp. Phys. 34, 409 (1979).

[11] T.T.M. Palstra et al., Phys. Rev. Lett. 61, 1662 (1988). M. Tinkham, Phys. Rev. Lett. 61, 1658 (1988). M. Inui, P.B. Littlewood and S.N. Coppersmith, Phys. Rev. Lett. 63, 2421 (1989). C.W. Hagen and R. Griessen, Phys. Rev. Lett. 62, 2857

(1989).

[12] C. Ebner and D. Stroud, Phys. Rev. B31, 165 (1985). S. John and T. Lubensky, Phys. Rev. B34, 4815 (1986).

[13] M.P.A Fisher, Phys. Rev. Lett. 62, 1415 (1989). D.S. Fisher, M.P.A. Fisher and D.A. Huse, submitted to Phys. Rev. B (1990).

[14] M.C. Marchetti and D. Nelson, submitted to Phys. Rev. B (1990).

[15] R.H. Koch et al., Phys. Rev. Lett. 63, 1511 (1989). R.H. Koch, V. Foglietti and M.P.A Fisher, Phys. Rev. Lett. 64, 2586 (1990).

[16] R. Griessen, Phys. Rev. Lett. 64, 1674 (1990); S.N. Coppersmith, M. Inui and P.B. Littlewood, Phys. Rev. 64, 2585 (1990); S. Martin and A. Hebard, to be published.

[17] C.A. Murray et al., Phys. Rev. Lett. 64, 2312 (1990).

[18] T.K. Worthington, F. Holtzberg and C.A. Field, Cryogenics 30, 417 (1990).

[19] Biomagnetic Technologies Inc., U.S.A.

[20] P.L. Gammel et al., Phys. Rev. B41, 2593 (1990).

[21] The dashed line in fig. 1 is calculated using Griessen's expression (ref.16) with B=6.0T, $U_o^*=85$meV, $\gamma=1.4$, $A=3\times10^{-10}$, $S_o=4\times10^{-7}$ and $\rho_n=6.4\times10^{-7}\,\Omega$m. For $U_o^*=30$meV, a more realistic value, the disagreement with the data is even more severe.

[22] S.R. Nagel and P.K. Dixon, J. Chem. Phys. 90, 3885 (1989).

[23] U. Welp et al., Phys. Rev. Lett. 62, 1908 (1989).

[24] H. Safar et al., submitted to Phys. Rev. Lett. (1990).

FIGURE CAPTIONS

Fig. 1. The inverse logarithmic derivative of the resistivity should vanish in any model with a phase transition. The vortex glass is represented by the solid line. The dashed line is the prediction of the TAFF model as formulated by Griessen (ref. 16). In the inset, the power law slope of the I-V curve is shown for two voltage ranges--$10^{-8} < V < 10^{-7}$ (O) and $10^{-7} < V < 10^{-6}$ (O).

Fig. 2. Fits to the vortex glass theory for the 6 Tesla data. The solid symbols are the linear resistivity with $R_N = .064\Omega$. The open symbols are the current where V/IR=2 with $J_o = 2.5 \times 10^3$ A/m^2.

Fig. 3. The scaled data (points). For comparison are the scaling function of Koch et al (open symbols) and the prediction of TAFF (line) are shown. The inset shows the I-V curves at constant temperature for the 6.0T data. The curves are spaced by approximately 0.1K, excluding 74.377K.

Fig. 4. The phase diagram for the vortex lattice. H_{c2} is taken from estimates of Welp et al. T_c is taken from the zero field resistive transition, which is sharp on this scale. The solid line is a 4/3 power law fit to the data. The dashed line is a linear fit.

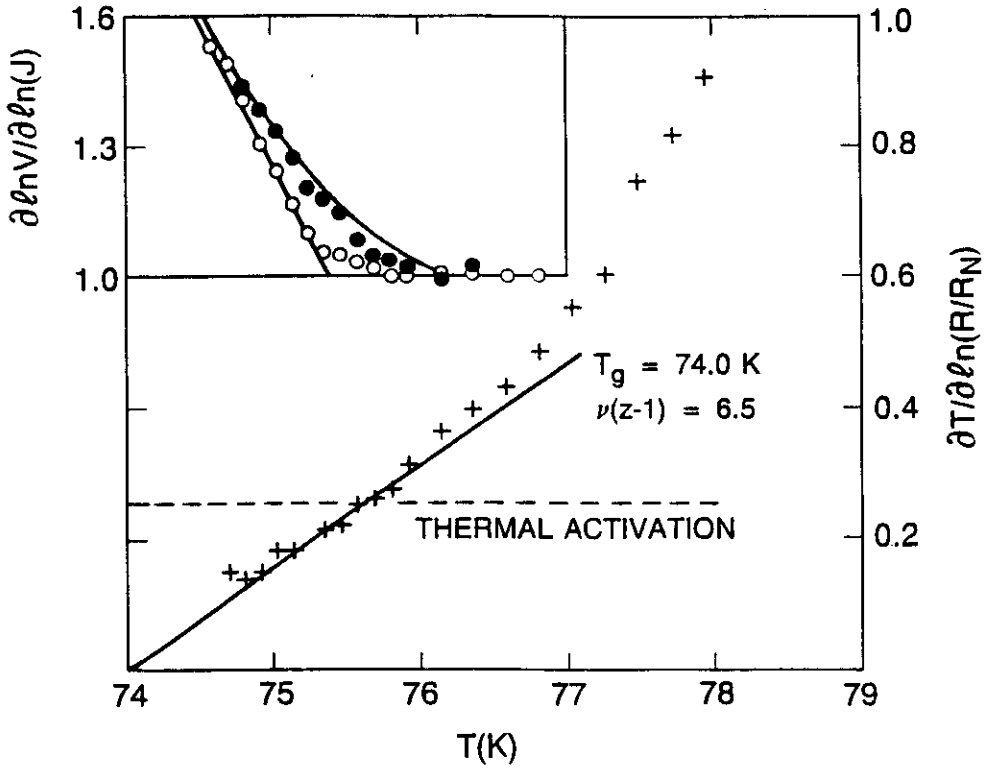

FIGURE 1

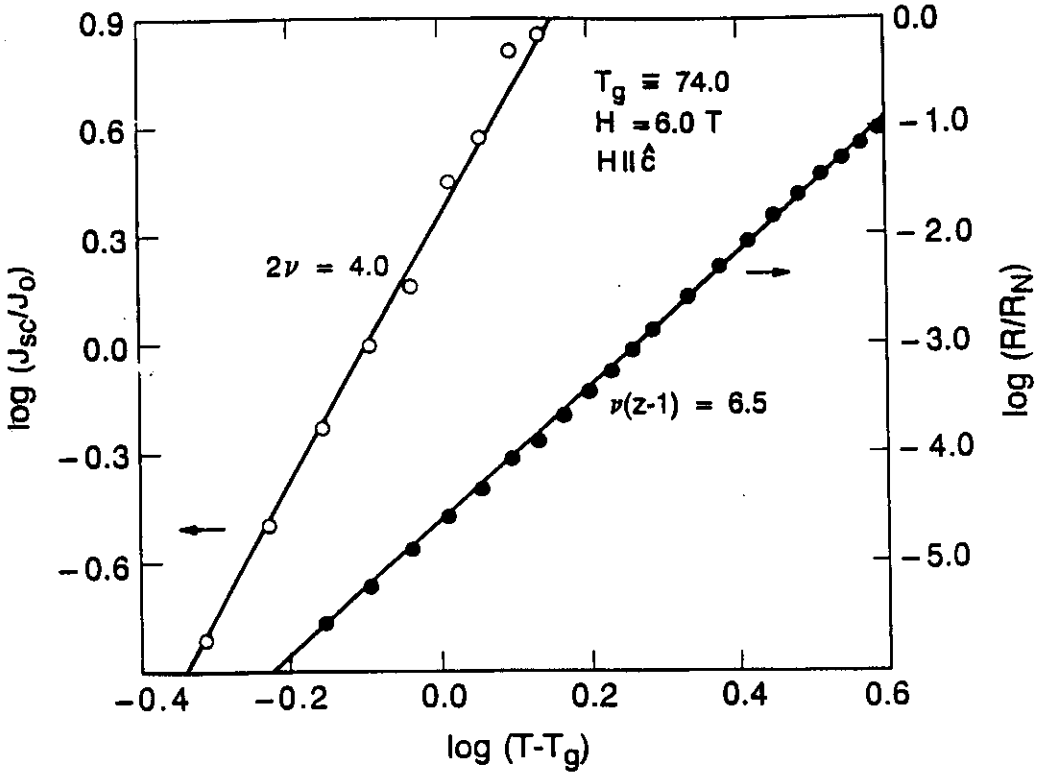

FIGURE 2

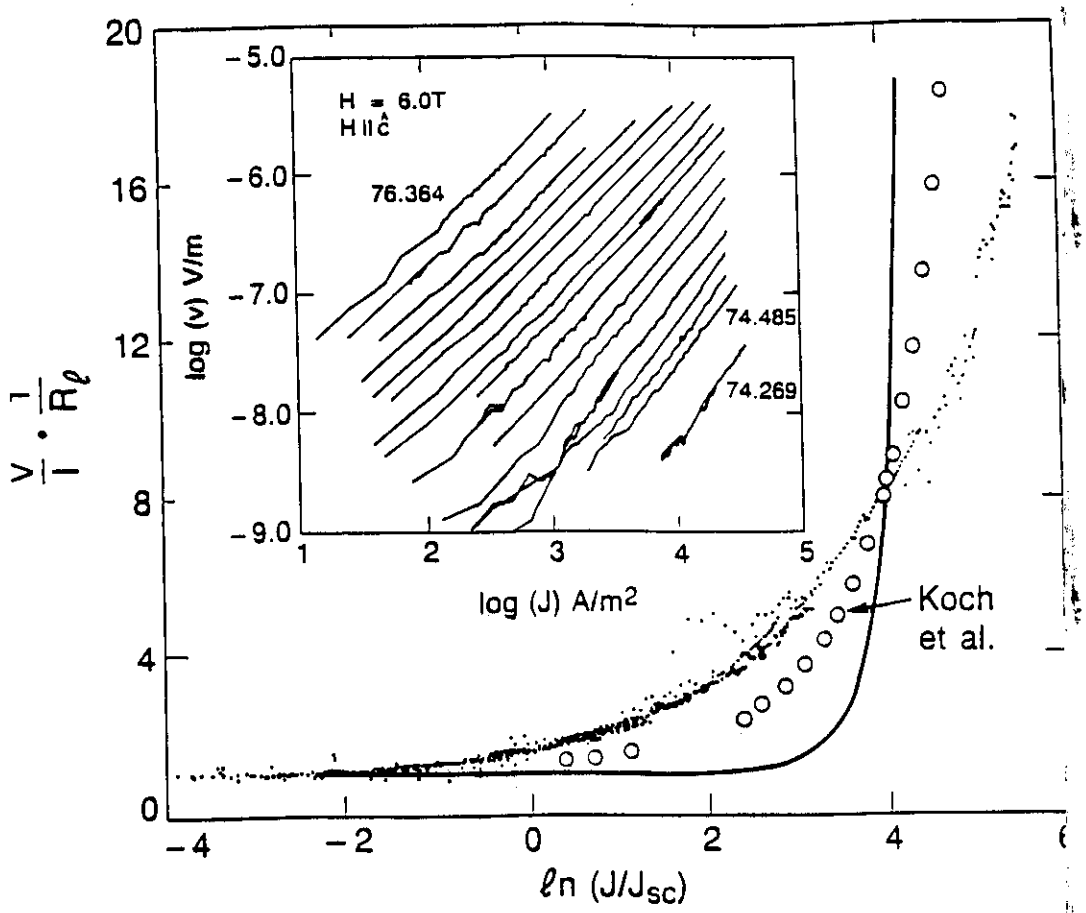

FIGURE 3

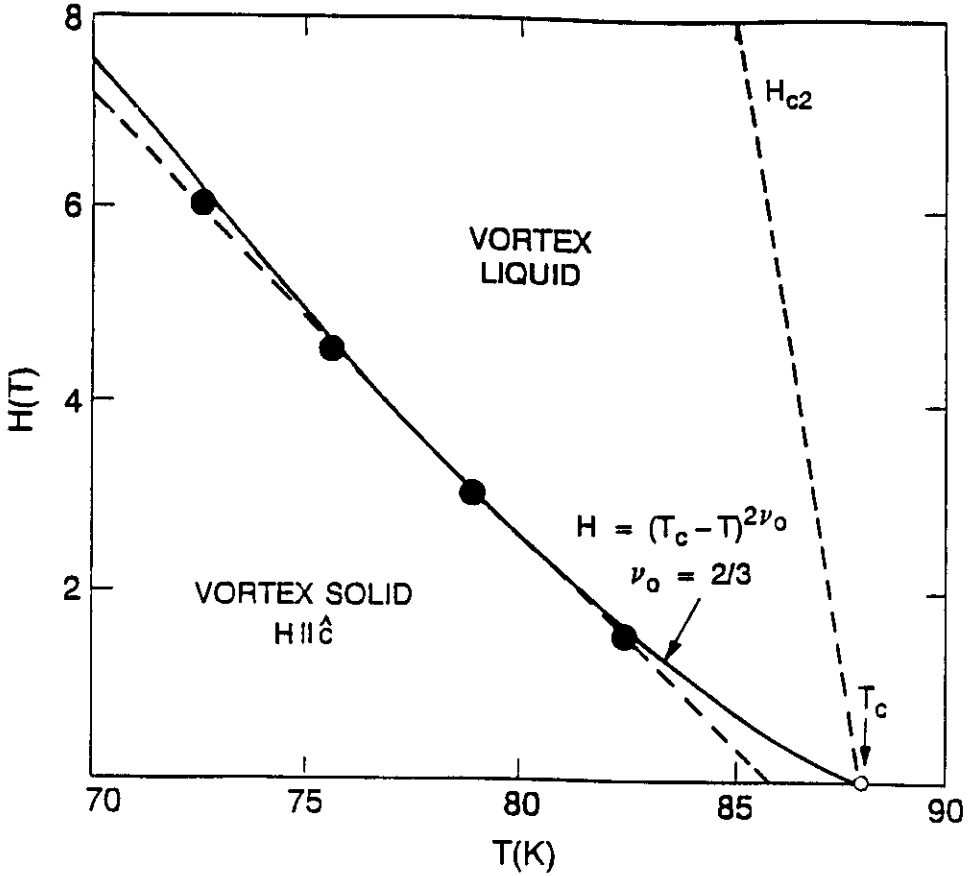
8
6
4
2
H(T)
70
75
80
85
90
T(K)
H_{c2}
VORTEX
LIQUID
$H = (T_c - T)^{2\nu_o}$
$\nu_o = 2/3$
VORTEX SOLID
$H \parallel \hat{c}$
T_c

FIGURE 4

TRANSLATIONAL AND BOND-ORIENTATIONAL ORDER IN THE VORTEX LATTICE OF THE HIGH-Tc SUPERCONDUCTOR $Bi_{2.1}Sr_{1.9}Ca_{0.9}Cu_2O_{8+\delta}$

D. G. Grier, C. A. Murray, C. A. Bolle [a], P. L. Gammel, and D. J. Bishop

AT&T Bell Laboratories
Murray Hill, New Jersey 07974

David Mitzi [b], and A. Kapitulnik

Stanford University
Stanford, California 94305"

ABSTRACT

We have investigated the microscopic ordering of the flux lattice in the mixed state of $Bi_{1.9}Sr_{2.1}Ca_{0.9}Cu_2O_{8+\delta}$ near H_{c_1} by image analysis of Bitter decorated samples. We observe a dramatic transition from strong isotropic disorder to hexatic order with increasing magnetic field. This transition occurs at a lower applied magnetic field for samples which are annealed in oxygen.

PACS Nos. 74.60.Ge, 74.70.Vy

12/4/90

[a] Present address: Instituto Balseiro, 8400 Bariloche, Rio Negro, Argentina.
[b] [b] Present address: IBM T. J. Watson Research Center, Yorktown Heights, New York 10598

Layered copper-oxide superconductors have a combination of properties not seen in conventional type-II superconducting materials including short superconducting coherence length, long magnetic penetration depth, very high mass anisotropy, and high critical temperature. The resulting rich and novel phenomenology has sparked considerable experimental and theoretical effort. One area which has received attention is the nature of the ordering of the magnetic flux lattice in the mixed state[1]. Measurements of bulk properties such as mechanical dissipation[2], transport[3], and magnetization[4], have been interpreted in light of the various predicted phase diagrams which include exotic new states of the vortex lattice including flux melting[5] [6], entangled flux liquids[7], hexatic flux liquids[8], and hexatic[9] vortex glasses[10]. However, these experimental techniques do not probe the microscopic order which not only differentiates among the proposed configurations, but also exposes the relevant physics of vortex pinning and entanglement.

In this Letter, we report observations of the development of long-range translational and bond-orientational microscopic order in the flux lattice of single crystal $Bi_{2.1}Sr_{1.9}Ca_{0.9}Cu_2O_{8+\delta}$ as a function of applied magnetic fields. Our experiments probe the region of the phase diagram at low applied fields between $H = H_{c_1}$ (for our demagnetization factor $H_{c_1} \approx 0.5G$) at which vortices are infinitely separated, and $H = B_{c_1}$ where the intervortex separation $a \sim 0.5$ μm becomes comparable to the in-plane magnetic penetration depth, $\lambda_{\parallel}$. In particular, we observe an abrupt transition from strong isotropic disorder to a phase with hexatic order. For oxygen-annealed samples, this transition shifts dramatically to lower fields.

Our single crystal BSCCO [2212] samples were prepared with a directional solidification technique described elsewhere[11]. Typically, they are rectangular slabs of width $w \approx 1$mm and thickness $d \approx 10-30\mu$m with the c-axis aligned along the short direction. Some samples were subsequently annealed at 600°C in 1 atm of oxygen for 24 hours and then quenched to room temperature while the rest were examined as made. Magnetization measurements of the unannealed samples indicate homogeneous bulk superconductivity with onset at $T_c = 88.5$ K and a transition width (10-90%) of 5 K. The annealed samples have onset temperatures ranging from 85.5 K to 86.5 K with transition widths of 2 K. X-ray diffraction shows that the lattice spacing along the c-axis shrinks from 30.89(1) Å to 30.80(1) Å after annealing, while the a and b spacings remain constant at 5.413(2) Å and 5.411(3) Å, respectively. High resolution XPS of the O_{1s} core levels shows that additional oxygen not only fills oxygen vacancies in the Bi-O plane, but also enters the lattice at other points. This structural change may affect the carrier mass anisotropy characteristic of layered superconductors. Torque magnetometry[12] indicates $\Gamma = (m_c/m_a)^{1/2} = 55$ for our unannealed samples. The measured room-temperature resistivity anisotropy[13] of our samples changes by less than 10% with annealing suggesting that oxygen annealing does not decrease Γ appreciably. While changes in Γ might be offset in these measurements by compensating changes in the carrier concentration and scattering time anisotropy, this is unlikely. Muon spin resonance[14] indicates that the a-b in-plane penetration depth is approximately $\lambda_{\parallel} \approx 0.30\mu$m. Assuming a superconducting coherence length of $\xi \approx 15-20$Å, the Ginzberg-Landau parameter $\kappa = \lambda_{\parallel}/\xi \approx 200$.

Twenty specimens cleaved in air along the Bi double layer were cooled immediately to 4.2 K in vacuum in applied magnetic fields ranging from 5 G to 100 G oriented normal to the superconducting a-b planes. Flux lines trapped in the samples are then located using the Bitter decoration technique[15] in which a Brownian "smoke" of ~50 Å diameter ferromagnetic Fe particles drifts through He buffer gas along magnetic field gradients to the surface. Particles reaching the surface are held in place by Van der Waals forces and are observed with a scanning electron microscope (SEM) after warming to room temperature. Samples reached a temperature of ~5K during the 1 second required for decoration. Two samples were decorated simultaneously to ensure uniform decorations.

It is important to realize that these field-cooled decoration experiments do not measure the equilibrium configuration of the vortices at 5K where the decoration takes place, but instead a configuration quenched in at a higher temperature, $T_f(H)$, where the microscopic configuration goes out of equilibrium. In the low density limit, we will assume this happens when vortices become individually, rather than collectively, pinned. At present there are no microscopic measurements of T_f. Macroscopic magnetization becomes irreversible for samples similar to those in our study, at a temperature T_{irr} that has been measured[16] to be very close to T_c at low applied fields ($T_{irr} = 0.99T_c$ at H = 5 G and $T_{irr} = 0.90T_c$ at H = 100G.) Bitter imaging experiments[17] on BSCCO in an applied field of 20G at ~15K, however, show vortex motion on the order of 1 μm during the 1 second required for decoration. Thus some thermal motion is taking place even at 15K, presumably due to the very weak pinning strengths in BSSCO, so that the configurations we observe are remnants of the equilibrium configuration at

$T_f \approx 15K < T_{irr}$.

At the highest magnetic fields of our study, particle interactions sometimes produce spurious pairs and even chains of particles. Such regions were avoided in our analysis. Some samples displayed "stripe" decoration features in which unusually large numbers of particles clump along straight lines extending across the sample. Preliminary high-resolution transmission electron microscope studies suggest that stripes may occur along boundaries between crystalline domains whose a- and b-axes are rotated by 90°. No twinning is observed in x-ray diffraction, however, so that these domains or stacking faults may occur below x-ray detectable levels. Since stripes affect the ordering of the neighboring vortex lattice, we only examined regions without them.

We have shown previously[18] for YBCO that the vortex density is $n_o = H/\phi_o$ to within experimental error. We find this to be true for the BSSCO samples as well. For this study, we digitized 42 SEM photographs of Bitter decorations using a video frame grabber at a resolution of 512 by 480 pixels and a dynamic range of 256 gray levels. Two or three pictures were taken near the center of each sample from regions separated by more than 500 μm. A typical digitized image contains approximately 4000 decoration clusters separated by approximately 8 pixels. SEM photographs of Bitter decorations of annealed samples at 69G, 23G, and 8G appear in Figures 1 (a), (b), and (c), respectively. The locations of the clusters were then determined to one pixel accuracy using an image processing technique described previously.[19] Gradients in the vortex density across images were determined to be less than 0.5%. Experimental uncertainty in vortex location arises both because of the irregular shapes of some clusters and also because of the inherent difficulty in placing a triangular lattice in registry with a square grid.

Figures 1 (d), (e), and (f) show Delaunay triangulations[20] for the images in Figures 1 (a), (b), and (c), respectively. Each vortex core is represented by a vertex in the triangulation, with bonds drawn to all nearest neighbor vortices. Triangles bordering topological defects such as disclinations (non 6-fold coordinated vortices) and edge dislocations (5-7-fold disclination pairs) in the vortex lattice are shaded. These triangulations and the pair correlation functions, g(r), calculated for the centers of the vortices, Figures 1 (g), (h), and (i), embody the major qualitative results of this Letter. At an applied field of 8G, the vortex density is $n_o = 0.75\mu m^{-2}$ and the vortex lattice is throroughly disordered. As the vortex density increases to 1.91 μm^{-2} (11G), much of the disorder abruptly vanishes, leaving only small concentrations of bound and unbound edge dislocations piercing the sample surface. The presence of free dislocations suggests that the flux lattice is hexatic under these conditions[21]. As the vortex density increases to 5.77 μm^{-2} (69G), we readily find defect-free regions extending beyond the experimental field of view. The increase in long-range order with increasing vortex density is also reflected in the g(r).

Above the disorder - hexatic transition, we observe a low density of unbound edge dislocations which decreases with increasing applied field. To further elucidate the development of long-range order in the vortex lattice, we have calculated the bond-orientational and translational correlation functions for the measured sets of vortex locations. The translational correlation function[22], $g_{\vec{G}}(r)$, is calculated from the order parameter for each site i: $\psi_{\vec{G}}(\vec{r_i}) = \exp(i\vec{G}\cdot\vec{r_i})$, where $\vec{G}$ is a first reciprocal lattice vector obtained from the power spectrum of the vortex locations. Figure 2 (a) shows

$g_{\vec{G}}(r)$ for the images in Figure 1. We have fit the correlation functions to a simple exponential decay[23] $g_{\vec{G}}(r) \sim \exp(-r/\xi_{\vec{G}})$ with correlation lengths $\xi_{\vec{G}}$ ranging from $1a$ for the 8 G sample to approximately $20a$ in the 69G example. The resolution limit for our imaging system is approximately $50a$ as determined by performing the same analysis on digitized perfect hexagonal lattices with random displacements of points by up to two pixels as would be expected from both registry and digitization errors.

Figure 3 (a) shows the range of correlation lengths measured for the least disordered spot on each sample with three different directions of $\vec{G}$ versus applied magnetic field for both annealed and unannealed samples. In both cases, the translational order is increasing with increasing magnetic field and shows no sign of saturating. Although the data points are scattered, their trend is reasonably consistent with the linear increase in correlation length with applied field predicted by Chudnovsky [23].

The 6-fold bond orientational order parameter at vortex location i is defined as $\psi_6(\vec{r_i}) = n_i^{-1} \sum_{j \varepsilon <nn>_i} \exp(i6\theta_{ij})$ where $<nn>_i$ is the set of n_i nearest neighbors and θ_{ij} is the angle made by the bond from site i to site j with respect to a fixed axis. The correlation function for this order parameter, $g_6(r)$, is plotted in Figure 2 (b) for the samples at 8G, 23G, and 69G. The solid lines are fits to the algebraic form $g_6(r) \sim r^{-\eta_6}$. The 23G sample has long range orientational order ($\eta_6 = 0.09$) while its translational order falls off rapidly ($\xi_{\vec{G}} \approx 3a$). This is the definitive signature of the hexatic phase. The 69G sample has both longer-range translational and orientational order, and no topological lattice defects within our sampling area. This is the most ordered vortex lattice we have observed for high T_c superconductors. The exponents, η_6, for the

samples selected for Figure 3 (a) appear in Figure 3 (b). The dashed line at $\eta_6 \approx 0.06$ shows the limit of our experimental resolution, determined by imaging a perfect hexagonal lattice, below which we can say that a sample has developed long-range orientational order, or $g_6(r) \rightarrow$ const.

For samples with $2a < \xi_{\vec{G}} < 10a$, the measured valued of $\xi_{\vec{G}}$ and η_6 are consistent with the measured density of edge dislocations, suggesting that topological defects determine the order in this regime. We note that the theories of vortex lattice melting[6][10] and glass transitions[10][23] which include only elastic interactions do not include the possibility of such topological defects.

For samples at higher fields with $10a < \xi_{\vec{G}} < 20a$, $\xi_{\vec{G}}$ is considerably smaller than the average distance between dislocations. Indeed, we see essentially no topological defects within the imaging area of 65 x 60 vortices. Suppression of $\xi_{\vec{G}}$ in this regime is caused by random lattice displacements which reflect random pinning and remnants of thermal motion above the microscopic quenching temperature, T_f, and experimental decoration inaccuracies.

We see a clear shift of the transition from disordered lattice to hexatic from 8G for the annealed samples to approximately 20 G for the as-made samples. This shift could result from the reduction in the density of oxygen vacancy pinning centers with high temperature oxygen annealing, and possibly from a change in effective mass anisotropy[6]. The abrupt transition from isotropic order to hexatic order could come about in several scenarios: 1) a crossover from pinning-induced disorder near H_{c_1}[24] to a regime dominated by thermal fluctuations; 2) a flux liquid to hexatic vortex glass

transition[6][10][23]; 3) remnants of high-temperature liquid and entangled hexatic liquid phases quenched in during field cooling[25].

We acknowledge helpful discussions with D. Huse, S. Martin, D. Nelson, A. Sudbo. Two of the authors would like to acknowledge support received from AT&T (D. B. M.) and the NSF (A. K.). This work was supported in part by the Joint Services Electronic Program under Grant No. N00014-84-K-0327 and by the Stanford Center for Materials Research through the NSF Department of Materials Research.

FIGURES

FIGURE 1:

(a - c) Scanning electron micrographs of Bitter decorations of oxygen-annealed BSCCO cooled to 4.2 K in magnetic fields of 69G, 23G, and 8G, respectively. The fields of view are (a) 27 x 25 μm^2, (b) 48 x 45 μm^2, and (c) 72 x 68 μm^2. (d - f) Delaunay triangulations corresponding to the images in (a - c), respectively. Shaded triangles adjoin vertices which are not 6-fold coordinated. (g - i) Azimuthally averaged pair correlation functions for the locations of vortex cores identified from the images in (a - c).

FIGURE 2:

(a) Translational correlation functions, $g_{\vec{G}}(r)$, calculated for the vortex locations identified from the images in Figure 1 (a - c). Diamonds correspond to the 69G sample, triangles to 23 G, and squares to 8 G. Solid lines are fits to the form $g_{\vec{G}}(r) = A \exp(-r/\xi_{\vec{G}})$.

(b) Bond-orientational correlation functions, $g_6(r)$, calculated for the vortex locations identified from the images in Figure 1 (a - c). Solid lines are fits to the form $g_6(r) = Ar^{-\eta_6}$.

FIGURE 3:

(a) Translational correlation lengths, $\xi_{\vec{G}}$, for annealed (open circles) and unannealed (filled circles) samples.

(b) Bond-orientational exponents, η_6, for annealed (open circles) and unannealed (filled circles) samples. The line at $\eta_6 = 0.06$ is the limit of our experimental resolution.

REFERENCES

1. P. L. Gammel, J. Appl., Phys. **67**, 4676 (1990).

2. P. L. Gammel, L. F. Schneemeyer, J. V. Wasczak, and D. J. Bishop, Phys. Rev. Lett. **61**, 1666 (1988).

3. R. Koch, V. Foglietti, W. J. Gallagher, G. Koren, A. Gupta, and M. P. A. Fisher, Phys. Rev. Lett. **63**, 1511 (1989); T. K. Worthington, F. H. Holtzberg, and C. A. Feild, Cryogenics **30**, 417 (1990).

4. P. H. Kes and C. J. van der Beek, Proceedings of the ICMC-90 Topical Conference on "High-Temperature Superconducting Materials", Garmisch-Partenkirchen, Germany, May 9-11, 1990; L. Lombardo, D. Mitzi, and A. Kapitulnik (to be published).

5. D. R. Nelson, Phys. Rev. Lett. **60**, 1973 (1988);

6. A. Houghton, R. A. Pelcovits, and A. Sudbo, Phys. Rev. **40**, 6763 (1989).

7. D. R. Nelson and H. S. Seung, Phys. Rev. B **39**, 9153 (1989).

8. M. C. Marchetti and D. R. Nelson, Phys. Rev. B **40**, 1910 (1990).

9. E. M. Chudnovsky, Phys. Rev. B **40** 11355 (1989).

10. M. P. A. Fisher, Phys. Rev. Lett. **62**, 1415 (1989); M. P. A. Fisher, D. Fisher, and D. Huse, Phys. Rev. B (1990).

11. D. B. Mitzi, L. W. Lombardo, A. Kapitulnik, S. S. Laderman, and R. D. Jacowitz, Phys. Rev. **B41**, 6564 (1990).

12. D. E. Farrell, S. Bonham, J. Foster, Y. C Chang, P. Z. Jiang, K. G. Vandervoort, D. J. Lam, V. G. Kogan, Phys. Rev. Lett. **63**, 782 (1989).

13. S. Martin, A. T. Fiory, R. M. Fleming, L. F. Schneemeyer, and J. V. Waszcak, Phys. Rev. **B41**, 846 (1990).

14. D. Harshman, private communication.

15. R. P. Huebener, Magnetic Flux Structures in Superconductors, (New York: Springer-Verlag, 1979), p. 100ff.

16. L. Lombardo, M. Ng, J. S. Urbach, D. B. Mitzi, and A. Kapitulnik (to be published).

17. R. N. Kleiman, P. L. Gammel, L. F. Schneemeyer, J. V. Waszczak, and D. J. Bishop, Phys. Rev. Lett. **62**, 2331 (1989)

18. P. L. Gammel, D. J. Bishop, G. J. Dolan, J. R. Kwo, C. A. Murray, L. F. Schneemeyer, and J. V. Wasczak, Phys. Rev. Lett. **59**, 2593 (1987).

19. D. H. Van Winkle and C. A. Murray, J. Chem. Phys. **89**, 3885 (1988).

20. F. F. Preparata and M. L. Shamos, Computational Geometry, an Introduction, (New York: Springer Verlag, 1985), and S. Fortune, Algorithmica **2**, 153 (1987).

21. D. R. Nelson, M. Rubinstein and F. Spaepen, Phil. Mag. A **46**, 105 (1982).

22. B. I. Halperin and D. R. Nelson, Phys. Rev. Lett. **41**, 121 (1978); D. R. Nelson and B. I. Halperin, Phys. Rev. **B19**, 2457 (1979).

23. E. M. Chudnovsky, (preprint), predicts an exponential form for $g_{\vec{G}}(r)$, using local values for the vortex lattice elastic constants. Sudbo, Pelcovits et al. (preprint) predict that, in regions of the phase diagram where nonlocal elastic constants are important, $g_{\vec{G}}(r)$ should have the form of a fast power law decay multiplied by a slowly decaying exponential. Our data over such small ~ $30a$ distances do not warrant attempts to fit to refined forms, but seem inconsistent with fits to pure power law decay.

~~24. Lattice a-b anisotropy and random orientation~~

25. M. C. Marchetti and D. R. Nelson, Phys. Rev. **B41**, 1910 (1990).

24 ~~26~~. D. R. Nelson and P. Le Dousal (preprint).

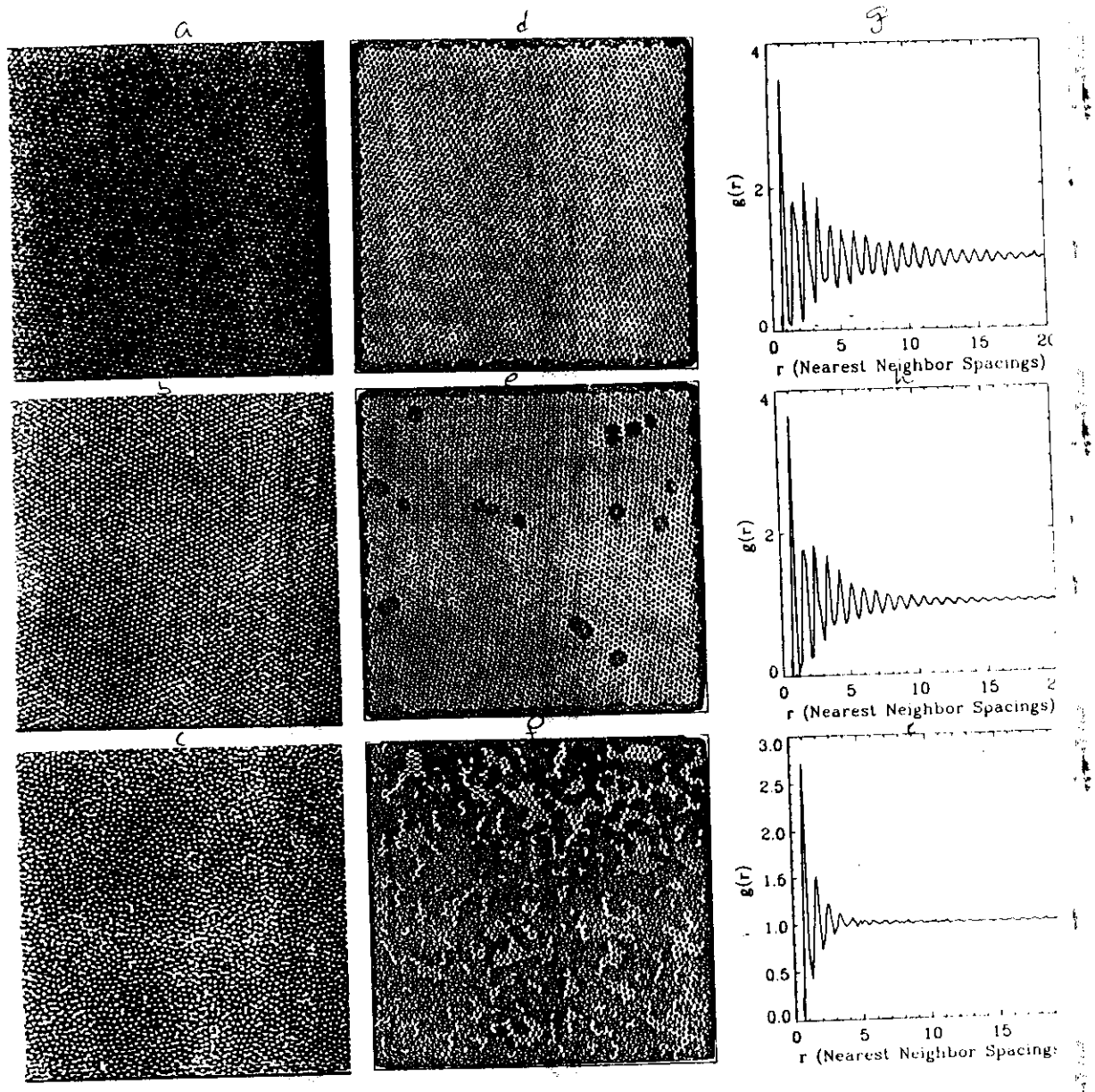

Figure 1

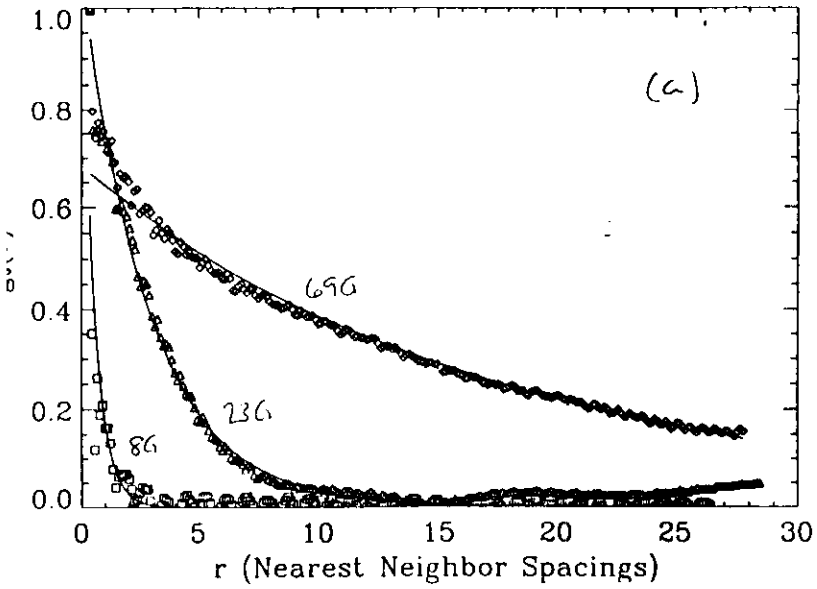

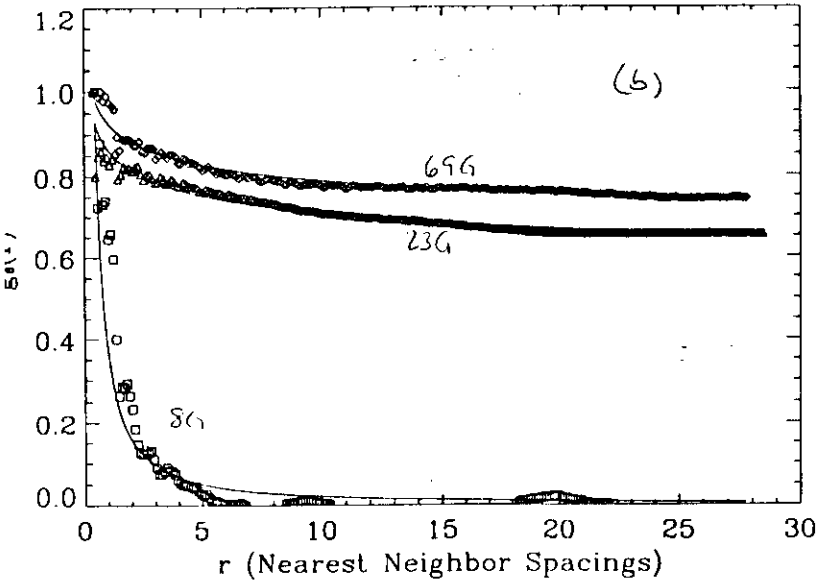

Figure 2

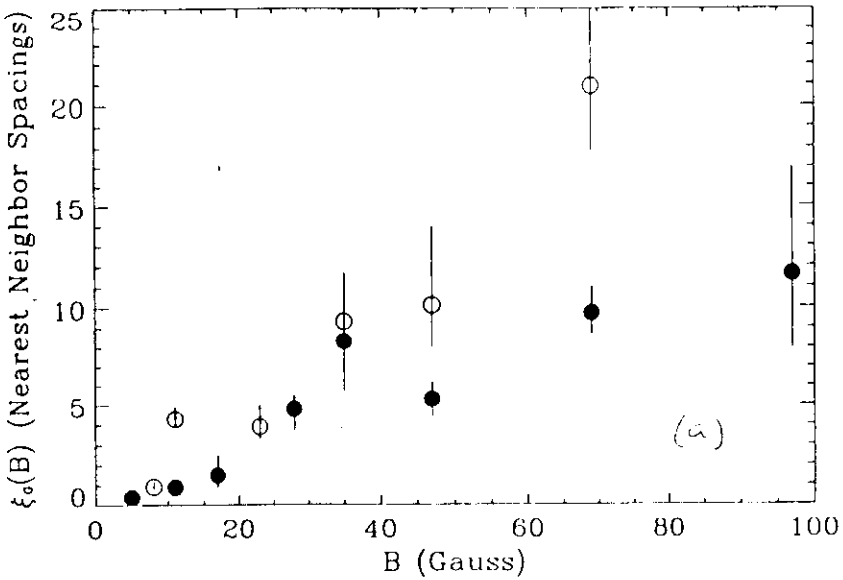

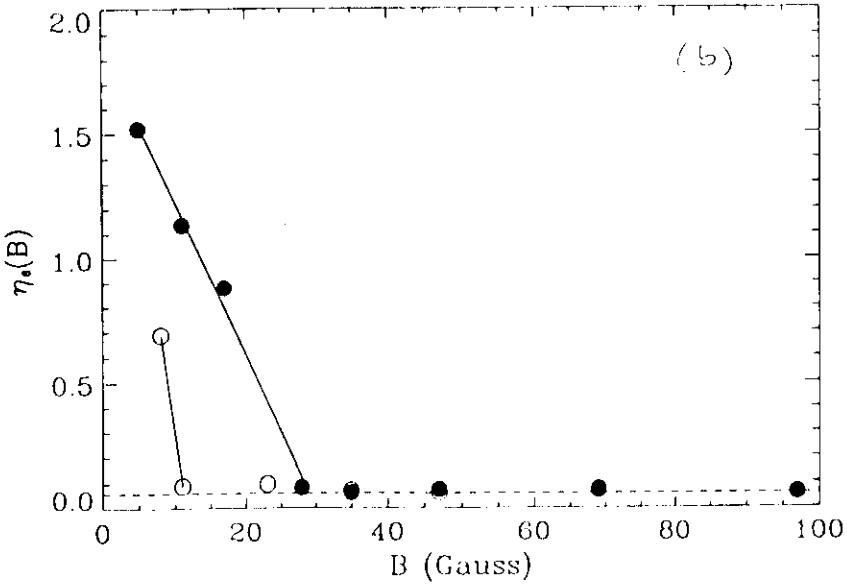

Figure 3

Observation of a Commensurate Array of Flux Chains in Tilted Flux Lattices in BSCCO Single Crystals

C. A. Bolle[a], P. L. Gammel, D. G. Grier, C. A. Murray and D. J. Bishop
ATT-Bell Laboratories
Murray Hill, New Jersey 07974

and

D. B. Mitzi[b] and A. Kapitulnik
Stanford University
Stanford, California 04305

Abstract

We report the observation of a novel flux lattice structure, a commensurate array of flux line chains. Our experiments consist of magnetic decoration of the flux lattices in high quality single crystals of BSCCO where the magnetic field is applied at an angle with respect to the conducting planes. For a narrow range of angles, the equilibrium structure is one with uniformly spaced chains with a higher line density of vortices than the background lattice. Our observations are in qualitative agreement with theories which suggest that in strongly anisotropic materials, the vortices can develop an attractive interaction in tilted magnetic fields.

PACS numbers: 74.60.Ge, 74.70.Vy

Observation of a Commensurate Array of Flux Chains in Tilted Flux Lattices in BSCCO Single Crystals

C. A. Bolle[a], P. L. Gammel, D. G. Grier, C. A. Murray and D. J. Bishop
ATT-Bell Laboratories
Murray Hill, New Jersey 07974

and

D. B. Mitzi[b] and A. Kapitulnik
Stanford University
Stanford, California 04305

Flux lattices in the high Tc superconductors have proven to be a rich and interesting area for research. Strong anisotropies and the importance of thermal fluctuations have combined to produce a variety of new structures and regimes not previously seen in flux lattices in conventional superconductors. Oval vortices[1], hexatics[2], liquids[3], and intrinsic pinning[4] have all been seen in studies of static flux lattice structures. Flux lattices have become important model systems to study the influence of disorder on positional and orientational correlations[5] as well as its effect on the character of phase transitions in the lattices[6].

In this letter we report the observation of a novel flux lattice structure which arises when the magnetic field is tilted with respect to the highly anisotropic conducting planes in single crystals of $Bi_{2.1}Sr_{1.9}Ca_{0.9}Cu_2O_{8+\delta}$ (BSCCO). We have found that for a narrow range of tilt angles, some of the flux lines form into a commensurate array of flux chains uniformly spaced along the sample. Our experiments provide supporting evidence for recent theories[7] which suggest that in strongly anisotropic materials, the normally purely repulsive interaction between flux lines develops a bound state at a finite separation.

Our experiments consist of the Bitter pattern technique[8] for decorating the magnetic flux lattices in high quality single crystals of BSCCO. The Bitter pattern technique uses very small ferromagnetic particles to sense the field distribution at the surface of a material. The "smoke" is made by evaporating a magnetic material in a background of inert (helium) gas. A freshly cleaved sample is first field-cooled to trap the flux. Magnetic Fe particles of size ~50Å are then formed by evaporation, thermalize in the gas, drift to the sample surface and preferentially decorate regions with strong magnetic field gradients. The surface Van der Waals forces hold the particles immobile. The sample is then warmed to room temperature and the lattice examined using a scanning electron microscope. More details of the technique as we implement it are given in previous work[9].

The single crystals were grown using a directional solidification process as described previously[10]. The crystals are typically in the form of thin sheets with basal plane dimensions of up to several cm^2 and thicknesses up to 100 μm. The lattice constants, a_0=5.413(2)Å, b_0=5.411(3)Å, and c_0=30.91(1)Å, were determined using a four-circle x-ray diffractometer. As is typical in these materials, an incommensurate periodicity of $4.7(1)b_0$ was observed along the b-axis. The crystals, as extracted from the melt, demonstrated a large, sharp (<5K 10-90% transition width) Meissner transition with an onset at 88.5K, indicative of a homogeneous, bulk superconductor. The crystals used for this experiment were not annealed. Torque magnetometry experiments[11] have shown that this system is three-dimensional with a large anisotropy parameter $\Gamma=(m_c/m_a)^{1/2}\approx 55$.

Shown in figure 1 is a micrograph of a flux lattice taken with an applied field B_0 of 35 Gauss at an angle θ = 70°. The dark spots indicate the vortices, separated by 1.4 μm on average. The geometry is as defined in the inset in figure 2. The a and b axes are oriented randomly with respect to the tilt axis as determined from many separate experiments. The obvious chain structures seen in the photo are always found to run "up and down hill" in the sample, independent of the a-b axes orientations. These chains have been seen for angles between 60 and 85 degrees at fields between 23 and 97 gauss. In the photo, the chains are separated by approximately 10 μm. This structure is the main result of this paper. The phenomenology of these features will now be discussed in detail.

Shown in figure 2 is data obtained for decorated flux lattices at angles between 0 and 90 degrees. The quantity $\tilde{B}$ is the measured average density of flux lines in a picture times the flux quantum. What is plotted is this quantity normalized by the applied field B_0 vs rotation angle. The simplest picture for the average density as a function of field which emerges is that the field component perpendicular to the c axis of the sample, given simply by $B_0\cos\theta$, forms the lattice that we see. The solid line shown in the figure is this dependence which fits the data quite well given the uncertainties.

Up to angles where we begin to see chains, we see no distortion or elongation beyond 4-5% of the hexagonal flux lattice. This already points to an important role of the anisotropy in this system. For an isotropic superconductor, ignoring surface effects, one would expect to see a distorted vortex lattice with a ratio of lattice parameters proportional to $\cos\theta$. This is simply due to the projection of a hexagonal

vortex lattice perpendicular to the applied field into the plane of the picture. More detailed comparisons with the distorted vortex lattices predicted[12] for tilted fields will be published elsewhere[5]. In addition over the range of fields we have studied, we see no effect of the field component parallel to the surface on either the positional or orientational correlation lengths. Also the parallel component of field does not seem to break the degeneracy of the orientational order with respect to the underlying crystal lattice or tilt direction. However when the chains form they do break the degeneracy of the orientational order. The chains always run up and down hill independent of the a and b directions in the crystal. As can be seen from the photo this locks in the orientational order in the hexagonal lattice between the chains and orients the lattice with one of the lattice vectors always parallel to the chains.

Shown in figure 3 is a plot of the perpendicular distance between chain vortices d as a function of the lattice parameter of the applied field $a_0=1.075(\phi_0/B_0)^{1/2}$ for all fields and angles θ. As shown in the inset in figure 3, D is the mean measured distance between the vortices in the ab plane and $d=D\cos\theta$ is the distance between vortices in a plane perpendicular to the applied field. What we see is that as the externally applied field is increased, the line density of vortices in the chains also increases. Also as the angle increases, the line density of the vortices D in the chains decreases. It is also clear that the interaction in the chains is relatively hard as the vortex spacing is seen to be constant over the length of the chain and constant from one chain to the next. However the photos suggest that interaction between chains is relatively soft as the distance between them is found to vary quite a bit.

The data for our decorations are tabulated in table 1. The last column gives the quantity $D/\tilde{a}_0$ where $\tilde{a}_0=a_0(\cos\theta)^{-1/2}$ is the lattice parameter due to B. Note that the values cluster around $(3/4)^{1/2}$. Shown in the inset of figure 4 is a Delaunay triangulation[2] for a chain formed at an angle of 70° at a field of 97 Gauss where the background lattice is ordered[2]. The decreased separation of vortices in the chains over the background lattice implies the existence of topological lattice defects. What we find in our images are dislocations strung along the chains, ordered into pairs with opposite Burgers vector. The dislocation pairs are roughly evenly spaced apart a distance c (equal to the average interchain distance) along the chain and can be viewed as an array of interstitials. In the triangulation, a dislocation is marked by a 5-fold coordinated vortex separated by one lattice spacing from a 7-fold coordinated vortex. The pairs consist of two dislocations with equal and opposite Burgers vectors. The cancellation of the strain field of a dislocation pair of equal and opposite Burgers vectors at large distances allows the lattice between the chains to be undisturbed.

Shown in figure 4 is a plot of the distance between chains c (see inset in figure 3) vs a_0. The data clearly show that the distance between chains depends strongly on the magnitude of the applied field and weakly on angle θ. The linear dependence suggests that c/a_0 is a constant or that the number of vortices between chains is a constant for a fixed angle, independent of the applied field and depends only weakly on angle if at all. The chain structure is then incommensurate with respect to the underlying crystal lattice but commensurate with respect to the flux lattice. This last point is evident in the triangulation shown in figure 4. The distance between chains is on average c. The line density of vortices in the chain is such that one accumulates one extra vortex along

the chain for every distance c traveled. Thus the structure that we see is the result of one and only one extra vortex line being added for every chain superlattice unit cell.

It is clear that the chains orient the flux lattice and their formation destroys the rotational degeneracy which exists in this system because there are no line defects to orient the flux lattice such as are found in twinned YBCO[4]. This suggests that tilted fields could be used to orient flux lattices which might be important for technological applications as well as in experiments such as neutron scattering in which one does not wish to obtain a powder pattern for the scattering.

Experimentally it is clear that the chains are formed by at least a weakening of the repulsive interaction between vortices in the direction orthogonal to the tilt axis $\hat{\omega}$ due to a tilt of the current paths with respect to the vortex axis resulting from the strong anisotropies in the system. The chains are roughly evenly spaced along the sample due to a repulsive interaction between them. The distance between them is presumably determined by a trade-off in the energy gained by forming a chain and the cost in energy due to the repulsive interactions between them.

The bound state which we suppose is the underlying driving force for the emergence of this structure has been discussed in several recent theoretical papers[7]. The general idea is that because of the strong anisotropy, the screening currents must run in the conducting planes and not in planes perpendicular to the axis of the vortex as for an isotropic superconductor.

There have been several calculations[7] for this situation within the effective mass approximation. Kogan et al have calculated the potential for a single vortex. A shallow attractive region develops in a direction perpendicular to the rotation axis. Parallel to the rotation axis the interaction is purely repulsive. Buzdin and Simonov have considered a similar situation, but examined the total energy for a chain of vortices near H_{c1}. In both calculations, the equilibrium line density along the chain had no field dependence in contradiction to the results presented here. In addition neither calculation gave any indication of a normal vortex lattice between the chains as is seen in our experiments. However we believe that these calculations have captured the essential physics and need only to be extended to finite vortex density to fully explain our data.

In conclusion we have observed a novel flux lattice structure which consists of uniformly spaced chains of vortex lines embedded in a background of an hexagonal flux lattice. These chains may arise from the formation of a bound state between vortices in strongly anisotropic materials in the presence of a tilted magnetic field. The chains appear to repel each other and the distance between them seems to be determined by a competition between the energy gained by forming a chain and that lost by not having them infinitely far apart. These chains provide a non-destructive way of orienting the flux lattice in a given direction without requiring the presence of line defects in the crystal.

We would like to thank L. Campbell for providing unpublished data on his calculations of vortex lattice parameters and V. Kogan, P. Littlewood, D. Huse, A. Sudbo, C. Varma and S. Coppersmith for many helpful discussions. Two of the authors would like to acknowledge support

received from ATT (D.B.M.) and the NSF (A.K.). This work was supported in part by the Joint Services Electronic Program under grant No. N00014-84-K-0327 and by the Stanford Center for Materials Research through the NSF Department of Materials Research.

a) present address, Instituto Balseiro, 8400 Bariloche, Rio Negro, Argentina

b) present address, IBM T. J. Watson Research Center, Yorktown Heights, New York 10598

References

1. G. J. Dolan, F. Holtzberg, C. Field, and T.R. Dinger, Phys. Rev. Lett. **62**, 2184 (1989).

2. C. A. Murray, P. L. Gammel, D. J. Bishop, D. B. Mitzi and A. Kapitulnik, Phys Rev. Lett. **64**, 2312 (1990).

3. R. N. Kleiman, P. L. Gammel, L. F. Schneemeyer, J. V. Waszczak, and D. J. Bishop, Phys. Rev. Lett. **62**, 2331 (1989).

4. G. J. Dolan,G. V. Chandrasekar, T. R. Dinger, C. Field, and F. Holtzberg, Phys. Rev. Lett. **62**, 827 (1989).

5. E. M. Chudnovsky, Phys. Rev. **B40**, 11357 (1989); E. M. Chudnovsky submitted to Phys. Rev.; A. Houghton, R. A. Pelcovits, and A. Sudbo, submitted to Phys. Rev.; C. A. Bolle, P. L. Gammel, D. Grier, C. A. Murray, D. J. Bishop, D. B. Mitzi and A. Kapitulnik, to be published.

6. M. P. A. Fisher, Phys. Rev. Lett. **62**, 1415 (1989) and D. S. Fisher, M. P. A. Fisher and D. A. Huse, submitted to Phys. Rev..

7. A. I. Buzdin and A. Yu Simonov, JETP Lett. **51**, 191 (1990); V. G. Kogan, N. Nakagawa and S. L. Thiemann, Phys. Rev. **B42**, 2631 (1990).

8. H. Trauble and U. Essmann, J. Appl. Phys. **25**, 273 (1968); N. V. Sarma, Phil. Mag. **17**, 1233(1968).

9. P. L. Gammel, D. J. Bishop, G. J. Dolan, J. R. Kwo, C. A. Murray, L. F. Schneemeyer, and J. V. Waszczak, Phys. Rev. Lett. **59**, 2592 (1987).

10. D. B. Mitzi, L. W. Lombardo, A. Kapitulnik, S. S. Laderman, and R. D. Jacowitz, Phys. Rev. **B41**, 6564 (1990).

11. D. E. Farrell, S. Bonham, J. Foster, Y. C. Chang, P. Z. Jiang, K. G. Vandervoort, D. J. Lam and V. . Kogan, Phys. Rev. Lett. **63**, 782 (1989).

12. L. J. Campbell, M. M. Doria, and V.G. Kogan, Phys. Rev. **B38**, 2439 (1988) and private communication.

Figure Captions

Figure 1: A region of the decorated crystal taken at an angle of 70° with an applied field of 35 Gauss. The dark regions are the vortices, with an average spacing of 1.4 μm. The chains run approximately perpendicular to the rotation axis, and define the orientation of the vortex lattice between chains. (The field of view is 75 μm by 60 μm)

Figure 2: The field $\tilde{B}=n\Phi_0$ defined from the vortex density n divided by the applied field B_0 is plotted against the rotation angle θ. At low angles, both the density $B=B_0\cos\theta$ and correlation functions (not shown) are equivalent to what would be generated by the normal component of B_0. The inset shows the sample geometry defining the rotation axis ω.

Figure 3: The inset shows the geometry of the chains in the crystal ab plane. The spacing along the the chain is D and between chains is c. The â direction is arbitrary. The spacing along chains projected perpendicular to the applied field direction d is defined as $d=D\cos\theta$. The data at all angles and applied fields are plotted against $a_0=4.808/(B_0)^{1/2}$, the vortex lattice constant for a hexagonal lattice created by the full applied field.

Figure 4: The spacing between chains c as defined in figure 3 is plotted vs a_0 for θ=70°. Data for three other angles is also shown. Because of chain wandering, there is a large error in this measurement. The inset in the lower right hand side shows a Delaunay triangulation for a region near a chain (dark line) taken at 70° and 97 Gauss. To accommodate the increased vortex density along the chain, pairs of dislocations (shaded regions) are formed.

Table #1

Angle (deg)	Field B (gauss)	Field $\tilde{B}$ (gauss)	D(μm)	c(μm)	d/c	$D/\tilde{a}_0$
10	35	36.0				
20	35	35.4				
40	35	28.2				
50	35	25.6				
55	35	21.6				
60	17		1.42	17.6	.040	.861
60	35	20.1				
65	23		1.32	16.0	.035	.856
65	35	16.1				
70	23		1.46	11.4	.044	.852
70	28		1.29	11.1	.040	.830
70	35	13.4	1.14	9.5	.042	.796
70	47	16.5	1.00	8.7	.039	.834
70	69	22.8	0.84	6.8	.042	.848
70	97	36.4	0.69	5.2	.045	.848
75	35	10.1	1.35	7.5	.047	.819
80	35	5.8	1.56	7.9	.034	.775
80	47		1.89	7.1	.046	1.09
85	35	3.7	1.80	8.3	.019	.634

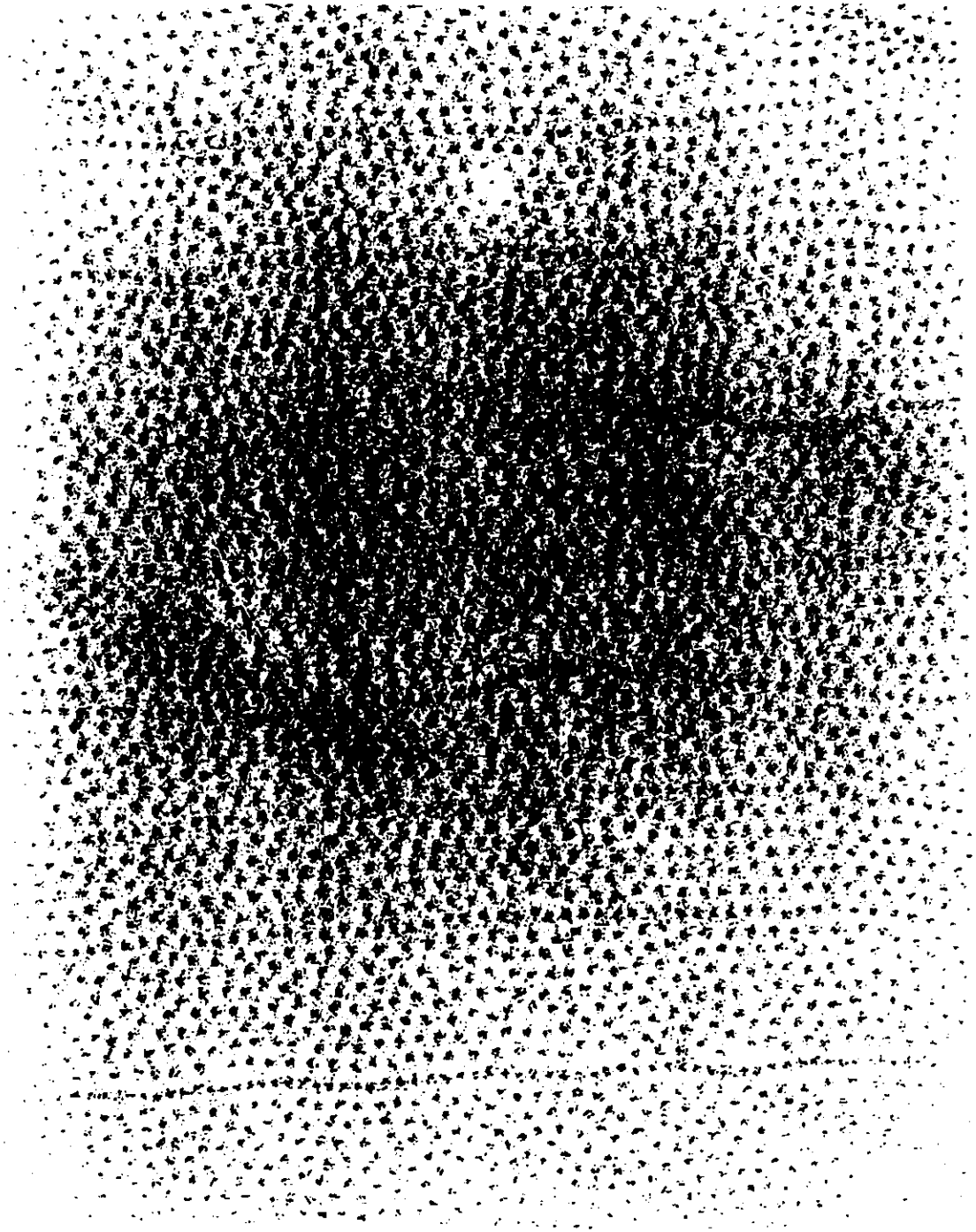

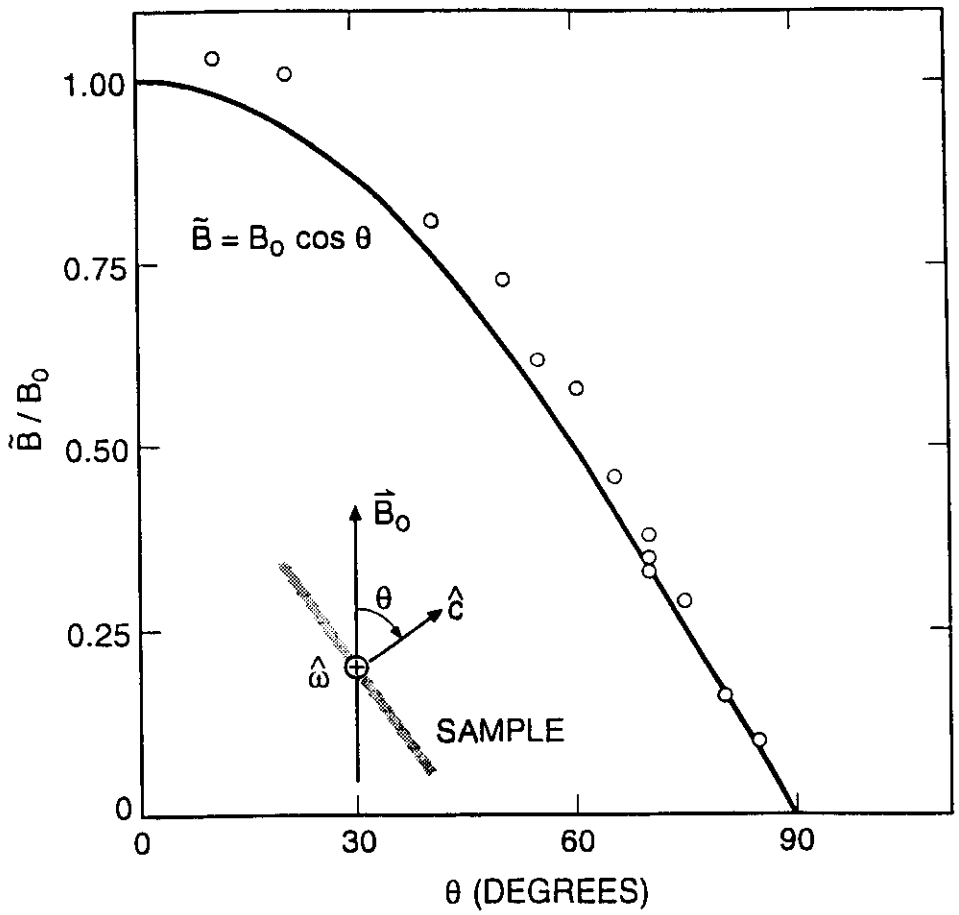
1.00
0.75
0.50
0.25
0
$\tilde{B} / B_0$
$\tilde{B} = B_0 \cos\theta$
$\vec{B}_0$
θ
$\hat{c}$
$\hat{\omega}$
SAMPLE
0
30
60
90
θ (DEGREES)

FIG. 2.

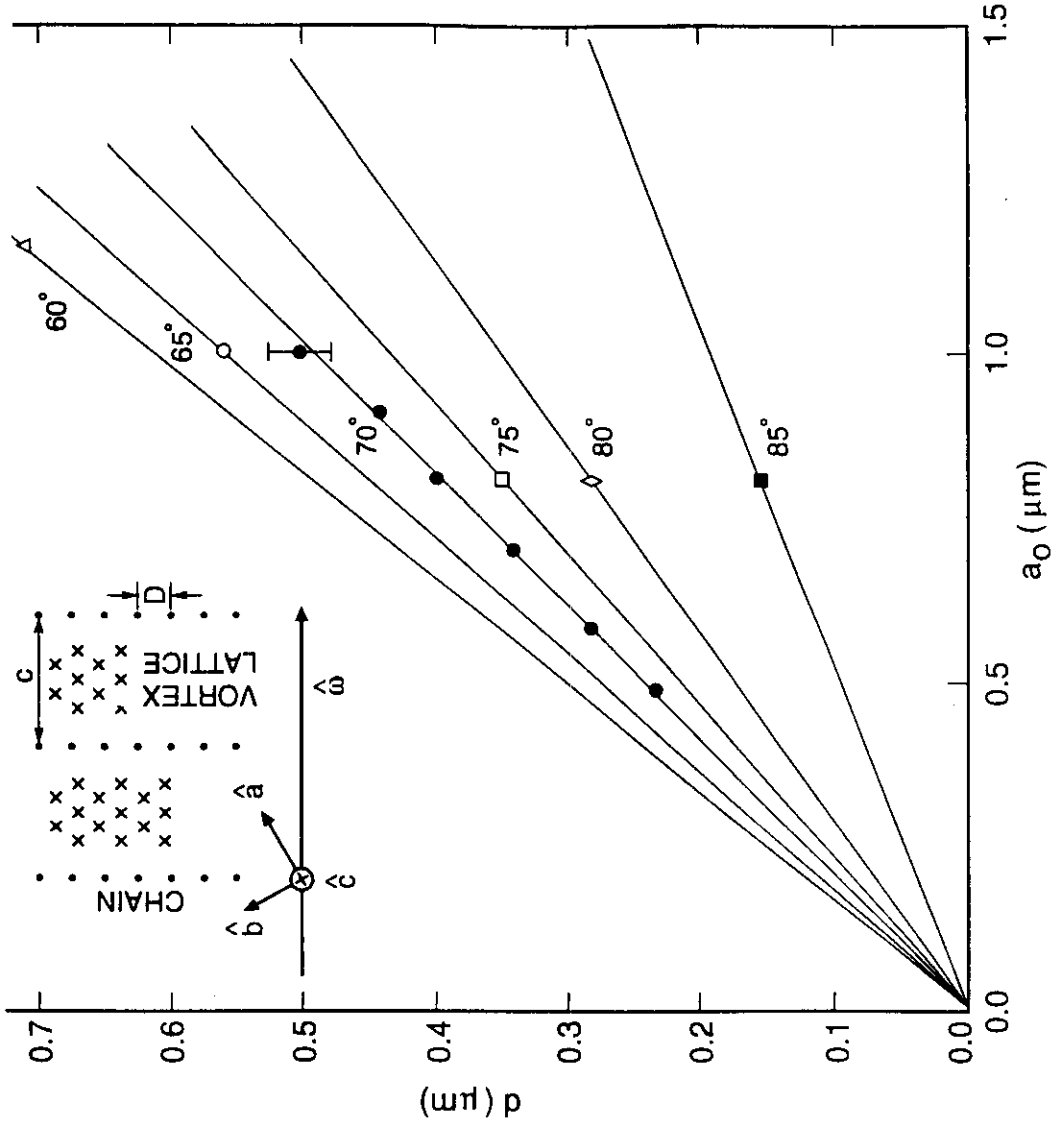
60°
65°
70°
75°
80°
85°
a_o (μm)
d (μm)
0.0
0.5
1.0
1.5
0.7
0.6
0.5
0.4
0.3
0.2
0.1
0.0
D
c
VORTEX LATTICE
CHAIN
ω̂
â
b̂
ĉ

FIG. 3.

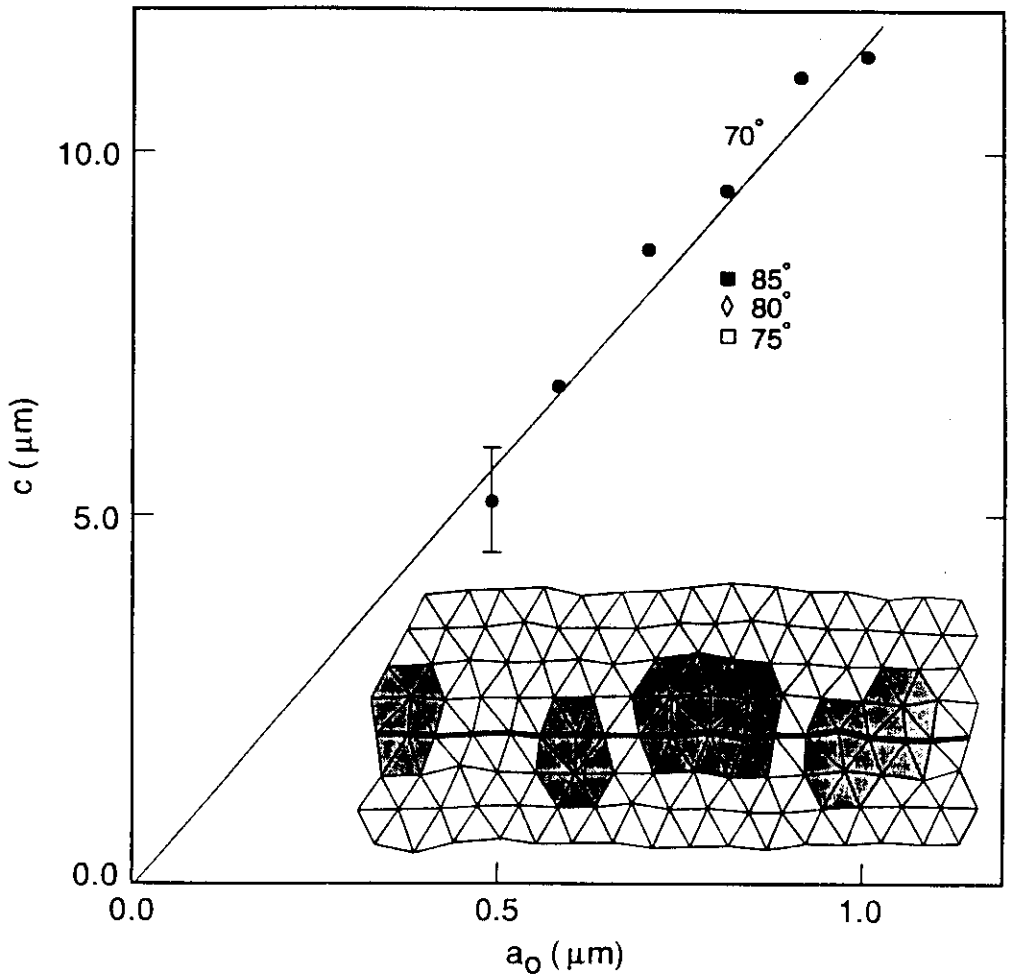
70°
85°
80°
75°
c (μm)
a_o (μm)
10.0
5.0
0.0
0.0
0.5
1.0

FIG. 4.